

MODEL-BASED ESTIMATION AND CONTROL IN SPARK IGNITION ENGINES USING LPV TECHNIQUES

A Dissertation

Presented to

the Faculty of the Department of Mechanical Engineering

University of Houston

In Partial Fulfillment

of the Requirements for the Degree

Doctor of Philosophy

in Mechanical Engineering

by

Rohit A. Zope

December 2011

UMI Number: 3500063

All rights reserved

INFORMATION TO ALL USERS

The quality of this reproduction is dependent upon the quality of the copy submitted.

In the unlikely event that the author did not send a complete manuscript and there are missing pages, these will be noted. Also, if material had to be removed, a note will indicate the deletion.



UMI 3500063

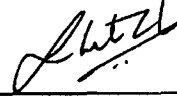
Copyright 2012 by ProQuest LLC.

All rights reserved. This edition of the work is protected against unauthorized copying under Title 17, United States Code.



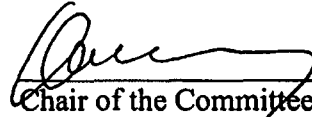
ProQuest LLC
789 East Eisenhower Parkway
P.O. Box 1346
Ann Arbor, MI 48106-1346

MODEL-BASED ESTIMATION AND CONTROL IN SPARK
IGNITION ENGINES USING LPV TECHNIQUES



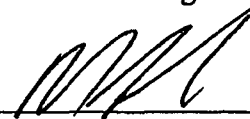
Rohit A. Zope

Approved:



Chair of the Committee
Karolos M. Grigoriadis, Professor
Mechanical Engineering

Committee Members:



Matthew A. Franchek,
Professor, Co-Chair,
Mechanical Engineering



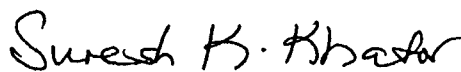
Leang-San Shieh, Professor,
Electrical and Computer Engineering



Gangbing Song, Professor,
Mechanical Engineering



Javad Mohammadpour,
Research Assistant Professor,
Mechanical Engineering



Suresh K. Khator, Associate Dean,
Cullen College of Engineering



Matthew A. Franchek,
Professor and Interim Chair,
Mechanical Engineering

Acknowledgements

The last four years of my life have been very rewarding and it just feels right to take this opportunity to express my heartfelt gratitude towards all involved in making this dissertation a success. First and foremost, I would like to thank my advisors, Professor Matthew Franchek and Professor Karolos Grigoriadis, for giving me the opportunity to come to the University of Houston to pursue graduate studies. Both Dr. Franchek and Dr. Grigoriadis have played a unique role in shaping my dissertation. I was introduced to the world of Linear Parameter Varying (LPV) systems by Dr. Grigoriadis and, ever since, I have been trying to learn more and apply the LPV systems theory to solve engineering problems. I consider myself lucky to have worked with Dr. Franchek, who in a certain way is responsible for instilling a sense of responsibility and accountability among the students. His words of appreciation to the smallest of my successful works (whenever that happened) made me believe in myself and egged me on to continue with the good work. I would like to thank Dr. Javad Mohammadpour, whom I look up to as a mentor and a dear friend. This work would not have been possible had it not been for the many discussions I had with him. I also thank Dr. L.S. Shieh and Dr. Gangbing Song, first, for serving as an examining member on my qualifying examination committee and, now, on my defense examination committee.

I wish to offer my special thanks to employees at Ford Motor Company: Stephen Smith, who gave me a chance to work as a research intern for two summers, Gopichandra Surnilla, for his expert advice and comments on my work relating to ethanol blend estimation and James Kerns, for the numerous discussions I had with him which made me learn and understand the niceties of SI engines.

I would like to mention my roommates, Rahul, Harshal, Rajat and Satadru, who kept my life outside school sensible and entertaining. Doctoral study is never a smooth ride, at least mine was not, and I have to give credit to my parents for their unwavering support and blessings. Thank you Aai and Baba for being my greatest

strength. It would be an understatement to thank my lovely wife who believed in me, shared the ups and downs and made infinite sacrifices to see me succeed. Thank you, my sweetheart, for all the unconditional love.

Last but not the least, I would like to thank the Almighty and my guru Most. Rev. Vishnu Maharaj Parnerkar for getting me to the US and seeing me through. My deepest and sincere gratitude for inspiring and guiding this humble being. May your blessings open up new vistas and allow me to scale unprecedented heights. Finally, I would like to dedicate this work to the little one who will soon be bringing bundles of joy and happiness to my family.

**MODEL-BASED ESTIMATION AND CONTROL IN
SPARK IGNITION ENGINES USING LPV TECHNIQUES**

An Abstract
of a
Dissertation
Presented to
the Faculty of the Department of Mechanical Engineering
University of Houston

In Partial Fulfillment
of the Requirements for the Degree
Doctor of Philosophy
in Mechanical Engineering

by
Rohit A. Zope
December 2011

Abstract

This dissertation addresses the problem of estimation and control in spark-ignited (SI) engines. In the first part of this thesis, we investigate the problem of estimating the ethanol content in an ethanol-gasoline blended fuel for use in flexible-fuel vehicles. A steady-state parametric model relating the engine speed, throttle angle, and air-fuel ratio to the fuel injector pulse-width is developed from physics. The parameters of this model are adapted and linked to the percentage of ethanol content via a suitably defined metric. The proposed steady-state model structure is experimentally validated on a 5.4L V8 Ford engine at the University of Houston's Engine Control Research Laboratory (UH-ECRL). The developed ethanol content estimation methodology is justified based on the combustion chemistry and physics involved. The methodology developed has a distinct advantage over previously proposed methods as it uses only the existing sensor set on a production vehicle.

The second part of the thesis examines the application of linear parameter varying (LPV) systems theory to SI engine sub-systems identification and control. LPV systems modeling and control have been investigated extensively in the literature. Nonlinear and/or time-varying systems can be cast into an LPV form and analyzed using the well established LPV controller synthesis techniques. In this thesis we present a method for identifying the model parameters of an LPV system and show how the LPV system identification problem can be reduced to a problem of linear regression. This methodology is validated by applying it to identify the intake manifold dynamics of an SI engine both in simulations using GT Power as well as experimentally at the UH-ECRL. Next, we consider the fueling control problem in SI engines. It is shown that the air and fuel path dynamics represent an LPV system with a parameter varying time-delay. Simulation study using the existing results in literature for design of an output feedback \mathcal{H}_∞ controller for the fueling control problem revealed the conservativeness of the delay-independent criteria. Hence, the focus of the last part of this thesis has been on developing new tractable results guaranteeing

closed-loop stability and \mathcal{H}_∞ performance of LPV time-delay systems using the less conservative delay-dependent conditions.

Table of Contents

Acknowledgements	iv
Abstract	vii
Table of Contents	ix
List of Figures	xii
List of Tables	xv
Chapter 1 Introduction	1
1.1 Flexible Fuel Vehicles	2
1.2 Linear Parameter Varying Systems	2
1.2.1 LPV System Stability and Performance Analysis	4
1.2.2 LPV Controller Synthesis	6
1.2.3 LPV Control in Automotive Systems	8
1.3 Outline of the Thesis	9
Chapter 2 Model-Based Ethanol Blend Estimation in Flexible-Fuel Vehicles	12
2.1 Introduction	12
2.2 Motivation	17
2.2.1 Model Structure Identification	17
2.3 First Principles Based Model	19
2.3.1 Air Path Dynamics	19
2.3.2 Fuel Path Dynamics	23

2.3.3	UEGO Sensor Dynamics	24
2.4	Description of the Experimental Facility	25
2.5	Main Results	26
2.5.1	Experimental Validation of the Proposed Model Structure	27
2.5.2	Ethanol Content Estimation Methodology	29
2.5.3	Correlation with Combustion Chemistry	32
2.6	Chapter Conclusions	34
Chapter 3 Parameter-Dependent Identification of the Intake Manifold		
System Dynamics in Spark Ignition Engines using LPV Methods		36
3.1	Introduction	36
3.2	Approach to LPV System Identification	38
3.3	Phenomenological Modeling of the Intake Manifold System in SI Engines	41
3.4	Problem Formulation	44
3.5	Simulation Results using GT-Power	46
3.6	Experimental Results	48
3.6.1	Training Data	48
3.6.2	Validation Data	50
3.7	Chapter Conclusions	52
Chapter 4 Delay-Dependent \mathcal{H}_∞ Control of LPV Time-Delay Systems		
with Application to Fueling Control in SI Engines		54
4.1	Introduction and Literature Review	54
4.2	Problem Statement and Preliminaries	58

4.3	\mathcal{H}_∞ Performance Analysis of Time-delay LPV Systems	60
4.3.1	LMI relaxation using slack variables	63
4.4	\mathcal{H}_∞ State Feedback Control of Time-Delay LPV systems	66
4.5	\mathcal{H}_∞ Output Feedback Control Design	67
4.6	Numerical Examples	73
4.7	Application to Fueling Control of SI Engines	78
4.7.1	LPV time-delayed Controller Design	83
4.7.2	Simulation Results	86
4.8	Chapter Conclusions	89
	Chapter 5 Conclusions, Contributions and Future Work	91
5.1	Summary and Assessment of the Dissertation	91
5.2	Future Research Directions	93
	References	96

List of Figures

Figure 2.1	3-dimensional plot showing the variation in fuel pulse-width as a function of throttle position and engine speed, for three fuel types tested on a 2005 Ford 5.4L PFI engine	18
Figure 2.2	Engine and dynamometer at the Engine Control Research Laboratory, University of Houston	26
Figure 2.3	Steady state operating points in terms of mass air flow and engine speed	27
Figure 2.4	Evolution of the parameter trajectory for E10 fuel blend	28
Figure 2.5	Comparison of actual V/s model estimated fuel pulse-width for E10 fuel	29
Figure 2.6	Vector lengths as a function of percentage ethanol content in the fuel blend	31
Figure 2.7	Ethanol blend estimator curve	31
Figure 2.8	Density corrected normalized vector length and FAR_s as a function of ethanol content	34
Figure 3.1	Throttle valve excitation input during GT-Power simulation study	46
Figure 3.2	Manifold pressure and engine speed trajectories during input excitation in GT-Power simulation	47
Figure 3.3	Estimated and sensor outputs with GT-Power simulation study	47
Figure 3.4	Throttle valve excitation input	48

Figure 3.5	Manifold pressure and engine speed trajectories during input excitation	49
Figure 3.6	a_1^0 coefficient trajectory	49
Figure 3.7	Throttle angle, manifold pressure and engine speed trajectories during validation	51
Figure 3.8	Sensor output and output of the identification algorithm	52
Figure 3.9	Sensor output and output of the identification algorithm with only 6 basis functions	53
Figure 4.1	γ varying with λ_2 and λ_3	74
Figure 4.2	Milling process	77
Figure 4.3	Blade rotation speed (rpm)	79
Figure 4.4	Displacement of mass 1 using results in Zhang et al. 2005 (solid line), and our results (dashed line)	79
Figure 4.5	Displacement of mass 2 using results in Zhang et al. 2005 (solid line), and our results (dashed line)	80
Figure 4.6	Control effort for the milling process example using results in Zhang et al. 2005 (solid line), and our results (dashed line)	80
Figure 4.7	Fuel path of an SI engine	82
Figure 4.8	Interconnection of the engine model and the controller	83
Figure 4.9	λ_{up} variation in response to disturbance with engine operating speed 1000 rpm	86
Figure 4.10	Δm_{O_2} variation in response to disturbance with engine operating speed 1000 rpm	87

Figure 4.11 λ_{up} variation in response to disturbance with engine operating speed 3500 rpm	87
Figure 4.12 Δm_{O_2} variation in response to disturbance with engine operating speed 3500 rpm	88
Figure 4.13 Engine speed variation	88
Figure 4.14 Disturbance profile	89
Figure 4.15 Closed loop λ tracking performance	89
Figure 4.16 Tracking performance: 90 -165 sec	90

List of Tables

Table 2.1	Properties of gasoline and ethanol	13
Table 2.2	Model parameters, model fit, vector length and angles for the seven fuel blends tested	30
Table 3.1	Normalized model coefficient values	50
Table 4.1	The resulting \mathcal{H}_∞ norms for $h_{max} = 1$ (Numbers as reported in the corresponding papers)	75
Table 4.2	The resulting \mathcal{H}_∞ norms for $h_{max} = 1.5$ (Numbers as reported in the corresponding papers)	75
Table 4.3	The maximum allowable time-delay	75

Chapter 1 Introduction

The term spark ignition (SI) engine refers to the internal combustion (IC) engine technology where the air-fuel mixture undergoes combustion when ignited by a spark from the spark plug. The fuel used in SI engines is primarily gasoline. The SI engine, as we know today, was invented by Nicolaus Otto and the first prototype was run in 1876 [1]. This engine had an overall efficiency of 14%. The thermodynamic cycle for this engine follows the Otto cycle, so named in honor of its inventor. Since its inception, the SI engine has been one of the main sources of energy for transportation. With an increasing emphasis on achieving substantial improvements in automotive fuel economy, automotive engineers are striving to develop engines having enhanced brake-specific fuel consumption (BSFC), and which can also comply with future stringent emission requirements. The SI engine technology has come a long way from carburetors to direct fuel injection, from no emission regulation to modern exhaust after-treatment technology. The silicon revolution made possible the use of digital controllers in the automotive industry and the control engineer has played a major role in developing today's modern engine sub-systems. Apart from increasing fuel economy and reducing emissions, the need as well as government mandate to lessen the nation's dependence on petroleum based fossil-fuels has led to increased research in the field of alternative fuel technology such as fuel cells, electric and hybrid vehicles and flexible-fuel vehicles (FFVs). In the first part of this dissertation, we address the problem of estimating the ethanol content in an FFV. In the second part, we investigate the use of linear parameter varying (LPV) techniques to identify and control different engine sub-systems.

1.1 Flexible Fuel Vehicles

A flexible-fuel vehicle or a dual-fuel vehicle is an alternative fuel vehicle with an internal combustion engine designed to run on more than one fuel, usually gasoline blended with either ethanol or methanol fuel with both the fuels stored in a common tank. Modern flex-fuel engines are capable of burning any proportion of the resulting blend in the combustion chamber and the fuel injection and spark timing are adjusted according to the actual blend as detected by an ethanol concentration sensor. The most common commercially available FFV in the world market is the ethanol flexible-fuel vehicle. Though technology exists to allow ethanol FFVs to run on any mixture of gasoline and ethanol, from pure gasoline up to 100% ethanol (E100) [2], North American and European flex-fuel vehicles are optimized to run on a maximum blend of 15% gasoline with 85% anhydrous ethanol called the E85 fuel. This limit in the ethanol content is set to reduce ethanol emissions at low temperatures and to avoid cold starting problems during cold weather conditions, at temperatures lower than 11 °C (52 °F) [3]. It is important to estimate the ethanol content in a blend accurately so that necessary optimization in terms of engine control strategy can be applied. The estimation of ethanol content in an FFV is the main topic of discussion in chapter 2, where a study of ethanol fuel properties and their effect on SI engine performance is outlined. In the following section we introduce the LPV systems in the context of their relevance to engine control and the work in this dissertation.

1.2 Linear Parameter Varying Systems

Linear parameter varying systems form a class of linear systems whose state-space entries depend continuously on a time-varying parameter vector $\rho(t)$ that is assumed to be unknown in advance, but is constrained *a priori* to lie in some known, bounded set, and its value is assumed to be either measurable or estimated in real-time. The

state-space representation of an LPV system is

$$\begin{aligned}
 \dot{x}(t) &= A(\rho(t))x + B_1(\rho(t))w(t) + B_2(\rho(t))u(t) \\
 z(t) &= C_1(\rho(t))x(t) + D_{11}(\rho(t))w(t) + D_{12}(\rho(t))u(t) \\
 y(t) &= C_2(\rho(t))x(t) + D_{21}(\rho(t))w(t),
 \end{aligned} \tag{1.1}$$

where $x(t)$, $w(t)$ and $u(t)$ represent the state vector, the exogenous input vector, and the control input vector, respectively; $z(t)$ and $y(t)$ represent the controlled output and system measurement vectors, respectively. The system state space matrices define a continuous mapping as $A, B_1, B_2, C_1, C_2, D_{11}, D_{12}, D_{21} : \mathbb{R}^s \rightarrow (\mathbb{R}^{n \times n}, \mathbb{R}^{n \times n_w}, \mathbb{R}^{n \times n_u}, \mathbb{R}^{n_z \times n}, \mathbb{R}^{n_y \times n}, \mathbb{R}^{n_z \times n_w}, \mathbb{R}^{n_z \times n_u}, \mathbb{R}^{n_y \times n_w})$. Such systems play a very important role in the context of gain-scheduling and have been studied extensively in the literature [4, 5]. LPV gain scheduling offers a distinct advantage over conventional adhoc gain scheduling approaches, since it involves direct synthesis of a controller rather than its construction from a family of local linear controllers designed by linear time-invariant methods. Other benefit of using LPV techniques resides in the fact that most non-linear and/or time-varying systems can be cast into an LPV representation. This is not the topic of discussion here and the interested reader is referred to [5, 6]. It is to be noted that the scheduling parameter $\rho(t)$ in the LPV system representation captures the time-varying or non-linear behavior of the original system. The knowledge of this scheduling parameter results in a systematic gain scheduling design guaranteeing closed-loop stability and performance over the entire range of parameter variation. The LPV control design approaches typically utilize norm based performance measures. In particular, the induced \mathcal{L}_2 norm is widely employed as a performance measure since this enables a degree of continuity to be maintained with linear \mathcal{H}_∞ theory in the sense that when the plant is linear time-invariant (LTI) the approaches are equivalent to linear \mathcal{H}_∞ design. The controller design involves solution to a linear matrix inequality (LMI) optimization problem [7–9], a convex problem [10] that can be solved efficiently in polynomial-time using existing solvers such as the one in Matlab.

1.2.1 LPV System Stability and Performance Analysis

Having introduced LPV systems in the previous section, we discuss the stability and performance analysis of LPV systems in this section. Stability of LPV systems can be studied by extending the Lyapunov theory as applied to LTI systems. In order to discuss the stability and performance we present some definitions fundamental to the study of LPV systems.

Definition 1.1 *Given a compact set $\mathcal{P} \subset \mathbb{R}^s$, the parameter variation set $\mathcal{F}_{\mathcal{P}}$ is defined as*

$$\mathcal{F}_{\mathcal{P}} \triangleq \{\rho \in C^0(\mathbb{R}_+, \mathbb{R}^s) : \rho(t) \in \mathcal{P}\}, \quad (1.2)$$

where C^0 is the set of piecewise continuous functions, \mathbb{R}_+ stands for the set of positive real numbers and \mathbb{R}^s denotes a vector with 's' real scalars.

Definition 1.2 *Given a compact set $\mathcal{P} \subset \mathbb{R}^s$, finite non-negative numbers $\{\nu_i\}_{i=1}^s$ and $\nu = [\nu_1, \nu_2, \dots, \nu_s]^T$, the parameter ν -variation set $\mathcal{F}_{\mathcal{P}}^\nu$ is defined as*

$$\mathcal{F}_{\mathcal{P}}^\nu \triangleq \{\rho \in C^1(\mathbb{R}_+, \mathbb{R}^s) : \rho(t) \in \mathcal{P}, |\dot{\rho}_i(t)| \leq \nu_i\}, \quad (1.3)$$

where C^1 denotes the class of piecewise continuously differentiable functions.

The parameter set $\mathcal{F}_{\mathcal{P}}$ includes time-varying trajectories where the parameter variation rates are unbounded whereas $\mathcal{F}_{\mathcal{P}}^\nu$ denotes a subclass of $\mathcal{F}_{\mathcal{P}}$ where the time-varying parameter trajectories are assumed to have bounded rates of variation. Note that $\rho \in \mathcal{P}$ denotes a vector in the compact subset of \mathbb{R}^s . The notion of quadratic stability for LPV systems is given by the following definition [11].

Definition 1.3 *Given a compact set $\mathcal{P} \subset \mathbb{R}^s$ and a function $A \in C(\mathbb{R}^s, \mathbb{R}^{n \times n})$, the function A is quadratically stable over \mathcal{P} if there exists a matrix $P \in \mathbb{S}_{++}^n$, such that for all $\rho \in \mathcal{F}_{\mathcal{P}}$,*

$$A^T(\rho)P + PA(\rho) < 0, \quad (1.4)$$

where \mathbb{S}^n denotes real symmetric $n \times n$ matrices and \mathbb{S}_{++}^n is the set of real symmetric positive definite $n \times n$ matrices.

This notion of quadratic stability can be extended to parameter dependent quadratic (PDQ) stability [12] by replacing the positive definite matrix P by a continuously differentiable matrix function $\tilde{P} : \mathbb{R}^s \rightarrow \mathbb{S}_{++}^n$ such that $\tilde{P}(\rho) > 0$ and

$$A^T(\rho)\tilde{P}(\rho) + \tilde{P}(\rho)A(\rho) \pm \sum_{i=1}^s \left(\nu_i \frac{\partial \tilde{P}}{\partial \rho_i} \right) < 0 \quad (1.5)$$

for all $\rho \in \mathcal{F}_{\mathcal{P}}^{\nu}$. If the function A is quadratically stable over \mathcal{P} , then the unforced LPV system (1.1) i.e. with $w = u \equiv 0$ defines a quadratically stable system. Further the quadratic stability implies exponential stability of the unforced LPV system. In the control design for LPV systems we typically use the induced \mathcal{L}_2 gain or the \mathcal{H}_{∞} norm as a performance measure which is defined as

Definition 1.4 *The induced \mathcal{L}_2 gain (or \mathcal{H}_{∞}) norm of the LPV system in (1.1) from w to z considering $u \equiv 0$ is defined by*

$$\|T_{zw}\|_{\infty} = \sup_{\rho \in \mathcal{F}_{\mathcal{P}}^{\nu}} \sup_{\|w\|_2 \neq 0} \frac{\|z\|_2}{\|w\|_2}, \quad (1.6)$$

where T_{zw} is an operator mapping w to z . $\|w\|_2$ is the 2-norm of the exogenous input and $\|z\|_2$ is the 2-norm of the desired controlled output vector.

Now we give a sufficient condition to check if the induced \mathcal{L}_2 -norm of an LPV system is less than a prescribed value γ using a parameter-dependent Lyapunov function.

Theorem 1.1 *Given a compact set $P \subset \mathbb{R}^s$, finite non-negative numbers $\{\nu_i\}_{i=1}^s$, and the LPV system in (1.1). If there exists a function $W \in \mathcal{C}^1(\mathbb{R}^s, \mathbb{S}_{++}^n)$, a positive scalar γ , such that $W(\rho) > 0$ and*

$$\begin{bmatrix} A^T(\rho)W(\rho) + W(\rho)A(\rho) + \sum_{i=1}^s \pm \left(\nu_i \frac{\partial W}{\partial \rho_i} \right) & B_1(\rho) & W(\rho)C_1^T(\rho) \\ * & -\gamma I_{n_w} & D_{11}^T(\rho) \\ * & * & -\gamma I_{n_z} \end{bmatrix} < 0 \quad (1.7)$$

for all $\rho \in \mathcal{F}_p^\gamma$ then the LPV system is parametrically dependent stable and satisfies the condition $\|T_{zw}\|_\infty \leq \gamma$.

Proof. Refer to [11]. Theorem 1.1 is a generalized form of the well known bounded real lemma and is used to derive the existence conditions for control synthesis.

Remark 1.1 The notation $\sum_{i=1}^s \pm(\cdot)$ is used to indicate that every combination of $+(\cdot)$ and $-(\cdot)$ should be included in the inequality. This means that the above 3×3 inequality actually represents 2^s different inequalities that correspond to the 2^s different combinations in the summation and must be checked simultaneously

Remark 1.2 In large symmetric matrix expressions, terms denoted by (\star) will be induced by symmetry. For instance with S symmetric we have

$$\begin{bmatrix} M + N + (\star) + S & \star \\ Q & P \end{bmatrix} \triangleq \begin{bmatrix} M + N + M^T + N^T + S & Q^T \\ Q & P \end{bmatrix}. \quad (1.8)$$

1.2.2 LPV Controller Synthesis

In this section we review the LPV controller synthesis problem guaranteeing a prescribed level of \mathcal{H}_∞ performance. Given the LPV plant in (1.1) the gain scheduled output feedback problem is to find a $n_k - th$ order dynamic controller with a state-space realization as

$$\begin{aligned} \dot{x}_k(t) &= A_k(\rho)x_k(t) + B_k(\rho)y(t), \\ u(t) &= C_k(\rho)x_k(t) + D_k(\rho)y(t), \end{aligned} \quad (1.9)$$

such that the closed loop system formed by the interconnection of the open-loop LPV system (1.1) and the controller in (1.9) is internally stable and guarantees an upper bound on the induced \mathcal{L}_2 norm given by definition 1.4. Two different methods exist for the synthesis of gain-scheduled output feedback controllers for LPV systems [13]. We present here the basic characterization method.

Theorem 1.2 Consider the LPV plant governed by (1.1), with parameter trajectories constrained by $\rho \in \mathcal{F}_P^\nu$. There exists a gain-scheduled output feedback controller (1.9) enforcing internal stability and a bound on the gain of the closed-loop system, whenever there exist parameter-dependent symmetric matrices X and Y , a parameter-dependent quadruple of state-space data $(\hat{A}_K, \hat{B}_K, \hat{C}_K, \hat{D}_K)$ such that the infinite dimensional LMI problem of (1.10) and (1.11) holds true.

$$\begin{bmatrix} XA + \hat{B}_K C_2 + (*) + \sum_{i=1}^s \pm \left(\nu_i \frac{\partial X}{\partial \rho_i} \right) & * \\ \hat{A}_K^T + A + B_2 \hat{D}_K C_2 & AY + B_2 \hat{C}_K + (*) - \sum_{i=1}^s \pm \left(\nu_i \frac{\partial Y}{\partial \rho_i} \right) \\ (XB_1 + \hat{B}_K D_{21})^T & (B_1 + B_2 \hat{D}_K D_{21})^T \\ C_1 + D_{12} \hat{D}_K C_2 & C_1 Y + D_{12} \hat{C}_K \\ * & * \\ * & * \\ -\gamma I & * \\ D_{11} + D_{12} \hat{D}_K D_{21} & -\gamma I \end{bmatrix} < 0 \quad (1.10)$$

$$\begin{bmatrix} X & I \\ * & Y \end{bmatrix} > 0 \quad (1.11)$$

In such a case, a gain scheduled controller of the form (1.9) is readily obtained using the following two step scheme.

- Solve for N and M , the factorization problem

$$I - XY = NM^T. \quad (1.12)$$

- Compute A_k, B_k, C_k and D_k as

$$A_k = N^{-1}(X\dot{Y} + N\dot{M}^T + \hat{A}_K - X(A - B_2\hat{D}_K C_2)Y) - \hat{B}_K C_2 Y - X B_2 \hat{C}_K) M^{-T}, \quad (1.13)$$

$$B_k = N^{-1}(\hat{B}_K - X B_2 \hat{D}_K), \quad (1.14)$$

$$C_k = (\hat{C}_K - \hat{D}_K C_2 Y) M^{-T}, \quad (1.15)$$

$$D_k = \hat{D}_K. \quad (1.16)$$

Proof. See [13].

Remark 1.3 *The LMI condition given by Theorem 1.2 corresponds to an infinite-dimensional convex optimization problem due to the parametric dependence. To obtain a finite-dimensional optimization problem, the parameter-dependent matrix functions X and Y can be approximated using a finite set of basis functions and a finite gridding of the parameter space can be used. As the LMIs are to be solved only at each of the grid points, this results in a set of finite-dimensional LMIs that can be solved numerically using commercial solvers.*

1.2.3 LPV Control in Automotive Systems

In this section we provide a motivation to the use of LPV gain-scheduling as it applies to automotive engine control. Gain scheduling of automobile engine controllers began in the early 1970s in conjunction with the use of microprocessor-based air-fuel mixture control and in response to the dual imperatives of improved fuel economy and reduction of exhaust emissions. Use of a catalytic converter requires precise control of the air-fuel ratio and necessitates feedback. This was traditionally accomplished using a signal from an exhaust gas oxygen (EGO) sensor located in the exhaust pipe. The EGO provides a two-state signal indicating that the air-fuel ratio is either lean or rich. Conventional (usually proportional plus integral) control results in a limit cycle about

the desired value. By using asymmetric gains with respect to the sign of the error, the limit cycle and thus the nominal air-fuel ratio can be shifted. Note that there is a substantial transport delay (load and engine-speed dependent) from the time the fuel-air mixture is inducted until the signal appears at the EGO sensor [14]. There are additional aspects of air-fuel regulation where LPV gain-scheduling techniques may be employed. These include closed-loop control of exhaust gas recirculation (EGR) which has gained importance beginning in the early 1980s, and variable camshaft timing where gain scheduling efforts are reported beginning in the mid 1980s. This motivates the research in application of LPV and/or LPV time-delay systems theory to engine control, and is the focus of the last part of this dissertation.

1.3 Outline of the Thesis

The results presented in this dissertation have either been already published or submitted for publication [15–22]. Each subsequent chapter consists of an adapted version of one or more of these articles. In this setup, every chapter is written as stand-alone, and there might be some overlap between the contents of the chapters. An attempt has been made to keep the notation consistent throughout the dissertation to prevent any confusion. An outline of the thesis is provided below.

In Chapter 2, we address the problem of estimating ethanol content in an ethanol-gasoline blend of an FFV. We investigate the use of a model-based approach relying only on the sensor set existing on a production vehicle. A parametric adaptive model is proposed based on first-principles modeling. The proposed model structure has three-terms and is based on steady-state operating conditions of the engine. The model structure is tested for fidelity using experimental data obtained at the University of Houston’s Engine Control Research Laboratory (UH-ECRL). Once the model structure is finalized we propose to use the changes in the model adapted coefficients

and link them to the percentage of ethanol content present in the blend. More specifically, we show that the three model coefficients form a vector whose length, or the 2-norm of the vector relates to ethanol content percentage. This hypothesis is further validated based on physics and the combustion chemistry. The methodology of ethanol estimation presented in this dissertation is a zero cost solution in the sense that we do not add any redundant sensor cost.

Chapter 1 has already given a brief overview of LPV systems with its importance and applications. In chapter 3, we examine the problem of identifying parameters of an LPV system. We start with a discrete time input-output representation of an LPV system. For such a system the model coefficients depend on the LPV scheduling parameter and their dependence is given by the basis functions. We simplify the LPV system identification problem to a problem of linear regression. The proposed method is used to identify the intake manifold dynamics of a 5.4L V8 Ford engine. The LPV system identification methodology presented allows use of a single experiment to collect data and identify model parameters as opposed to an LTI approach where numerous experiments need to be performed corresponding to distinct operating speed-load conditions of the SI engine.

Controlling the ratio of the air-fuel mixture in SI engines is a widely discussed problem in the automotive literature and the contents of chapter 4 are motivated by the same. However, in the material presented, we first discuss the analysis and control synthesis for LPV time-delay systems and then conclude the discussion with the fueling control problem as an application. This is mainly done to emphasize the fact that the work presented is the first in literature to discuss output feedback control of LPV time-delay systems in the delay-dependent framework. We investigate the conditions to satisfy asymptotic stability and \mathcal{H}_∞ performance requirements for LPV time-delay systems. Our choice of the Lyapunov-Krasovskii functional to derive the stability and performance analysis conditions allows for fast-varying delays. The

analysis conditions derived are then relaxed using the so-called *slack* variables. The introduction of slack variables is shown to reduce the conservativeness and leads to an LMI condition for synthesis of a delayed feedback controller. Both state feedback and output feedback controller synthesis conditions are derived. We use two examples from literature to evaluate the performance of our method for the design of the state feedback controller. In the case of the output feedback controller design, these being the first results no comparison is proposed. However, the fueling control in SI engines is investigated to provide an application and validate the presented design methodology. We formulate the SI engine dynamics as an LPV system with a time-delay where the engine speed acts as a scheduling parameter. The time-delay appears as a parameter-varying delay with a known upper bound as well as a known bound on the rate of change of parameter variation. All this information is used in the controller design process. Simulations performed using a model in Matlab-Simulink validate the novel results presented.

Finally, chapter 5 gives the conclusions, summarizes the important contributions of this dissertation work and provides remarks about future research directions.

Chapter 2 Model-Based Ethanol Blend Estimation in Flexible-Fuel Vehicles

2.1 Introduction

Petroleum based fossil fuels are a dominant source of energy for transportation. The United States (US) transportation sector relies on petroleum for 95% of its energy, consuming approximately 140 billion gallons of gasoline each year [23]. Light duty vehicles account for 77% of the transportation energy used. These figures indicate our dependence on fossil fuels, mainly petroleum. Alternative fuels have been explored for several decades, but have attracted more attention recently due to rising petroleum costs and the pressing need to reducing vehicle emissions. In 2007, the federal government proposed a plan to reduce the US gasoline usage by 20% in the next ten years [24]. A key implication of this is the need for scientists and engineers to develop renewable and alternative fuels and such vehicles. Ethanol as an alternative fuel has attracted a lot of attention in recent years. Because of ethanol's excellent miscibility with common gasoline, it can be used as an additive to partially replace gasoline content of automotive fuel. Such mixtures are normally named after the amount or percentage of ethanol they contain. For example, a mixture containing 85% ethanol and 15% gasoline by volume is referred to as E85. In the United States, E85 is used as an alternative to gasoline. Ethanol is used in high concentrations in some regions like Brazil, Sweden and North America, but globally it is used in lower concentrations of 10% or less. Even in regions where ethanol is used in high concentrations, gasoline is still widely used. As discussed in chapter 1, FFVs can operate on gasoline or any ethanol blend concentration. However, they need an adaptive engine

Table 2.1: Properties of gasoline and ethanol

Property	Gasoline	Ethanol
Chemical formula	$C_4 - C_{12}$	C_2H_5OH
Composition (C,H,O)	86,14,0	52,13,35
Lower heating value (MJ/kg)	42.4	26.8
Self Ignition Temperature ($^{\circ}C$)	~ 300	420
Density (kg/m^3)	745	790
Research Octane Number (RON)	92	111
Stoichiometric Air-Fuel Ratio	14.6	9.0
Dielectric Constant	2	24.3
Latent heat of vaporization (kJ/kg)	390	840
Boiling Point Temperature ($^{\circ}C$)	20-300	78.5

management system to support and meet the emission requirements without sacrificing performance or drivability. Conventional gasoline is prepared through distillation of crude oil in refineries and is a mixture of many different hydrocarbon compounds. Ethanol is produced by fermentation and distillation of sugars, or by hydration of ethylene from petroleum. These differing production processes result in fuels with widely varying properties. The characteristics of ethanol differ from those of gasoline as shown in Table 2.1.

Nakata et al. (2006) and the numerous references therein describe in detail the effect of ethanol fuel on SI engines performance. As observed from Table 2.1 ethanol has high anti-knock quality due to its high octane number as compared to gasoline. This allows the ignition timing to be advanced resulting in higher torque production. With E100 the engine torque increases by 20% as compared to 92 Research Octane Number (RON) gasoline fuel [25]. The high octane number of ethanol also allows engines to operate at higher compression ratios than that possible with gasoline. Experimental studies [26] have shown a 29% increase in engine power with E50 fuel, when the compression ratio is increased from 6:1 to 10:1. The use of ethanol as an alternative to gasoline results in reduction of harmful exhaust gas emissions. Reduction in NOx emissions is observed owing to the charge cooling effect which can be

attributed to the higher latent heat of vaporization of ethanol [25,27]. Koc et al. in 2009 conducted experiments with three different fuels (E0, E50 and E85) by running the engine at eight different engine speeds ranging from 1500 rpm to 5000 rpm in increments of 500 rpm. Stoichiometric air-fuel ratio was maintained during all the experiments and the engine was allowed to reach stable condition before any measurements were recorded. Engine torque, fuel consumption and pollutant emissions (CO, HC and NO_x) were measured during the experiments. The engine was normally run at the maximum brake torque (MBT) spark timings and no special optimization/tuning was done for ethanol fuel. A significant reduction in HC emissions is observed with increasing ethanol content in the fuel and has been attributed to the oxygen enrichment caused by ethanol addition.

The operation with ethanol provides improved torque and horsepower over gasoline. Feedgas emission levels are also lower than those with gasoline. However, this advantage is diminished at the tailpipe due to the long catalytic converter light-off times that result from the lower combustion temperatures which characterize alcohol fuels. The lower heating value of ethanol results in an increase in the brake specific fuel consumption (BSFC). However, increasing BSFC due to lower energy content of ethanol-gasoline blends may be improved by increasing compression ratio [28]. Considerable hardware modifications are necessary to a dedicated gasoline engine to avoid the problems arising due to the corrosive nature of alcohol fuels [29]. Stodart et al. (1998) investigated the problem of improving cold start performance in FFVs and proposed the installation of a separate tank and injector to deliver gasoline to the combustion chamber during the cold start phase.

To exploit the favorable properties of ethanol fuel and thus improve fuel economy and engine performance, it is necessary to accurately know the ethanol content in any fuel blend. One of the most important advantages of knowing the correct ethanol

content in a fuel blend is for the engine management system to supply appropriate quantity of fuel during cold start and hence overcome any cold starting issues. Capacitance based sensors [30] could be used to differentiate the fuel blends based on the differing dielectric constant of ethanol and gasoline. However, such sensors have associated accuracy and reliability issues and with an after-market price tag of approximately \$500 the sensors are cost prohibitive. Alternatively, ethanol content estimation can be realized by attributing the feedback based fuel correction after a refill event to the change in concentration of ethanol in the fuel blend. This exhaust gas oxygen (EGO) sensor based ethanol estimation is cost effective, as it involves no additional sensors but becomes unreliable in the case of mass air flow sensor errors. Typically, the MAF sensor has associated with it an error of $\pm 7\%$. It has been shown in [31] that a 5% error in the MAF sensor reading results in a 30% error in percent ethanol estimation. This emphasizes the need of a robust approach to ethanol content estimation.

Presented in [32] are the engineering challenges of estimating ethanol content on a sensorless system subject to real world issues. It is shown that the accuracy of estimating ethanol content is severely compromised due to the stacked-up production tolerances of the components involved. Ahn et al. (2008) presented a model-oriented approach investigating the sensitivity of ethanol content estimation to modeling and sensor errors. Specifically, errors in air charge estimate, mass air flow (MAF) sensor, and manifold temperature sensor are considered. The conclusion points out the high sensitivity of ethanol estimation and motivates the need of redundant algorithms with fusion of other sensors. Ahn et al. (2009) propose the use of a manifold absolute pressure (MAP) sensor along with the MAF sensor to estimate cylinder air flow under MAF sensor drifts and hence prevent severe mis-estimation of ethanol content in FFVs. Huff and Prevost (2001) have described a different way of looking at this problem, using engine roughness to determine the percent alcohol in fuel and compensate for any changes so that drivability is not affected. Under cold starting

conditions, the oxygen sensor takes a predetermined amount of time to warm up and provide reliable air-fuel ratio information. During this time the engine runs in open loop control and can run rough. Engine roughness which is the second derivative of engine speed can be used to determine if the engine is running lean and hence determine the extent by which the air-fuel ratio needs to be enriched. The variations in engine roughness are also caused by changes in the manifold air pressure and engine speed and hence, entry conditions have been defined to use the criteria of engine roughness for estimating ethanol content. The effect of ethanol concentration on cylinder pressure evolution in direct-injection flex-fuel engines has been studied in [33]. A physics-based lumped parameter model for cylinder pressure evolution during the compression stroke in direct-injection (DI) engines is presented. Oliverio et al. (2009) and Ahn et al. (2010) proposed the use of an in-cylinder pressure sensor and presented experimental results. However, the proposed method requires the engine to operate in single injection as well as split injection modes to generate a residue that captures the charge cooling effect and hence requires modifications to the engine. A detailed investigation of analyzing various uncertainties involved in fuel blend estimation for bio-diesel as well as ethanol-gasoline blends has recently appeared in the literature [34].

All the approaches reviewed involve the addition of an otherwise redundant sensor hence increasing production costs. In this chapter, a parametric adaptive model-based approach to ethanol estimation is proposed. Using information from production sensors a model relating the fueling command to the engine speed, throttle angle and air-fuel ratio (AFR) is developed. Adaptation in the model parameter coefficients is used to estimate the fuel composition of the fuel blend. Experimental results are presented to validate the proposed approach.

2.2 Motivation

Detailed in this section is the motivation for the fuel blend estimation approach presented in this work. A steady-state fuel path model structure is identified and used in the ethanol estimation process. Identifying a low order yet high-fidelity model structure is very important, as the accurate estimation of ethanol content is based on the identified fuel path model. The ethanol estimation strategy utilizes the observed change in model parameter coefficients to predict the ethanol content in an ethanol-gasoline fuel blend.

2.2.1 Model Structure Identification

A comparison of the fuel properties for ethanol and gasoline shows a significant change in the stoichiometric ratio of combustion. For the same amount of air mass flow, 48.97% more by mass of E85 fuel, is required as compared to gasoline to achieve stoichiometry. As the modern day automobiles use a linear exhaust gas oxygen sensor in the fueling control loop, $\lambda \triangleq \frac{A/F}{\text{Stoichiometric } A/F}$ is maintained close to unity with excursions happening only during short transients or as a result of catalyst modulation. In an SI engine running in closed-loop air-fuel ratio control, the fuel mass flow relates linearly to the air mass flow and inversely to the stoichiometric AFR (AFR_s) of the fuel. Engines are often equipped with a MAF sensor that estimates the air flow past the throttle plate. However, MAF sensors are prone to aging and drift errors [35]. To overcome this problem, the MAF sensor is eliminated in our work and the air-flow is characterized using only throttle angle and engine speed information. The fuel injector pulse-width is chosen as an output.

To motivate our model formulation we present some typical experimental results obtained of our engine facility at the UH-ECRL. Shown in Fig. 2.1 is the fuel injector pulse-width (PW) plotted as a function of throttle position and engine speed, for three

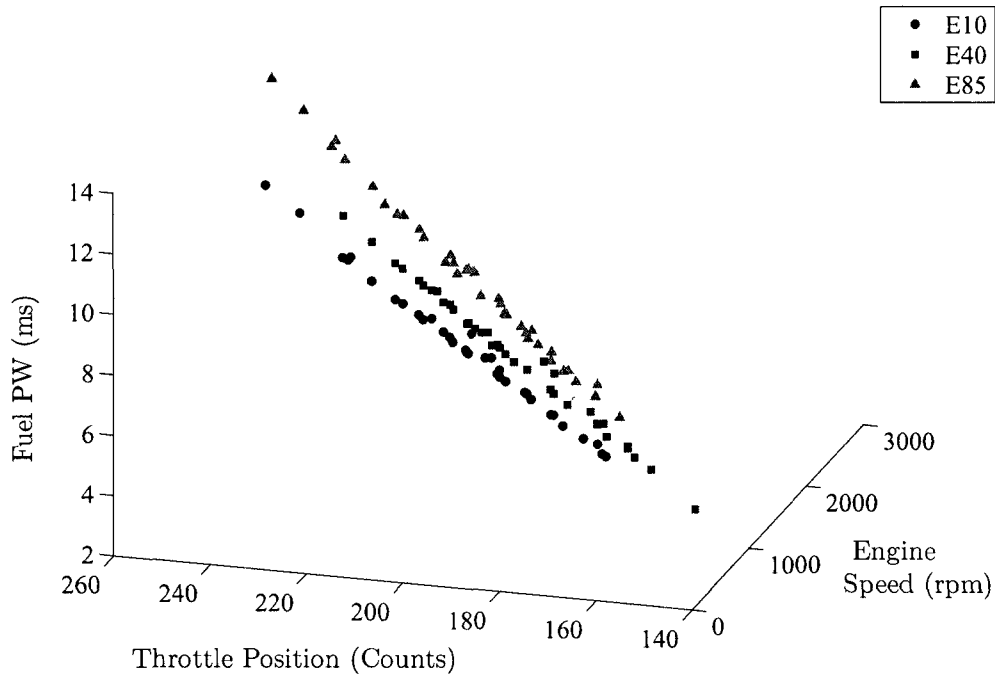


Figure 2.1: 3-dimensional plot showing the variation in fuel pulse-width as a function of throttle position and engine speed, for three fuel types tested on a 2005 Ford 5.4L PFI engine

different fuel blends with the engine running in closed-loop fueling control. Throttle position is measured using an existing sensor, which feeds a voltage signal to an analog to digital converter (ADC). The output of ADC is in counts and relates directly to the throttle angle opening. Shown in the 3-dimensional (3-d) plot of Fig. 2.1 is a comparison of the fuel injector's pulse-width for different fuels under specific steady state conditions of throttle position and engine speed. Each point on the 3-d plot corresponds to one steady state operating point of the engine, where the throttle was held fixed and the speed was controlled using a dynamometer load. With E10 fuel, the pulse-width was recorded at approximately 35 such steady state points. Similar tests were repeated with E40 and E85 fuel. It is to be noted that the pulse-widths corresponding to a particular fuel-blend cloud together. Thus, it can be observed from Fig. 2.1 that fuel PW is a good indicator of the fuel blend for similar operating conditions of the engine. This sets the foundation of this work. To summarize the

objective, we seek a steady state model of the form

$$PW = f(\psi^i, N^j, \lambda^k), \quad (2.1)$$

where PW is the fuel pulse-width command, ψ is the throttle angle, N the engine speed and λ is the universal exhaust gas oxygen (UEGO) sensor measured normalized air-fuel ratio. In (2.1), f is a polynomial function in the variables ψ , N and λ . The powers $i, j, k \in \mathbb{Z}$ where \mathbb{Z} denotes the set of integers. The variable λ is included in the required model structure to account for any non-stoichiometric operation of the engine, as dictated by the catalyst modulation controller.

2.3 First Principles Based Model

A physics-based approach is used to motivate the model structure relating engine speed, throttle position and air-fuel ratio to fuel pulse-width command in an SI engine under steady-state conditions. A mean value model of an SI engine is derived and simplified to a low order polynomial-type model to be used in determining appropriate regressor-type models.

2.3.1 Air Path Dynamics

The air induction system on an SI engine consists of a throttle body, intake manifold and intake valves. Mathematical model for the air path of an internal combustion engine is well established and can be explained by the intake manifold filling and emptying dynamics [1]. The dynamics governing the intake manifold pressure is obtained by differentiating the ideal gas law,

$$P_m V_m = m R T_m, \quad (2.2)$$

where P_m , V_m , T_m and m denote pressure in the intake manifold, volume of the intake manifold, temperature and mass of the air in the intake manifold, respectively. R is

the ideal gas constant. Differentiating (2.2) gives

$$\dot{P}_m = \frac{RT_m}{V_m} \dot{m} + \frac{mR}{V_m} \dot{T}_m. \quad (2.3)$$

Due to slow temperature variation the \dot{T}_m term has been shown to not contribute significantly to the manifold dynamics and can be neglected [36]. The net mass flow rate of air into the intake manifold is the difference of the mass air flow past the throttle, $\dot{m}_{a,th}$ and the air flow into the cylinders, $\dot{m}_{a,cyl}$. The throttle mass air flow rate, $\dot{m}_{a,th}$ can be modeled using standard orifice equations for one-dimensional steady compressible flow [1] as

$$\dot{m}_{a,th} = C_d A_{th}(\psi) \frac{P_a}{\sqrt{RT_a}} \Upsilon \left(\frac{P_m}{P_a} \right), \quad (2.4)$$

where ψ is the throttle angle, $A_{th}(\psi)$ is the throttle plate open flow area, C_d is the flow discharge coefficient and P_a , T_a denote the ambient pressure and temperature, respectively. The functions $A_{th}(\psi)$ and $\Upsilon \left(\frac{P_m}{P_a} \right)$ are given by

$$A_{th}(\psi) = \frac{\pi d_{th}^2}{4} (1 - \cos \psi), \quad (2.5)$$

where d_{th} represents the throttle plate diameter, and

$$\Upsilon \left(\frac{P_m}{P_a} \right) = \begin{cases} \sqrt{\frac{2\gamma}{\gamma-1} \left(r_p^{\frac{2}{\gamma}} - r_p^{\frac{\gamma+1}{\gamma}} \right)}, & \text{if } r_p > \left(\frac{2}{\gamma+1} \right)^{\frac{\gamma}{\gamma-1}} \\ \gamma^{\frac{1}{2}} \left(\frac{2}{\gamma+1} \right)^{\frac{\gamma+1}{2(\gamma-1)}}, & \text{if } r_p \leq \left(\frac{2}{\gamma+1} \right)^{\frac{\gamma}{\gamma-1}}. \end{cases} \quad (2.6)$$

The constant $\gamma = 1.4$ is the ratio of specific heats for air and $r_p = \frac{P_m}{P_a}$. For ethanol content estimation, a polynomial approximation to the nonlinear equation in (2.4) is sought. Equation (2.5) can be written as a Taylor series expansion leading to

$$A_{th}(\psi) = \frac{\pi d_{th}^2}{4} \left(1 - 1 + \frac{\psi^2}{2!} - \frac{\psi^4}{4!} + \dots \right) \quad (2.7)$$

$$\approx a_0 \psi^2 + a_1 \psi^4, \quad (2.8)$$

for some coefficients a_0 and a_1 . We consider engine operation at throttle angles resulting in un-choked air flow conditions. In a naturally aspirated engine $P_m < P_a$, except

at wide open throttle conditions, when $P_m \rightarrow P_a$. Under these assumptions, the expression for the function $\Upsilon \left(\frac{P_m}{P_a} \right)$ can be expanded using the generalized binomial theorem as

$$\begin{aligned} \Upsilon \left(\frac{P_m}{P_a} \right) &= \sqrt{\frac{2\gamma}{\gamma-1}} \left(\frac{P_m}{P_a} \right)^{\frac{1}{\gamma}} \left[1 - \left(\frac{P_m}{P_a} \right)^{\frac{\gamma-1}{\gamma}} \right]^{\frac{1}{2}} \\ &= \sqrt{\frac{2\gamma}{\gamma-1}} \left[\left(\frac{P_m}{P_a} \right)^{\frac{1}{\gamma}} - \frac{1}{2} \left(\frac{P_m}{P_a} \right) + \frac{1}{8} \left(\frac{P_m}{P_a} \right)^{\frac{2\gamma-1}{\gamma}} \dots \right] \\ &\approx b_0 P_m^{\frac{1}{\gamma}} + b_1 P_m + b_2 P_m^{\frac{2\gamma-1}{\gamma}}, \end{aligned} \quad (2.9)$$

for some coefficients b_0 , b_1 and b_2 . Substituting the value of γ in (2.9) results in

$$\Upsilon \left(\frac{P_m}{P_a} \right) \approx b_0 P_m^{\frac{5}{7}} + b_1 P_m + b_2 P_m^{\frac{9}{7}}. \quad (2.10)$$

Substituting the expressions (2.8) and (2.10) in (2.4) leads to a polynomial expression for mass air flow past the throttle plate as

$$\dot{m}_{a,th} \approx C_d \frac{P_a}{\sqrt{RT_a}} (a_0 \psi^2 + a_1 \psi^4) (b_0 P_m^{\frac{5}{7}} + b_1 P_m + b_2 P_m^{\frac{9}{7}}). \quad (2.11)$$

The coefficient of discharge C_d is a function of the throttle angle. However, this effect can be lumped in the a_i coefficients and hence no separate polynomial dependence is considered. This leads to the polynomial expression

$$\dot{m}_{a,th} \approx c_0 \psi^2 P_m^{\frac{5}{7}} + c_1 \psi^2 P_m + c_2 \psi^2 P_m^{\frac{9}{7}} + c_3 \psi^4 P_m^{\frac{5}{7}} + c_4 \psi^4 P_m + c_5 \psi^4 P_m^{\frac{9}{7}}, \quad (2.12)$$

for some coefficients c_i . This completes the approximation for mass air flow past the throttle plate in a polynomial form.

The dynamics governing intake of air charge into the cylinders, can be modeled by comparing engine behavior to a volumetric pump [1,37]. The cylinder air flow for a 4-stroke engine is given by

$$\dot{m}_{a,cyl} = \frac{\eta_{vol} \rho_{a,m} V_d N}{2}, \quad (2.13)$$

where η_{vol} is the volumetric efficiency, $\rho_{a,m}$ is the density of air in the intake manifold and V_d is the total displaced volume of all cylinders. Using the ideal gas law in (2.2), (2.13) can be written as

$$\dot{m}_{a,cyl} = \frac{\eta_{vol} V_d N}{2RT_m} P_m. \quad (2.14)$$

As is a common practice [38, 39], the volumetric efficiency can be expressed as a polynomial function of manifold pressure P_m and engine speed N as

$$\eta_{vol} = d_0 + d_1 N + d_2 N^2 + d_3 N^3 + d_4 P_m. \quad (2.15)$$

Substituting (2.15) in (2.14) gives

$$\begin{aligned} \dot{m}_{a,cyl} &= e_0 N P_m + e_1 N^2 P_m + e_2 N^3 P_m + e_3 N^4 P_m + e_4 N P_m^2 \\ &\approx e_0 N P_m + e_1 N^2 P_m + e_2 N^3 P_m + e_4 N P_m^2, \end{aligned} \quad (2.16)$$

where the coefficients e_i are given by, $e_i = d_i \frac{V_d}{2RT_m}$. Under steady state operation, (2.3) gives $\dot{m}_{a,th} = \dot{m}_{a,cyl}$. Equating (2.12) and (2.16) permits a solution to mass air flow into the cylinders, using only engine speed N and throttle angle ψ . The variable P_m is thus eliminated. This leads to an expression involving non-integer powers of P_m . A simplified model can be obtained by considering only integer powers of P_m in (2.12) as

$$\dot{m}_{a,th} \approx c_1 \psi^2 P_m + c_5 \psi^4 P_m. \quad (2.17)$$

Solving for P_m from (2.17) and (2.16) and substituting back in (2.17) gives an expression for mass air flow into the cylinders, MAF_{cyl} as

$$\begin{aligned} MAF_{cyl} &= \frac{c_1 \psi^2}{e_4} \left(-e_0 - e_1 N - e_2 N^2 - e_3 N^3 + c_1 \frac{\psi^2}{N} + c_5 \frac{\psi^4}{N} \right) \\ &\quad + \frac{c_5 \psi^4}{e_3} \left(-e_0 - e_1 N - e_2 N^2 - e_3 N^3 + c_1 \frac{\psi^2}{N} + c_5 \frac{\psi^4}{N} \right) \\ &\approx f_0 \psi^2 + f_1 \psi^2 N, \end{aligned} \quad (2.18)$$

where in the approximation only the first few significant terms are considered and f_0 , f_1 are model coefficients. Equation (2.18) needs to be divided by the engine

speed to convert the mass air flow rate from g/sec to g/cycle or g/intake-event. This is necessary as the steady state model relates the fuel PW commanded by the Powertrain Control Module (PCM), a per intake event quantity, to the air flow per cycle. Hence, the mass air flow rate into the cylinders per intake event is given as a function of throttle angle and engine speed as

$$MAF_{cyl/intake} = f_0 \frac{\psi^2}{N} + f_1 \psi^2. \quad (2.19)$$

2.3.2 Fuel Path Dynamics

Fuel path dynamics have been studied extensively in the past [39,40]. For a port fuel-injected system, the fuel puddling phenomenon is used to explain the dynamics relating the injected fuel mass to the fuel mass actually entering the cylinders. Under steady-state operation of the engine, the fuel mass in the cylinder would equal the injector command. The fuel system is designed such that the volumetric fuel flow rate is proportional to the injection pulse-width command as given by

$$PW = K_{f_{pw}} \dot{m}_{f,c}, \quad (2.20)$$

where $K_{f_{pw}}$ is a constant characterizing the fuel injector's slope and $\dot{m}_{f,c}$ is the fueling command, in mass from the PCM. Fuel injectors' are usually specified by the rate at which they can inject fuel, for example cc/min or lb/hr. Fuel injectors' slope is the inverse of this quantity. Under steady state operation, the actual fuel mass flow in the cylinders is equal to the fueling command, giving the equation

$$\dot{m}_{f,cyl} = \dot{m}_{f,c}, \quad (2.21)$$

where $\dot{m}_{f,cyl}$ is the actual fuel mass in the cylinders.

2.3.3 UEGO Sensor Dynamics

The UEGO sensor is used to measure the air-fuel ratio in the exhaust gas of an SI engine. The UEGO sensor located in the exhaust manifold reads the normalized air-fuel ratio λ which is defined as

$$\lambda = \frac{\dot{m}_a/\dot{m}_f}{AFR_s}, \quad (2.22)$$

where AFR_s is the mass ratio of air-fuel for stoichiometric combustion. Associated with the UEGO sensor dynamics is a time delay and a first order lag [38]. The delay is a result of the transport of exhaust gas species from the cylinder exhaust port downstream to the location of the UEGO sensor. The first order lag captures the dynamics associated with the gas mixing as well as the sensor response. In frequency domain, this results in the following expression for the sensed value of the normalized air-fuel ratio λ

$$\lambda(s) = e^{-Ts} \frac{1}{\tau s + 1} \lambda_{cyl}(s), \quad (2.23)$$

where T , τ denote the time delay and the time constant respectively. The in-cylinder AFR denoted as λ_{cyl} is given as

$$\lambda_{cyl} = \frac{MAF_{cyl/intake}/\dot{m}_{f,cyl}}{AFR_s}. \quad (2.24)$$

Under steady-state operation λ_s equals λ_{cyl} . Substituting (2.19), (2.20) and (2.21) in (2.24) results in a steady state model for the fuel injection PW command

$$PW = \frac{K_{fpw}}{\lambda AFR_s} \left(f_0 \frac{\psi^2}{N} + f_1 \psi^2 \right). \quad (2.25)$$

A Taylor series expansion of the function $\frac{1}{\lambda}$ in the vicinity of stoichiometry gives

$$\begin{aligned} \frac{1}{\lambda} &= 1 - 1(\lambda - 1) + \dots \\ &\approx 2 - \lambda. \end{aligned} \quad (2.26)$$

Use of the above Taylor series approximation for $\frac{1}{\lambda}$ is justified as $0.98 < \lambda < 1.02$ near stoichiometry which is the typical excursion for catalyst modulation. Substituting

(2.26) in (2.25) gives

$$\begin{aligned}
 PW &= \frac{K_{f_{pw}}}{AFR_s} \left(f_0 \frac{\psi^2}{N} + f_1 \psi^2 \right) (2 - \lambda) \\
 &= \frac{2K_{f_{pw}}}{AFR_s} \left(f_0 \frac{\psi^2}{N} + f_1 \psi^2 \right) - \lambda \frac{K_{f_{pw}}}{AFR_s} \left(f_0 \frac{\psi^2}{N} + f_1 \psi^2 \right). \quad (2.27)
 \end{aligned}$$

As a final outcome the following modification of (2.27) is proposed

$$PW = \theta_1 \psi^2 + \theta_2 \left(\frac{\psi^2}{N} \right) + \theta_3 \lambda, \quad (2.28)$$

where θ_i form the model coefficients (parameters). The advantage of (2.28) over (2.27) is that the number of regressor multiplications are reduced. This form relates sensor faults to specific coefficient(s) within the model and from this isolation, sensor diagnostics can be performed. Combining the sensor diagnostics component of (2.28) along with its ethanol estimation capability enables the estimation robustness.

2.4 Description of the Experimental Facility

This study was undertaken at the University of Houston Engine Control Research Laboratory. The engine and dynamometer setup is as shown in Fig. 2.2. The engine used is a 2005 Ford 5.4-L V8 sequential multi-port fuel injected, spark ignition engine, controlled by a Ford production PCM. The interface to this PCM is provided by a memory emulator. The engine is equipped with the production sensors. The sensors of interest are the throttle position sensor, crankshaft position sensor and the UEGO sensor. The software used for data acquisition and throttle reference commands is by Accurate Technologies. The software runs on a Dell computer which communicates with the memory emulator via the USB port. The software has two components called the ‘‘ATI VISION’’ and the ‘‘ATI No-Hooks’’. The ATI VISION allows for the monitoring and measurement of signals that the PCM broadcasts, whereas the ATI No-Hooks allows access to RAM variables internal to the PCM, which are

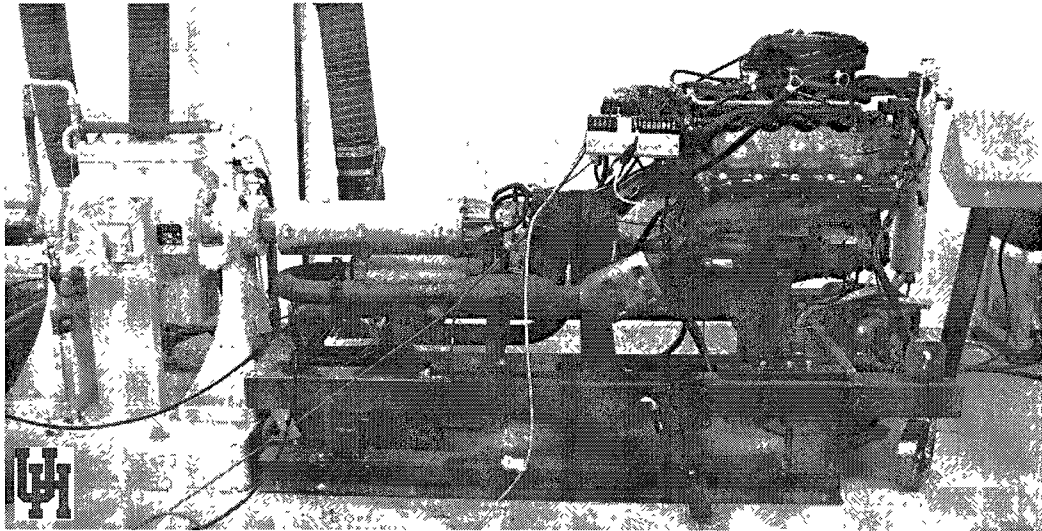


Figure 2.2: Engine and dynamometer at the Engine Control Research Laboratory, University of Houston

otherwise only viewable or measurable. The engine is coupled to a 175-hp eddy current dynamometer controlled by a DyneSystems InterLoc-V controller. To achieve steady-state at different operating conditions, the throttle plate was controlled using the No-Hooks software, whereas the torque load on the engine was controlled using the dynamometer controller. Fuel injectors were left in control of the Ford PCM.

2.5 Main Results

The steady-state fuel pulse-width model (2.28) forms the basis for the ethanol estimation methodology proposed in our work. The model coefficients (parameters) are related to the percent ethanol content in the fuel blend. A recursive least squares (RLS) identification approach is used to identify on-line the model parameters during steady state engine operation. A metric based on the identified parameter coefficients is proposed that can be linked directly to the ethanol content present in the ethanol-gasoline fuel blend. Specifically, we propose to use changes in the length of the coefficient vector to identify a change in the fuel ethanol content. The presented

ethanol content estimation methodology is further correlated to combustion chemistry. In the next sub-section we present the experimental validation of the proposed model structure followed by validation of the proposed ethanol content estimation method.

2.5.1 Experimental Validation of the Proposed Model Structure

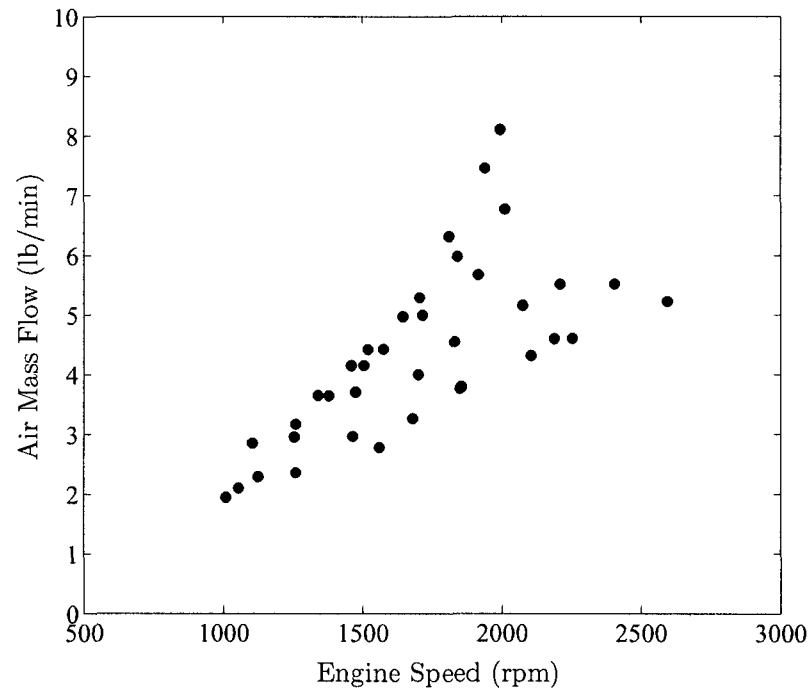


Figure 2.3: Steady state operating points in terms of mass air flow and engine speed

Seven different fuel blends obtained by volumetric mixing of gasoline or E0 and E85 are used in this study. For validation purposes, a Siemens fuel composition sensor is used to measure the actual ethanol content in the fuel-blend. With a known fuel composition in the tank, the engine is operated at steady-state covering the speed - air mass points as shown in Fig. 2.3. At each steady-state, the engine speed is controlled using the throttle, load is controlled using the dynamometer and all the relevant

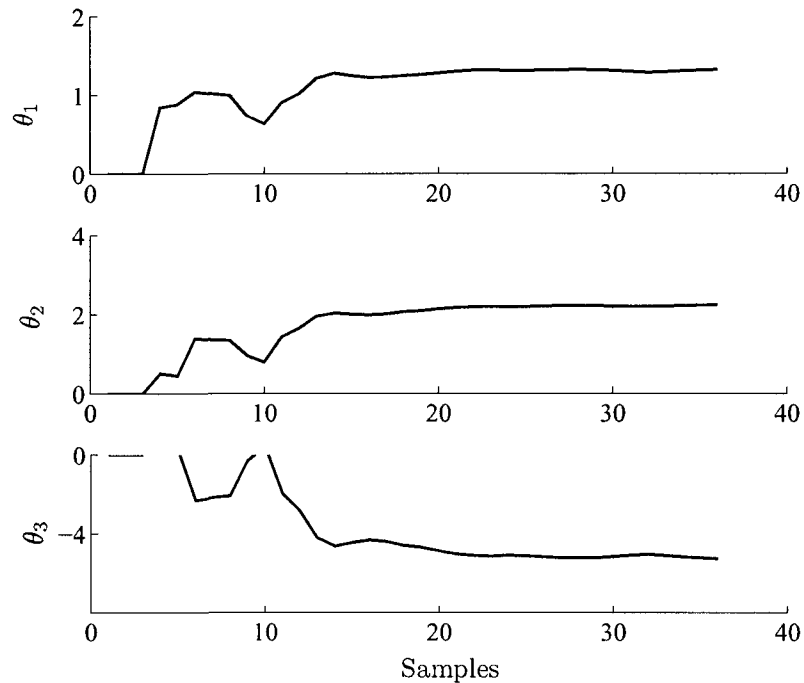


Figure 2.4: Evolution of the parameter trajectory for E10 fuel blend

data recorded using the ATI-VISION recorder software. RLS parameter estimation is used to identify the model parameters. Prior to parameter estimation, the recorded variables are scaled to provide magnitude normalization. The engine speed in rpm is divided by 1000 whereas the throttle position measured in counts is divided by 100. A detailed analysis of parameter estimation using RLS can be found in [41] and [42]. Shown in Fig. 2.4 is the parameter convergence, as the RLS algorithm proceeds with the experimental data obtained using E10 fuel. Each sample represents one steady state operating point of the engine, where the engine speed and throttle position are held constant. As is evident from Fig. 2.4, the theta coefficients converge to their steady-state values after approximately 25 samples of data, which is approximately < 10 seconds on a Dell machine with Intel core 2 Duo, 1.8 GHz processor and 2 GB RAM. Shown in Fig. 2.5 is a comparison of model estimated fuel PW command with the actual fuel PW command from the PCM for E10 fuel. The values of the estimated unknown model parameters θ_i for all fuel blends, as identified by the RLS

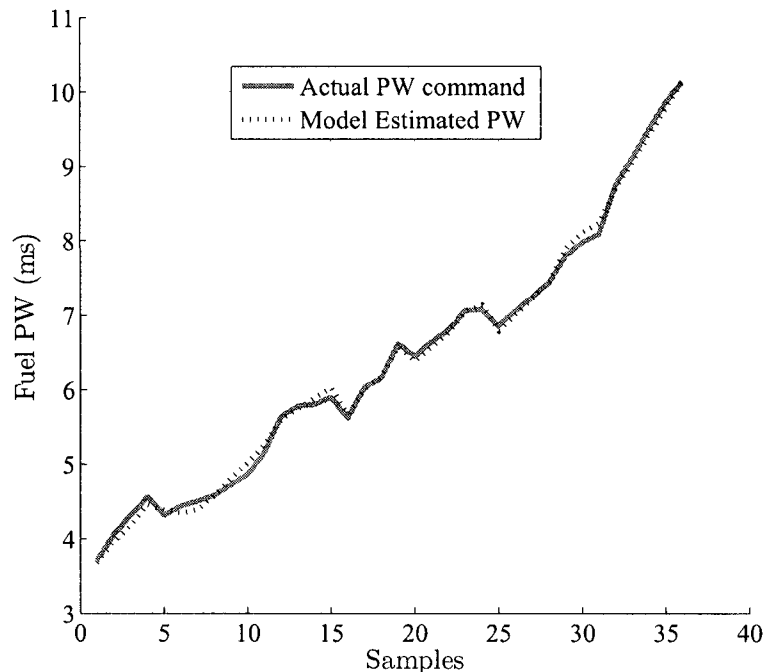


Figure 2.5: Comparison of actual V/s model estimated fuel pulse-width for E10 fuel estimation algorithm are shown in Table 2.2. Also, presented is the parameter vector length L_{EXX} which is the 2-norm of the estimated parameter vector θ . The accuracy of each model is measured by a model fit calculation defined as

$$Model\ Fit\ (\%) = \left(1 - \frac{\|y - \hat{y}\|}{\|y - mean(y)\|} \right) \times 100, \quad (2.29)$$

where y is the actual fuel PW and \hat{y} denotes the model estimated fuel PW. The model fit used here is the R^2 coefficient of determination, a statistical measure of how well the regression line approximates the real data points [43]. In Table 2.2 it is worth noting that as expected the coefficient vector length increases with increasing percentage of ethanol content in the fuel blend.

2.5.2 Ethanol Content Estimation Methodology

Presented in this section is a methodology for estimating the ethanol content in a given fuel blend. The fidelity of the proposed model structure has been validated

Table 2.2: Model parameters, model fit, vector length and angles for the seven fuel blends tested

	E0	E10	E30	E40	E60	E70	E85
θ_1	1.258	1.32	1.429	1.473	1.591	1.662	1.799
θ_2	2.145	2.234	2.337	2.461	2.692	2.802	3.012
θ_3	-4.95	-5.26	-5.585	-5.778	-6.198	-6.527	-7.084
Model Fit (%)	94.28	95.22	92.41	94.5	92.36	93.6	93.42
Vector Length L_{EXX}	5.539	5.865	6.221	6.451	6.942	7.295	7.91
Vector Angle (in $^\circ$)	0	0.457	0.719	0.356	0.131	0.194	0.385

using experimental data. As has been observed the model parameters change with varying ethanol content. The three model parameters $[\theta_1 \ \theta_2 \ \theta_3]^T$ form a vector in the 3-dimensional space spanned by the three input regressors. The parameter vector corresponding to E0 fuel is considered as a reference (nominal) vector denoted as $\theta^{E0} = [\theta_1^{E0} \ \theta_2^{E0} \ \theta_3^{E0}]^T$. The length of this vector L_{E0} acts as a reference length for comparison. Let the normalized vector length be defined as

$$\tilde{L}_{EXX} = \frac{L_{EXX} - L_{E0}}{L_{E0}}. \quad (2.30)$$

The normalized vector length denotes a percentage change with respect to the reference vector length L_{E0} . The vector length L_{EXX} and the normalized vector length \tilde{L}_{EXX} as a function of percent ethanol content is shown in Fig. 2.6. The ethanol content estimation methodology is based of predicting the percent ethanol in a fuel blend knowing the normalized coefficient vector length associated with it. Shown in Fig. 2.7 is a least squares curve fit through the \tilde{L}_{EXX} data points used to design the fuel blend estimator. The fuel-blend estimator equation is given by

$$\% \text{ Ethanol} = -156.76 \tilde{L}_{EXX}^2 + 267.476 \tilde{L}_{EXX}. \quad (2.31)$$

It is noted that a variation in the ethanol content will change the length of the parameter vector θ but will not affect the directionality. Potential changes in the directionality of the vector would imply a faulty situation, e.g., a sensor fault and

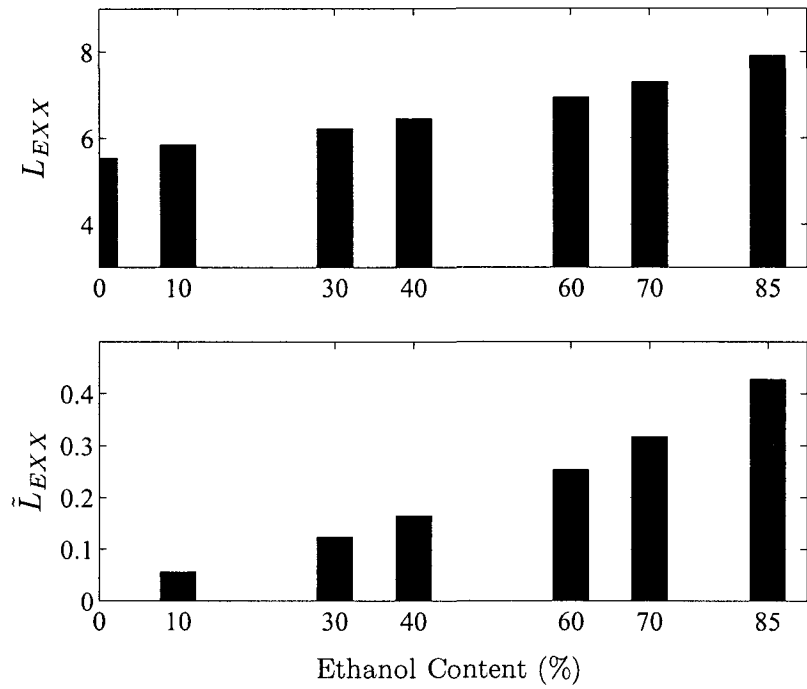


Figure 2.6: Vector lengths as a function of percentage ethanol content in the fuel blend

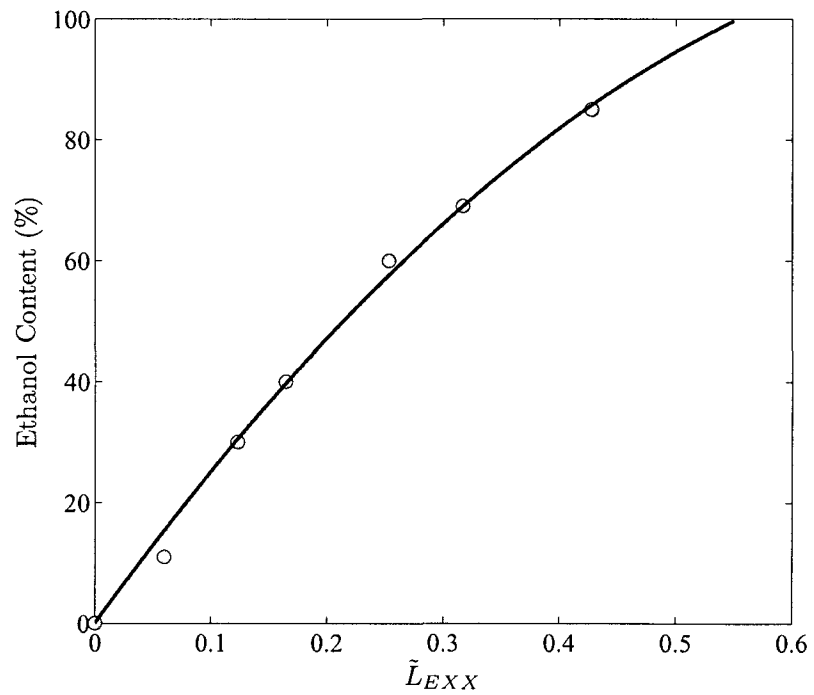
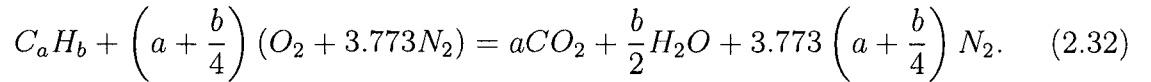


Figure 2.7: Ethanol blend estimator curve

can be used to provide diagnostics information. Considering the parameter vector corresponding to E0 fuel as the nominal vector, the angle made by each of the other vectors corresponding to different fuel blends can be calculated using the dot product and is presented as the last entry in Table 2.2. It is evident that the angular variation is within 1° implying that all the parameter vectors point in the same direction.

2.5.3 Correlation with Combustion Chemistry

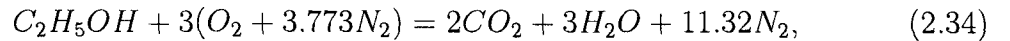
Presented in this section is a relation between the coefficient vector length and the stoichiometric fuel-air ratio (FAR_s). The complete combustion of a general hydrocarbon fuel with average molecular composition C_aH_b with air is [1]



Let $y = b/a$ be the ratio of hydrogen to carbon atoms in the hydrocarbon fuel. The molecular weights of oxygen, atmospheric nitrogen, atomic carbon and atomic hydrogen are respectively, 32, 28.16, 12.011 and 1.008. The stoichiometric air-fuel ratio is given by

$$\left(\frac{A}{F}\right)_s = \left(\frac{F}{A}\right)_s^{-1} = \frac{(1 + y/4)(32 + 3.773 \times 28.16)}{12.011 + 1.008y}. \quad (2.33)$$

For gasoline $y = 1.87$ [1] and (2.33) gives the stoichiometric air-fuel ratio for gasoline as 14.6. The stoichiometric combustion equation for ethanol E100 is



and $(A/F)_s = 9.00$. Ethanol-gasoline blend is denoted by EXX, where XX denotes the percentage of ethanol by volume in the mixture. The AFR_s and also the FAR_s variation as a function of ethanol content can be determined using (2.32) and (2.34) where (2.32) and (2.34) are multiplied by the number of moles of gasoline and ethanol present in the mixture. The number of moles n present in volume V of a particular fuel depend on the density ρ and the molecular weight M of the fuel. Knowing the

densities and molecular weights and using the fundamental relation $V = \frac{nM}{\rho}$ the number of moles present in a volumetric mixture can be calculated. To compare the variation in FAR_s and normalized coefficient vector length \tilde{L}_{EXX} as a function of percent ethanol content, we define a normalized value for the stoichiometric fuel-air ratio as

$$\widetilde{FAR}_s = \frac{FAR_s - FAR_{s,E0}}{FAR_{s,E0}}. \quad (2.35)$$

The parameter vector length L_{EXX} is indicative of the percentage ethanol content based on the fact that the model parameters have incorporated the effect of FAR_s and K_{fpw} among other engine parameters, see (2.27). Given K_{fpw} is a constant allows a meaningful comparison of \tilde{L}_{EXX} and \widetilde{FAR}_s . A fuel injector delivers a fixed volume of fuel at constant pressure and pulse-width. So for fuel with varying density the same PW would result in different mass of fuel being injected. This in-effect implies that K_{fpw} actually changes with changing ethanol content if not accounted for explicitly by the PCM software which is the case at hand. Hence, to have a meaningful comparison the vector lengths need to be corrected based on the density of the fuel under test. Table 2.1 specifies the density for E0 and E100 fuels. Assuming a linear change in density, as the ethanol content is changed from 0 % to 100 % a scaling to the vector length is proposed as

$$L_{EXX,\rho} = L_{EXX} \times \frac{\rho_{EXX}}{\rho_{E0}}, \quad (2.36)$$

where $L_{EXX,\rho}$ is the density corrected vector length for fuel blend EXX . ρ_{EXX} and ρ_{E0} denote the density of the fuel blend EXX and $E0$ respectively. The corrected vector length is then normalized using (2.30) and shown in Fig. 2.8 is the combined plot of $\tilde{L}_{EXX,\rho}$ and \widetilde{FAR}_s as a function of percentage ethanol content in the fuel blend. As is evident from Fig. 2.8 the plots coincide as expected. This analysis validates the proposed ethanol estimation methodology based on the chemistry of the process involved.

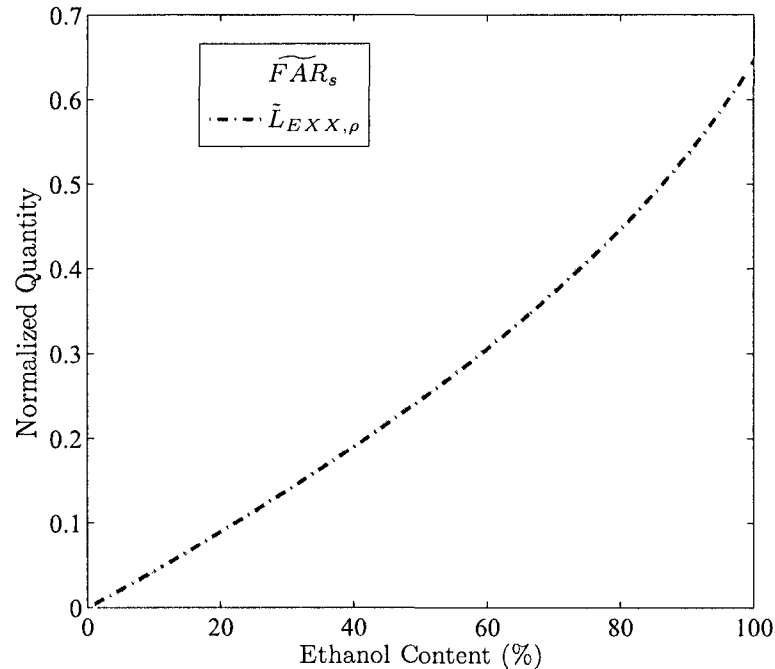


Figure 2.8: Density corrected normalized vector length and \widetilde{FAR}_s as a function of ethanol content

2.6 Chapter Conclusions

In this chapter, a method for estimation of ethanol content in flex-fuel vehicles using the existing sensor set is presented. Throttle position measurement along with engine speed, gives an estimate of mass air-flow rate in the cylinders. Use of throttle position sensor as opposed to the MAF sensor, eliminates any sensitivity issues associated with the MAF sensor. A parametric model relating the fueling command to ethanol content is developed based on first-principles modeling of the air path and fuel path dynamics. The model coefficients are estimated using RLS methods and are shown to capture the effect of changing fuel composition. Adaptation in the model coefficients is used to estimate the ethanol content. The proposed approach has been validated experimentally, at the UH-ECRL. This work has focussed on providing a proof of concept, relating the estimated parameter vector length to fuel composition. Sensor measurement inaccuracies/uncertainties can be addressed with the proposed

approach by looking at the direction of the coefficient vectors to provide a diagnostic capability. This additional diagnostics capability is deemed out of the scope of the current work and hence not investigated here.

Chapter 3 Parameter-Dependent Identification of the Intake Manifold System Dynamics in Spark Ignition Engines using LPV Methods

3.1 Introduction

The literature on identification of linear time-invariant (LTI), as well as linear time-varying (LTV) systems is vast [41, 42]. However, the literature on identification on linear parameter-varying (LPV) systems is yet to mature. The problem of LPV system identification based on state-space representation has been the focus of interest in the past few years. The first work addressing the identification of LPV systems with linear fractional parameter dependence appears in [44]. It showed that the identification of an LPV system with one scheduling parameter, one input and full state measurement can be cast as a recursive least-squares problem. Furthermore, it was shown that the parameter estimates are consistent in a noise-free case and can be further extended to a noisy measurement case, by considering an instrumental variable approach. Some of the recent work on state-space based LPV system identification can be found in [45, 46] whose methods are based on sub-space identification. A nonlinear optimization problem needs to be solved to search for the optimal parameters. Verdult provides a general framework for sub-space identification of LPV systems, describes a practical dimension reduction method for subspace identification and formulates the non-linear optimization based identification problem [45]. Some drawbacks of these methods are the long time required for the optimization

methods to converge, as well as, the absence of guarantees for convergence to the global optimizers. There are few results reported on input/output-based LPV system identification. The LPV system identification problem based on an input-output description of the LPV systems has been investigated in [47–49]. The authors in [47] study the identification of discrete LPV systems and derive conditions on the persistency of excitation in terms of the inputs and the scheduling parameter trajectories. An excellent work describing in detail the different methods for identification of LPV systems is Toth’s doctoral dissertation [50]. The approach we consider in this chapter for identification of LPV systems is somewhat similar to the one in [47], where some basis functions of the appropriate LPV parameters are defined *a priori*. However, the formulation is different in the sense that the method presented here introduces a new regressor vector to augment the basis functions and the system data using a Kronecker product. Using the proposed formulation, it would be possible to utilize standard least-squares optimization methods in the literature.

The presented LPV system identification is motivated by the modeling and control of internal combustion engines. The process model for an internal combustion (IC) engine with spark ignition is inherently nonlinear. The dynamic equations for the manifold system of an SI engine are developed by employing the principles of conservation of mass and energy, and assuming that the vaporized constituents satisfy the equation of state. We seek a parameter identification approach to enable us to rely on the engine’s input-output data to adapt the system model in real-time. This would be beneficial for the design of adaptive controllers based on the identified parameters. Due to the nonlinear nature of the system dynamics governing the intake manifold, in this chapter we tackle the system identification problem in an LPV setting, where a quasi-LPV model is initially extracted from the nonlinear model.

This chapter is organized as follows. This section has given an introduction and a brief literature review of system identification as applied to LPV systems. Section

3.2 describes the proposed LPV identification framework and presents the main results of this chapter. In section 3.3 we discuss the development of a first-principles based model for intake manifold in SI engines, as an application of the proposed results. Section 3.4 shows how the first-principles based model derived in section 3.3 is cast into an input-output form suitable for the application of the proposed identification method. In section 3.5 we give an application of the LPV system identification methodology presented using an SI engine model developed in the simulation environment of GT-Power. A further validation of the proposed method follows in section 3.6 where we have used experimental data obtained from the SI engine at UH-ECRL. Finally a conclusion to this chapter is provided in section 3.7.

3.2 Approach to LPV System Identification

The LPV system identification problem based on an input-output description has been investigated in [47, 48]. In this section, we discuss the problem under study and present an RLS-based algorithm for its solution. It is noted that the identification method we propose here is different from that in [47] as explained before. Consider a quasi-LPV system represented as

$$A(q^{-1}, \rho_k)y(k) = B(q^{-1}, \rho_k)u(k) + n_k, \quad (3.1)$$

where q^{-1} is the backward shift operator, ρ_k is the vector of external measurable parameters, and n_k is the modeling error consisting of bounded disturbance and unmodeled dynamics. In the above formulation, $u(k)$ and $y(k)$ are the sequences of the inputs and outputs, respectively. Notice that the system represented by (3.1) would have a structure similar to a linear time-invariant system if the parameters ρ_k were frozen. The polynomials A and B are defined as

$$\begin{aligned} A(q^{-1}, \rho_k) &= 1 + a_1(\rho_k)q^{-1} + \dots + a_n(\rho_k)q^{-n}, \\ B(q^{-1}, \rho_k) &= b_1(\rho_k)q^{-1} + \dots + b_m(\rho_k)q^{-m}. \end{aligned} \quad (3.2)$$

The coefficients of the polynomials A and B have the structure

$$\begin{aligned} a_i(\rho_k) &= a_i^0 + f_1(\rho_k)a_i^1 + \dots + f_{N-1}(\rho_k)a_i^{N-1}, \\ b_j(\rho_k) &= b_j^0 + f_1(\rho_k)b_j^1 + \dots + f_{N-1}(\rho_k)b_j^{N-1}, \end{aligned} \quad (3.3)$$

where $i \in \{1, \dots, n\}$, $j \in \{1, \dots, m\}$ and a_i^r , b_j^r are constant values and $f_r(\rho_k)$ are known basis functions of the online measurable variables ρ_k . Reformulating the original LPV system (3.1) by concatenating the vectors resulted from the collected data yields

$$\begin{aligned} A(q^{-1}, \rho_k) &= 1 + q^{-1}(a_1^0 + a_1^1 f_1 + \dots + a_1^{N-1} f_{N-1}) + \\ &\quad \dots + q^{-n}(a_n^0 + a_n^1 f_1 + \dots + a_n^{N-1} f_{N-1}), \\ B(q^{-1}, \rho_k) &= q^{-1}(b_1^0 + b_1^1 f_1 + \dots + b_1^{N-1} f_{N-1}) + \dots \\ &\quad + q^{-m}(b_m^0 + b_m^1 f_1 + \dots + b_m^{N-1} f_{N-1}). \end{aligned} \quad (3.4)$$

Substituting the above two equations back into the LPV model (3.1) results in the compact form

$$y(k) = \phi_k \Xi + n(k), \quad (3.5)$$

where

$$\begin{aligned} \phi_k &= [-y(k-1), -y(k-2), \dots, -y(k-n); \\ &\quad u(k-1), u(k-2), \dots, u(k-m)] \end{aligned}$$

is the regression vector and we have

$$\begin{aligned} \Xi &= \begin{bmatrix} a_1^0 + a_1^1 f_1 + \dots + a_1^{N-1} f_{N-1} \\ \vdots \\ a_n^0 + a_n^1 f_1 + \dots + a_n^{N-1} f_{N-1} \\ b_1^0 + b_1^1 f_1 + \dots + b_1^{N-1} f_{N-1} \\ \vdots \\ b_m^0 + b_m^1 f_1 + \dots + b_m^{N-1} f_{N-1} \end{bmatrix} \\ &= \mathcal{V}^0 + f_1 \mathcal{V}^1 + \dots + f_{N-1} \mathcal{V}^{N-1}, \end{aligned}$$

where $\mathcal{V}^i = [a_1^i, \dots, a_n^i, b_1^i, \dots, b_m^i]^T$ for $i = 0, \dots, N-1$. Finally, it is easy to obtain the expression

$$y(k) = \Gamma_k \Theta + n(k), \quad (3.6)$$

where

$$\begin{aligned} \Gamma_k &= G_k \otimes \phi_k, \quad G_k = [1, f_1, \dots, f_{N-1}], \\ \Theta^T &= [(\mathcal{V}^0)^T, (\mathcal{V}^1)^T, \dots, (\mathcal{V}^{N-1})^T]. \end{aligned}$$

Here $\Theta \in \mathcal{R}^{(m+n)N \times 1}$ is the vector including the unknown variables of the input-output representation of the LPV system in (3.1), and \otimes denotes the Kronecker product. Due to the determined structure in (3.6), a classical parameter identification algorithm such as RLS or LMS may be used. For the linear regressor model, an iterative scheme is used as given by

$$\hat{\Theta}_{k+1} = \hat{\Theta}_k + \lambda_k L_k \left(y(k) - \Gamma_k^T \hat{\Theta}_k \right), \quad (3.7)$$

where λ_k is the forgetting factor and $(\hat{\cdot})$ represent the estimates. A Weighted Recursive Least Square (WRLS) method is used to determine the iterative equations for updating L_k at each step. To this purpose, we consider the cost function to be minimized as

$$V(t, \Theta) = \frac{1}{2} \sum_{k=1}^t \lambda^{t-k} (y(k) - \Gamma_k^T \Theta)^2. \quad (3.8)$$

The equations obtained to solve the above problem iteratively are

$$L_k = \frac{P_{k-1} \Gamma_k}{\lambda + \Gamma_k^T P_{k-1} \Gamma_k}, \quad (3.9)$$

$$P_k = \frac{1}{\lambda} \left[P_{k-1} - \frac{P_{k-1} \Gamma_k \Gamma_k^T P_{k-1}}{\lambda + \Gamma_k^T P_{k-1} \Gamma_k} \right]. \quad (3.10)$$

It is noted that the described procedure for parameter identification works only for the LPV systems including a single output; however, the method can be easily extended

for systems with multiple outputs. Following the same lines as in [41], the iterative equations obtained for MIMO systems parameter identification are

$$L_k = P_{k-1}\Gamma_k(\lambda\Lambda_k + \Gamma_k^T P_{k-1}\Gamma_k)^{-1}, \quad (3.11)$$

$$P_k = \frac{1}{\lambda} [P_{k-1} - P_{k-1}\Gamma_k(\lambda\Lambda_k + \Gamma_k^T P_{k-1}\Gamma_k)^{-1}\Gamma_k^T P_{k-1}], \quad (3.12)$$

and the estimate of the parameters is updated from

$$\hat{\Theta}_{k+1} = \hat{\Theta}_k + \lambda L_k (y(k) - \Gamma_k^T \hat{\Theta}_k). \quad (3.13)$$

The above iterative equations are determined from minimizing the cost function

$$V(t, \Theta) = \frac{1}{2} \sum_{k=1}^t \lambda^{t-k} (y(k) - \Gamma_k^T \Theta)^T \Lambda_k^{-1} (y(k) - \Gamma_k^T \Theta), \quad (3.14)$$

at each iteration. Note that in the above cost function the matrix Λ_k is used to weight the different output channels in the cost function.

3.3 Phenomenological Modeling of the Intake Manifold System in SI Engines

In this section, we describe the steps necessary for identification of parameters of interest using a simplified nonlinear model of the intake manifold system of SI engines. An application of LPV gain scheduling to charge control of an SI engine appears in [51, 52], where an LFT model of the intake model is derived. Here, we follow the approach presented in [15] to model the dynamics of the intake manifold of an SI engine. For the sake of completeness, the model is described here.

The intake manifold filling and emptying dynamics of an SI engine can be represented as [1]

$$\dot{P}_m = \frac{RT_m}{V_m} (\dot{m}_{a,th} - \dot{m}_{a,cyl}), \quad (3.15)$$

where P_m denotes the pressure in the intake manifold, V_m represents the manifold volume and T_m is the temperature of the intake manifold. $\dot{m}_{a,th}$ denotes the mass of air flow past the throttle plate and the air flow into the cylinders is represented by $\dot{m}_{a,cyl}$. The throttle mass air flow rate, $\dot{m}_{a,th}$ can be modeled using the standard orifice flow equation for one-dimensional steady compressible flow [1] as

$$\dot{m}_{a,th} = C_d A_{th}(\alpha) \frac{P_a}{\sqrt{RT_a}} \Psi \left(\frac{P_m}{P_a} \right), \quad (3.16)$$

where α is the throttle angle, $A_{th}(\alpha)$ is the flow area of the throttle, R is the gas constant, C_d is the flow discharge coefficient and P_a , T_a denote the ambient pressure and temperature, respectively. The functions $A_{th}(\alpha)$ and $\Psi \left(\frac{P_m}{P_a} \right)$ are given by

$$A_{th}(\alpha) = \frac{\pi d_{th}^2}{4} (1 - \cos \alpha), \quad (3.17)$$

where d_{th} represents the throttle diameter and

$$\Psi \left(\frac{P_m}{P_a} \right) = \begin{cases} \sqrt{\frac{2\gamma}{\gamma-1} \left(r_p^{\frac{2}{\gamma}} - r_p^{\frac{\gamma+1}{\gamma}} \right)}, & \text{if } r_p > \left(\frac{2}{\gamma+1} \right)^{\frac{\gamma}{\gamma-1}} \\ \gamma^{\frac{1}{2}} \left(\frac{2}{\gamma+1} \right)^{\frac{\gamma+1}{2(\gamma-1)}}, & \text{if } r_p \leq \left(\frac{2}{\gamma+1} \right)^{\frac{\gamma}{\gamma-1}}. \end{cases} \quad (3.18)$$

The constant $\gamma = 1.4$ is the ratio of specific heats for air, and $r_p = \frac{P_m}{P_a}$. Equation (3.17) can be rewritten using the Taylor series expansion leading to

$$\begin{aligned} A_{th}(\alpha) &= \frac{\pi d_{th}^2}{4} \left(1 - 1 + \frac{\alpha^2}{2!} - \frac{\alpha^4}{4!} + \frac{\alpha^6}{6!} \dots \right) \\ &\approx p_0 \alpha^2 + p_1 \alpha^4 + p_2 \alpha^6, \end{aligned} \quad (3.19)$$

for some coefficients p_0 , p_1 and p_2 . The expression for the function $\Psi \left(\frac{P_m}{P_a} \right)$ can be expanded using the generalized binomial theorem to get

$$\begin{aligned} \Psi \left(\frac{P_m}{P_a} \right) &= \sqrt{\frac{2\gamma}{\gamma-1}} \left(\frac{P_m}{P_a} \right)^{\frac{1}{\gamma}} \left[1 - \left(\frac{P_m}{P_a} \right)^{\frac{\gamma-1}{\gamma}} \right]^{\frac{1}{2}} \\ &\approx s_0 P_m^{\frac{1}{\gamma}} + s_1 P_m + s_2 P_m^{\frac{2\gamma-1}{\gamma}}, \end{aligned} \quad (3.20)$$

for some coefficients s_0 , s_1 and s_2 . Substituting the value of γ in (3.20) results in

$$\Psi \left(\frac{P_m}{P_a} \right) \approx s_0 P_m^{\frac{5}{7}} + s_1 P_m + s_2 P_m^{\frac{9}{7}}. \quad (3.21)$$

Substituting the expressions (3.19) and (3.21) into (3.16) leads to a polynomial expression for the mass of air flow past the throttle plate as given by (3.22)

$$\dot{m}_{a,th} \approx C_d \frac{P_a}{\sqrt{RT_a}} (p_0 \alpha^2 + p_1 \alpha^4 + p_2 \alpha^6) (s_0 P_m^{\frac{5}{7}} + s_1 P_m + s_2 P_m^{\frac{9}{7}}) \quad (3.22)$$

The coefficient of discharge, C_d is also a function of the throttle angle, whose effect can be incorporated in the p_i coefficients and hence no separate polynomial dependence is considered. This leads to the following polynomial expression for $\dot{m}_{a,th}$ with new coefficients c_i as

$$\begin{aligned} \dot{m}_{a,th} &\approx c_0 \alpha^2 P_m^{\frac{5}{7}} + c_1 \alpha^2 P_m + c_2 \alpha^2 P_m^{\frac{9}{7}} \\ &\quad + c_3 \alpha^4 P_m^{\frac{5}{7}} + c_4 \alpha^4 P_m + c_5 \alpha^4 P_m^{\frac{9}{7}} \\ &\quad + c_6 \alpha^6 P_m^{\frac{5}{7}} + c_7 \alpha^6 P_m + c_8 \alpha^6 P_m^{\frac{9}{7}} \\ &= \mu(\alpha, P_m), \end{aligned} \quad (3.23)$$

where $\mu(\cdot)$ gives the functional dependence of $\dot{m}_{a,th}$ on the engine parameters throttle angle and manifold pressure. The cylinder air flow for a 4-stroke engine is given by [1]

$$\dot{m}_{a,cyl} = \frac{\eta_{vol} V_d N}{2RT_m} P_m, \quad (3.24)$$

where η_{vol} is the volumetric efficiency, V_d is the total displaced volume of all the cylinders and N is the engine speed. As is a common practice [38, 39] the volumetric efficiency is expressed as a polynomial function of P_m and N as in

$$\eta_{vol} = d_0 + d_1 N + d_2 N^2 + d_4 P_m. \quad (3.25)$$

Substituting (3.25) in (3.24) gives

$$\begin{aligned} \dot{m}_{a,cyl} &= e_0 N P_m + e_1 N^2 P_m + e_2 N^3 P_m + e_3 N P_m^2 \\ &= \xi(N, P_m), \end{aligned} \quad (3.26)$$

for some coefficients e_i , with $\xi(\cdot)$ giving the dependence of $\dot{m}_{a,cyl}$ on the engine parameters speed and manifold pressure. Substituting (3.23) and (3.26) in (3.15) models

the intake manifold dynamics. The throttle valve opening α is manipulated using a simple first-order system with the bandwidth of w_{thr} . Finally, the overall system dynamics is represented by

$$\begin{aligned} \dot{P}_m &= \beta_m(\mu(\alpha, P_m) - \xi(N, P_m)), \\ \dot{\alpha} &= -w_{thr}\alpha + w_{thr}\alpha_{ref}, \end{aligned} \tag{3.27}$$

where $\beta_m = \frac{RT_m}{V_m}$ is a constant associated the manifold volume and temperature and α_{ref} is the reference throttle input. The speed that the engine runs at depends on the applied load. The torque and speed production dynamics can be modeled; however, it is not required in this study since the engine speed is a measurable quantity and we aim to identify only the intake manifold dynamics.

3.4 Problem Formulation

In order to use the results of the LPV system identification methodology presented in section 3.2, the system to be identified needs to be formulated in an input-output representation. This section details the steps necessary, to formulate the problem we plan to solve. Assuming the manifold pressure P_m , engine speed N , and the throttle angle α as the measurable scheduling parameters, an LPV representation for the system dynamics in (3.27) can be written as

$$\begin{aligned} \dot{x}(t) &= A(\rho)x(t) + B(\rho)u(t), \\ y(t) &= C(\rho)x(t), \end{aligned} \tag{3.28}$$

where ρ is the scheduling parameter vector, $u(t)$ is the input and $y(t)$ is the output to be modeled. To demonstrate the proposed approach, the air flow past the throttle is chosen as the output and the reference throttle opening serves as the input. The

parameter-dependent state-space matrices are given as

$$\begin{aligned}
x &= \begin{bmatrix} P_m \\ \alpha \end{bmatrix}, \quad u = \alpha_{ref}, \quad \rho = \begin{bmatrix} P_m & N & \alpha \end{bmatrix}^T \\
A(\rho) &= \begin{bmatrix} -\beta_m \frac{\xi(N, P_m)}{P_m} & \beta_m \frac{\mu(\alpha, P_m)}{\alpha} \\ 0 & -w_{thr} \end{bmatrix}, \quad B(\rho) = \begin{bmatrix} 0 \\ w_{thr} \end{bmatrix}, \\
C(\rho) &= \begin{bmatrix} 0 & \frac{\mu(\alpha, P_m)}{\alpha} \end{bmatrix}.
\end{aligned} \tag{3.29}$$

The continuous-time state-space representation in (3.28) is discretized using the backward difference approximation with a sampling time T_s , to obtain

$$\begin{aligned}
x(k+1) &= (I + T_s A(\rho))x(k) + T_s B(\rho)u(k), \\
y(k) &= C(\rho)x(k).
\end{aligned} \tag{3.30}$$

The input-output representation of (3.30) is then obtained as

$$y(k) = (1 - w_{thr}T_s)y(k-1) + \left(\frac{\mu(\alpha, P_m)}{\alpha} w_{thr}T_s \right) u(k-1). \tag{3.31}$$

To associate the obtained model with the input-output representation that is useful for the LPV parameter identification, we define a set of basis functions as

$$\begin{aligned}
f_1(\rho) &= \alpha P_m^{\frac{5}{7}}, & f_2(\rho) &= \alpha P_m, & f_3(\rho) &= \alpha P_m^{\frac{9}{7}}, \\
f_4(\rho) &= \alpha^3 P_m^{\frac{5}{7}}, & f_5(\rho) &= \alpha^3 P_m, & f_6(\rho) &= \alpha^3 P_m^{\frac{9}{7}}, \\
f_7(\rho) &= \alpha^5 P_m^{\frac{5}{7}}, & f_8(\rho) &= \alpha^5 P_m, & f_9(\rho) &= \alpha^5 P_m^{\frac{9}{7}}.
\end{aligned} \tag{3.32}$$

It is interesting to note that the non-linear terms in $\xi(N, P_m)$ do not play a role in forming the basis functions, due to the output selection. With the basis functions defined as above, the input-output representation in (3.31) is of the form (3.1), as required by the LPV identification algorithm. More specifically, we have

$$\begin{aligned}
A(q^{-1}, \rho_k) &= 1 - (1 - w_{thr}T_s)q^{-1}, \\
B(q^{-1}, \rho_k) &= \left(w_{thr}T_s \frac{\mu(\alpha, P_m)}{\alpha} \right) q^{-1}, \\
&= [w_{thr}T_s(c_0 f_1(\rho) + c_1 f_2(\rho) + c_2 f_3(\rho)) \\
&\quad + c_3 f_4(\rho) + c_4 f_5(\rho) + c_5 f_6(\rho)) \\
&\quad + c_6 f_7(\rho) + c_7 f_8(\rho) + c_8 f_9(\rho)]q^{-1}.
\end{aligned} \tag{3.33}$$

As can be seen from the above formulation the coefficients b_j from (3.3) correspond to the product of $w_{thr}T_s$ and the coefficients c_i from (3.23). The a_i and b_j coefficients of (3.3) are to be identified using the proposed RLS based system identification technique.

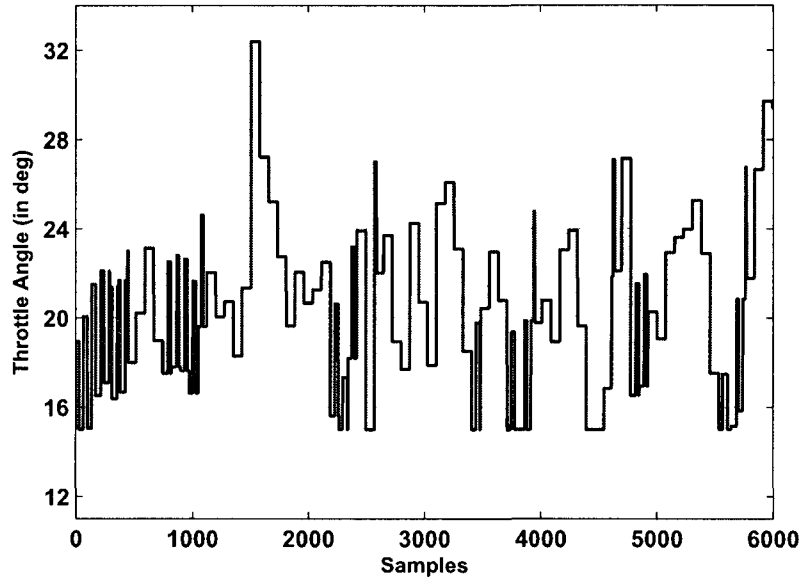


Figure 3.1: Throttle valve excitation input during GT-Power simulation study

3.5 Simulation Results using GT-Power

GT-Power, the industry standard tool for engine model identification and vehicle simulation, was used to validate numerically the proposed approach. A 4-cylinder SI engine model was developed in the GT-Power simulation environment and coupled with Matlab-Simulink. Fig. 3.1 shows the throttle angle excitation input used for identifying the parameter-dependent intake model. Fig. 3.2 shows the corresponding manifold pressure and speed variations and shown in Fig. 3.3 are the results of the identification method presented in this chapter.

The proposed LPV identification algorithm was implemented on the data collected

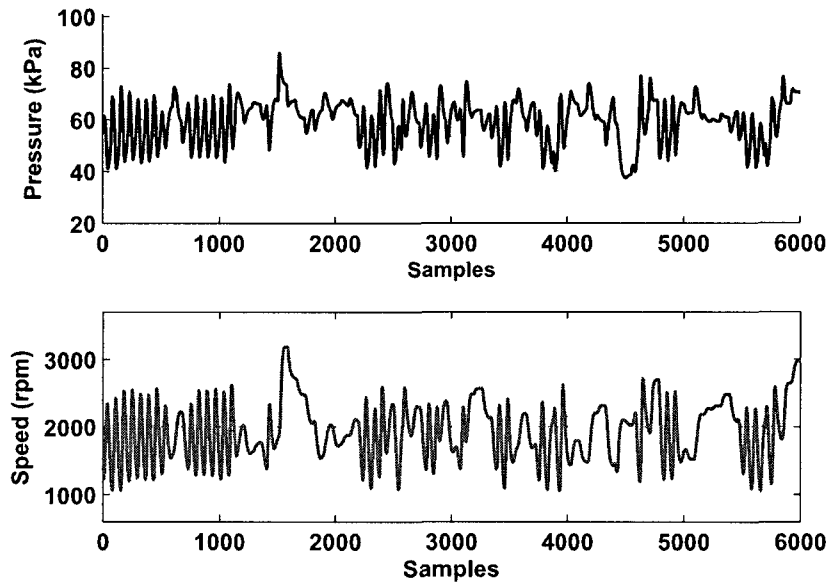


Figure 3.2: Manifold pressure and engine speed trajectories during input excitation in GT-Power simulation

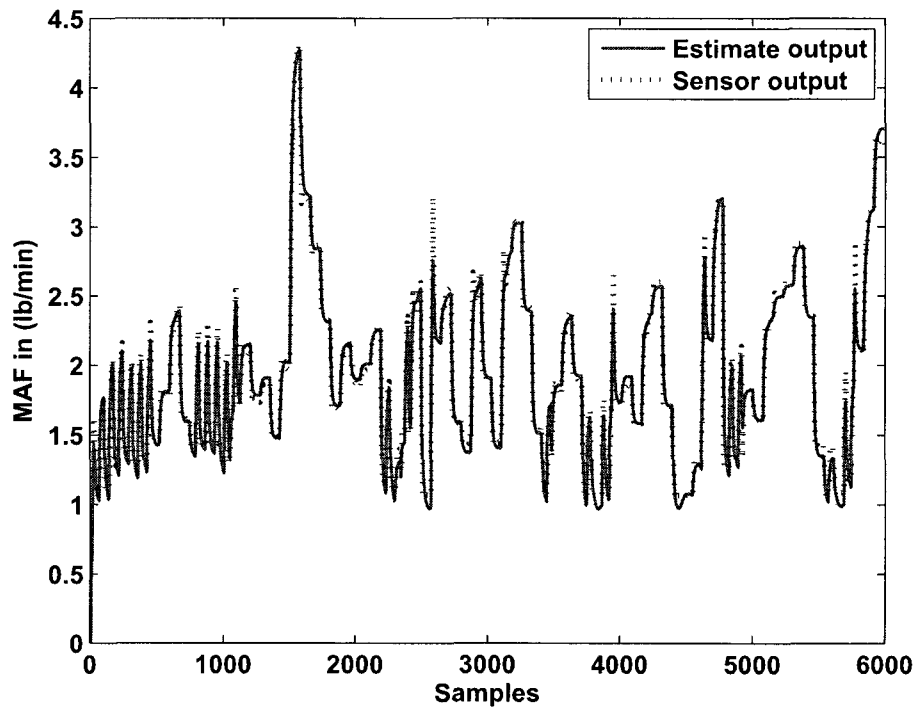


Figure 3.3: Estimated and sensor outputs with GT-Power simulation study

from simulations, with the forgetting factor value $\lambda = 1$. Fig. 3.3 shows the comparison of the model estimated mass air flow, with the sensor obtained value. As can be seen the model estimates track the sensor output values very well.

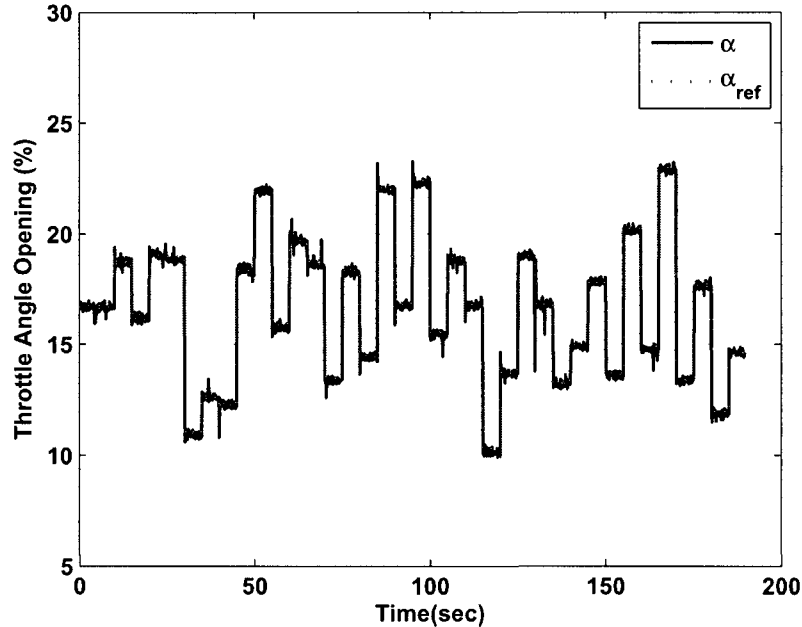


Figure 3.4: Throttle valve excitation input

3.6 Experimental Results

3.6.1 Training Data

Experiments were performed at the UH-ECRL to validate the proposed LPV identification algorithm. A brief description of the engine setup used is already provided in section 2.4. Here we elaborate the types of signals used in the identification methodology. A random Gaussian signal with appropriate range of variation was used to excite the throttle angle input. All relevant data was recorded. Fig. 3.4 shows the throttle excitation and Fig. 3.5 shows the trajectories of the relevant engine parameters. Manifold pressure is measured in kPa and the engine speed is measured in

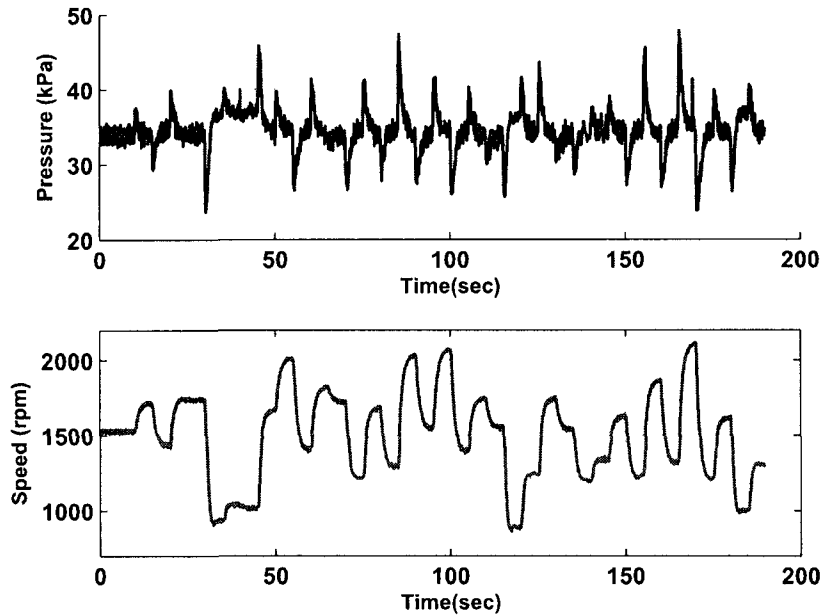


Figure 3.5: Manifold pressure and engine speed trajectories during input excitation

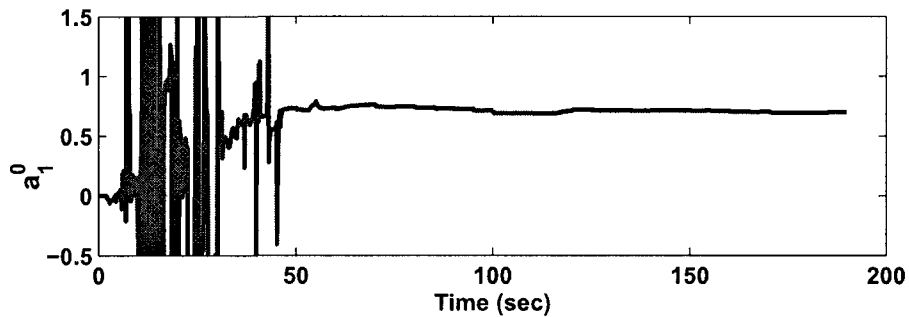


Figure 3.6: a_1^0 coefficient trajectory

revolutions per minute (rpm). The input-output data is collected from the engine at a 10 Hz sampling rate, corresponding to a sampling time $T_s = 100$ ms. The proposed identification method is implemented with a forgetting factor $\lambda = 1$. Fig. 3.6 shows the convergence of the a_1^0 identified coefficient. Similar convergence was obtained for the other identified coefficients but is not shown here. Shown in Table 3.1 are the values of the identified coefficients after normalization. During the validation phase presented in the following sub-section we use the identified model coefficients to predict the mass air flow across the throttle and compare it with the actual value of mass

Table 3.1: Normalized model coefficient values

Normalized Coefficient	Value
a_1^0	0.72
b_1^1	7.407
b_1^2	-9.748
b_1^3	3.330
b_1^4	-5.372
b_1^5	7.312
b_1^6	-2.529
b_1^7	1.015
b_1^8	-1.383
b_1^9	0.476

air flow measured using a sensor.

3.6.2 Validation Data

As mentioned before a random Gaussian signal was used as an input excitation in order to identify the model coefficients. To validate the results of the identification algorithm, another data set was obtained, where the throttle was modulated manually as a driver in a car would. The engine was applied a dynamometer load similar to the one used during identification/training phase. Fig. 3.7 shows the throttle angle, manifold pressure and engine speed during the engine run for the validation case. It is to be noted that the throttle perturbations during this validation phase are in the same magnitude range as with the training data. This is obvious because the identified model is expected to hold good only for the data range used during the identification process. Also the variation in engine speed as seen from Fig. 3.7 is from approximately 1000 rpm to 2000 rpm, very similar to the one seen in Fig. 3.5. Similar is the case with the observed manifold pressure. The mass air flow across the throttle was estimated, based on the coefficient values obtained during identification phase (shown in Table 3.1) and this estimate was compared with the actual MAF sensor

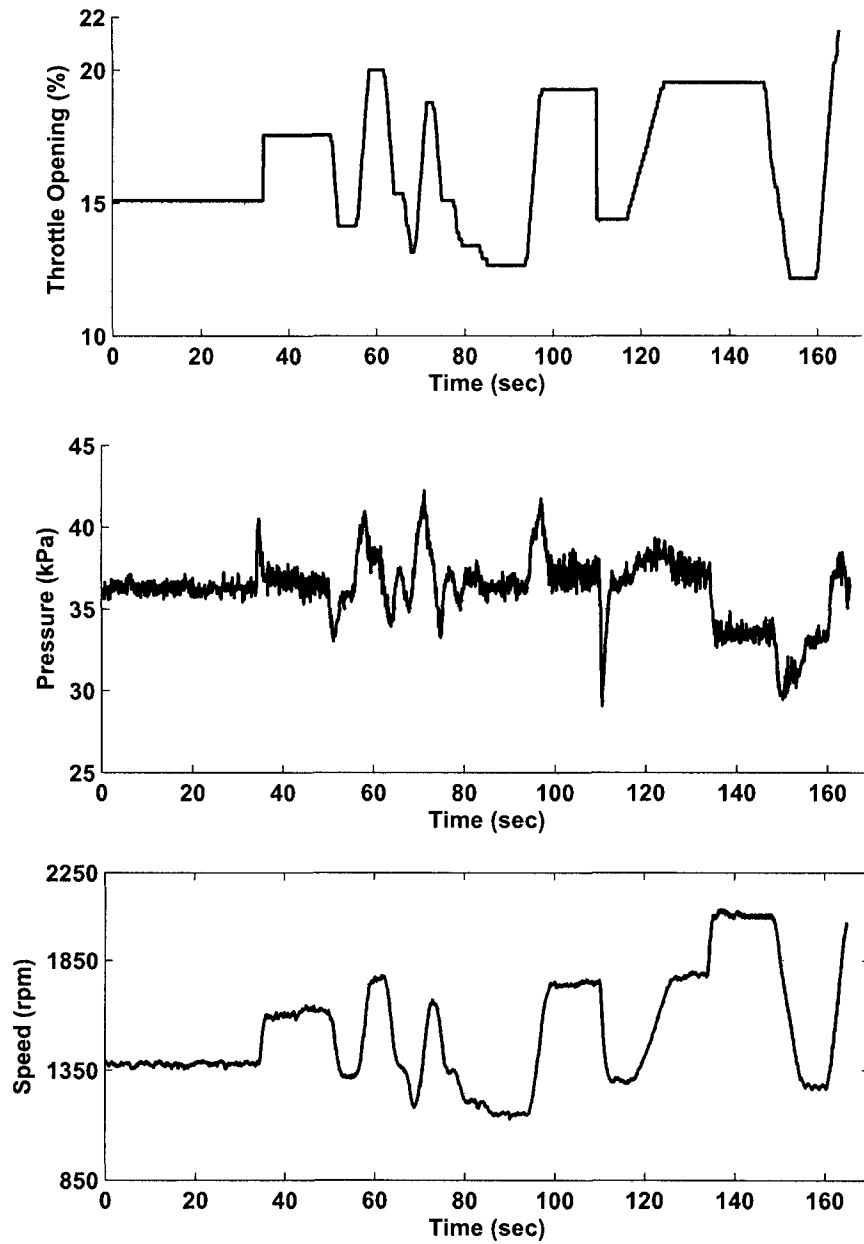


Figure 3.7: Throttle angle, manifold pressure and engine speed trajectories during validation

obtained value. This comparison is shown in Fig. 3.8. As is evident, the estimate tracks the sensor output value very well. For comparison sake Fig. 3.9 shows the results of using only the first six basis functions from (3.32). The results deteriorate even further if only three basis functions are used and is not shown here.

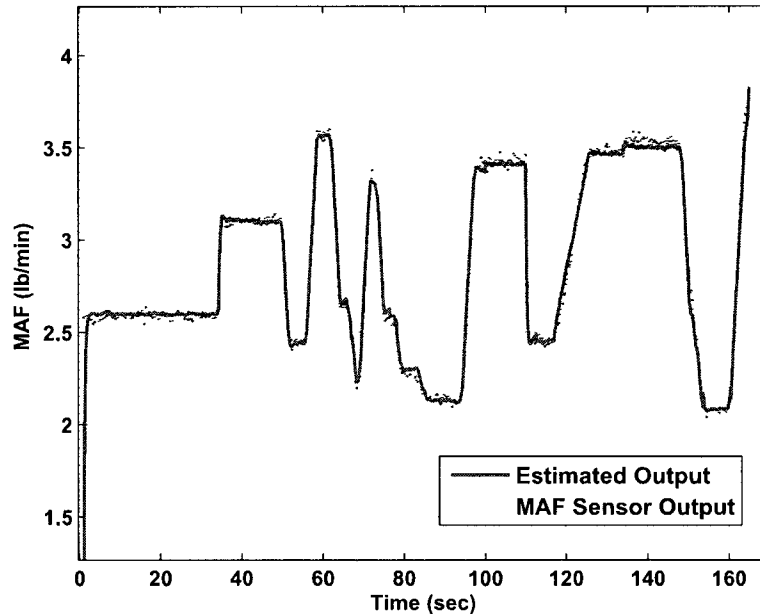


Figure 3.8: Sensor output and output of the identification algorithm

3.7 Chapter Conclusions

This chapter illustrates the successful application of parameter-dependent model identification to the intake manifold of an SI engine. The LPV system identification problem is posed as a recursive least squares problem, by introducing a new regressor vector to augment the basis functions and the system data using the Kronecker product. A non-linear model of the intake manifold is derived from the first-principles and cast into an LPV form. The derived continuous time LPV state-space model is then discretized and cast into an input-output form, to which the proposed method of identification can be applied. The proposed approach has been validated with

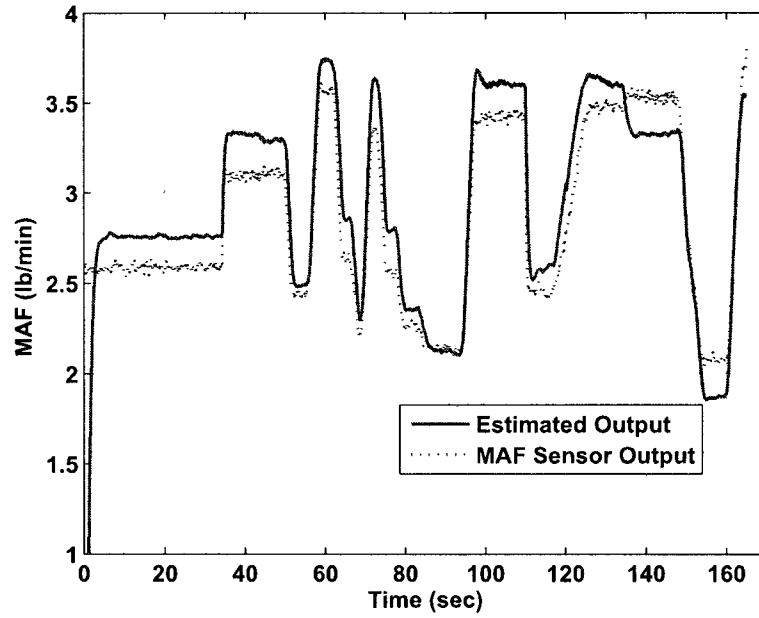


Figure 3.9: Sensor output and output of the identification algorithm with only 6 basis functions

simulations in GT-Power and with experimental data obtained from a 5.4-L V8 Ford engine, housed at the UH-ECRL.

Chapter 4 Delay-Dependent \mathcal{H}_∞ Control of LPV Time-Delay Systems with Application to Fueling Control in SI Engines

In this chapter the delay-dependent stability and \mathcal{H}_∞ control of LPV systems with fast-varying time-delays is examined. This work is motivated by the inability of the existing output feedback control synthesis methods for LPV time-delay systems to provide a feasible controller for the fueling control problem in SI engines.

4.1 Introduction and Literature Review

Dynamic systems with time delays appear frequently in engineering and biological systems. Time delays may be constant or time-varying, point-wise or distributed, deterministic or stochastic. The most obvious example of time delay in a system is the delay introduced by the interconnection of two subsystems that are separated by a significant physical distance resulting in transport or transmission delays between the sub-systems. Delays often describe the time to effect coupling or interconnection between dynamics through propagation or transport phenomena in shared environments, or through heredity and competition in population dynamics. Time delays complicate the controller design process as they often induce instability in the feedback control system [53]. The mathematical formulation of a time-delay system results in a system of functional differential equations (FDEs) which are infinite dimensional, as opposed to ordinary differential equations (ODEs) that describe finite-dimensional

systems. Stability analysis and control of time-delay systems is a subject of great practical and theoretical importance and has been studied extensively in the controls literature for decades. For example refer the monographs [54–60] and the numerous references therein. Richard in [61] provides a good overview of some recent advances and open problems in time-delay systems.

Stability of time-delay systems can be broadly studied using either frequency domain or time domain methods. The discussion in this chapter is restricted to the use of time domain methods and more specifically to the employment of Lyapunov-based methods. Existing stabilization results for delay systems are concerned with either one of the following two types of stabilization: delay-independent stabilization or delay-dependent stabilization. Delay-independent stabilization is based on conditions that are independent of the size of the delay and has been studied extensively in the literature [62–68]. It is well known that delay-independent criteria for stabilization lead to conservative results specially for systems with small time delays, as stability is guaranteed for all non-negative values of time delays. Delay-dependent criteria ensure stabilization and a prescribed level of performance of the system for magnitudes of the delays smaller than a given bound. This knowledge of a bound on the size of the time-delay allows for reduced conservatism compared to the delay-independent approach. Development of the delay-dependent stability conditions and control has been investigated in [69–77] among many others.

Linear parameter-varying (LPV) systems provide a systematic way of computing gain-scheduled controllers for nonlinear and/or time-varying systems when formulated in the LPV framework. Stability analysis and control synthesis problems for LPV systems have been investigated extensively in the literature [12, 13, 78–80]. The above results, however, do not consider systems with delay in their dynamics. LPV systems with time delays often appear in many engineering applications. In fact, in parameter-varying systems often the magnitude of the delay changes as a function of varying

parameters in the system. For instance, the transport delay in an internal combustion engine is a known function of the engine speed and mass air flow. Similarly, parameter-varying time delays also appear in many manufacturing processes such as the milling process, where the changes in system dynamics result in variable time delays. Stability analysis and control of such LPV time-delay systems has attracted a lot of attention in the last decade. One of the first work appeared in [81], where the authors analyzed a time-delay LPV system and developed a delay-independent condition, with an additional restriction of keeping the kernel of the integral term parameter-independent. State feedback controller synthesis conditions guaranteeing a desired induced \mathcal{L}_2 gain performance were also presented in [81]. The authors in [82] developed stability tests for LPV time-delay systems using both delay-independent and delay-dependent conditions. However, the delays are assumed to be constant (not parameter varying) and no controller synthesis conditions were provided. The authors in [83] provide the delay-independent and delay-dependent stability analysis results for quadratic stability and affine quadratic stability and further discuss \mathcal{L}_2 gain state feedback control using delay-independent conditions. Improvements over the result of [81] are presented in [84] along with new results discussing the $\mathcal{L}_2 - \mathcal{L}_\infty$ gain control. Output feedback control synthesis has been discussed in [85, 86] again using the delay-independent conditions. Delay-dependent \mathcal{H}_∞ control result for LPV systems with state delays first appeared in [87]. However, the rate information for the delay variation has not been used resulting in conservative results. The authors in [88] examined state feedback \mathcal{H}_∞ control of LPV time-delay systems with a rate bounded time-varying delay. Their approach uses a model transformation introducing additional dynamics in the system. This shortcoming is overcome in the work of [89], where an equivalent descriptor model transformation first introduced in [90], along with Park's inequality [91] for bounding cross terms is used to derive less conservative results. Additional results concerning control and filtering of LPV time-delay systems appear in [92–94].

Despite a large number of research articles appeared in the past decade on the control of time-delay LPV systems, \mathcal{H}_∞ control of LPV time-delay systems based on output feedback is still an open problem with more efforts directed towards reducing the design conservatism. It is well known that the choice of an appropriate Lyapunov-Krasovskii functional is crucial for deriving stability conditions. The conservatism of the existing delay-dependent conditions stems from two sources: one is the model transformation used and the other is the inequality bounding techniques usually employed for some cross terms encountered in the analysis and synthesis conditions. The Lyapunov-Krasovskii functional used in this work is borrowed from [95] and modified to allow for the dependence of the time-varying delay on the scheduling parameter. This type of Lyapunov-Krasovskii functionals avoids any model transformation or any bounding of the cross terms. The only conservatism introduced by this method comes from the initial choice of the Lyapunov-Krasovskii functional and the use of the Jensen's inequality [59] employed to bound an integral term in the derivative of Lyapunov-Krasovskii functional. The main advantage of these functionals is their simplicity and the lower number of matrix variables involved in the Lyapunov-Krasovskii functional, thus reducing products between data matrices and decision variables and making them potentially interesting candidates for the stabilization and control design purposes. In this chapter, a bounded real lemma, which is an LMI analysis condition guaranteeing a prescribed level of \mathcal{H}_∞ performance is derived for the time-delay LPV system. Before substituting the closed-loop system state-space matrices and deriving synthesis conditions, the LMI conditions are relaxed using the approach presented in [97], which introduces *slack* variables. Existence conditions for synthesis of a state feedback controller are derived. It is shown that the proposed results for state feedback control synthesis have a potential to reduce conservativeness as compared to methods in literature. To develop existence conditions for an output feedback control, we substitute the output feedback controller dynamics in the closed-loop which results in bilinear matrix inequality (BMI) conditions. These

conditions corresponding to the closed-loop system are linearized using a nonlinear transformation leading to the final delayed-feedback output controller synthesis conditions. The structure of the feedback controller is assumed to have a delay term in its dynamics.

The notation used in this chapter is standard. \mathbb{R} stands for the set of real numbers. \mathbb{R}^n and $\mathbb{R}^{k \times m}$ denote the set of real vectors of dimension n and the set of real $k \times m$ matrices, respectively. The transpose of a real matrix M is denoted as M^T and its null-space by $\ker(M)$. \mathbb{S}^n denotes real symmetric $n \times n$ matrices and \mathbb{S}_{++}^n is the set of real symmetric positive definite $n \times n$ matrices. $\mathcal{C}(J, K)$ denotes the set of continuous functions from a set J to a set K .

4.2 Problem Statement and Preliminaries

Consider the following state-space representation of an LPV system with a time-delay in the state:

$$\begin{aligned}
(\Sigma_\rho) : \quad & \dot{x}(t) = A(\rho)x(t) + A_h(\rho)x(t - h(\rho(t))) + B_1(\rho)w(t) + B_2(\rho)u(t) \\
& z(t) = C_1(\rho)x(t) + C_{1h}(\rho)x(t - h(\rho(t))) + D_{11}(\rho)w(t) + D_{12}(\rho)u(t) \\
& y(t) = C_2(\rho)x(t) + C_{2h}(\rho)x(t - h(\rho(t))) + D_{21}(\rho)w(t) \\
& x(\theta) = \phi(\theta), \forall \theta \in [-h(\rho(0)) \ 0],
\end{aligned} \tag{4.1}$$

where $x(t) \in \mathbb{R}^n$ is the system state vector, $w(t) \in \mathbb{R}^{n_w}$ is the vector of exogenous disturbance with finite energy in the space $\mathcal{L}_2[0 \ \infty)$, $u(t) \in \mathbb{R}^{n_u}$ is the input vector, $z(t) \in \mathbb{R}^{n_z}$ is the vector of controlled outputs, $y(t) \in \mathbb{R}^{n_y}$ is the vector of measurable outputs, $\phi(\cdot)$ denotes the initial system condition, and h is a differentiable scalar function representing the parameter-varying time-delay. We assume that the delay is bounded and that the function h lies in the set

$$\mathcal{H} := \{h \in \mathcal{C}(\mathbb{R}^s, \mathbb{R}) : 0 \leq h(t) \leq h_{max} < \infty, \forall t \in \mathbb{R}_+\}. \tag{4.2}$$

The initial condition function ϕ is a given function in $\mathcal{C}([-h_{max} \ 0], \mathbb{R}^n)$. Wherever needed, the notation $x_t(\theta)$ is used to denote $x(t + \theta)$ for $\theta \in [-h_{max} \ 0]$, that is, x_t is the infinite dimensional state of the system. The state space matrices $A(\cdot)$, $A_h(\cdot)$, $B_1(\cdot)$, $B_2(\cdot)$, $C_1(\cdot)$, $C_{1h}(\cdot)$, $C_2(\cdot)$, $C_{2h}(\cdot)$, $D_{11}(\cdot)$, $D_{12}(\cdot)$, $D_{21}(\cdot)$ are assumed to be known continuous functions of a time-varying parameter vector $\rho(\cdot) \in \mathcal{F}_p^\nu$, i.e., we consider bounded parameter trajectories with bounded rates for the parameter variation. Notice that, the parametric dependence of the delay on ρ results in a given delay bound h_{max} , since ρ is restricted to lie in the given parameter set \mathcal{P} . Bounding the rate of variation of the parameter vector ρ allows the use of parameter dependent Lyapunov Krasovskii functionals resulting in less conservative analysis and synthesis conditions [12, 13].

In this chapter, we are interested in an \mathcal{H}_∞ design as the performance specification for the closed-loop system. This chapter takes advantage of a number of lemmas to prove some of the technical results. The two important ones are described below.

Lemma 4.1 *Projection Lemma.* *Given a symmetric matrix $\Psi \in \mathbb{R}^{m \times m}$ and two matrices \mathcal{C} , \mathcal{D} of appropriate dimensions, the following problem*

$$\Psi + \mathcal{C}^T \Theta^T \mathcal{D} + \mathcal{D}^T \Theta \mathcal{C} < 0 \quad (4.3)$$

is solvable in a matrix Θ of compatible dimension if and only if

$$Ker^T(\mathcal{C})\Psi Ker(\mathcal{C}) < 0, \quad Ker^T(\mathcal{D})\Psi Ker(\mathcal{D}) < 0, \quad (4.4)$$

where $Ker(\mathcal{C})$ and $Ker(\mathcal{D})$ are any basis of the kernel or null space of \mathcal{C} and \mathcal{D} , respectively.

Proof. Refer to [96]

Lemma 4.2 *Jensen's Lemma.* *Let ϕ be a convex function and $f(x)$ is a function*

integrable over $[a, b]$, $a < b$. Then, the inequality in (4.5) holds

$$\phi \left(\int_a^b f(x) dx \right) \leq (b-a) \int_a^b \phi(f(x)) dx \quad (4.5)$$

Proof. Refer to [59].

The Jensen's inequality is often used in the \mathcal{H}_∞ norm analytical computation of integral operators in time-delay systems framework. It is also used in approaches based on Lyapunov-Krasovskii functionals as an efficient bounding technique. An example of one such application is given as

$$\left(\int_{t-h}^t \dot{x}(\theta) d\theta \right)^T P \left(\int_{t-h}^t \dot{x}(\theta) d\theta \right) \leq h \int_{t-h}^t \dot{x}(\theta)^T P \dot{x}(\theta) d\theta, \quad (4.6)$$

with $P = P^T > 0$. The convex function is $\phi(z) = z^T P z$ and $f(t) = \dot{x}(t)$.

4.3 \mathcal{H}_∞ Performance Analysis of Time-delay LPV Systems

Consider the unforced (i.e., $u \equiv 0$) time-delay LPV system

$$\begin{aligned} (\Sigma_{\rho w}) : \quad \dot{x}(t) &= A(\rho)x(t) + A_h(\rho)x(t - h(\rho(t))) + B_1(\rho)w(t), \\ z(t) &= C_1(\rho)x(t) + C_{1h}(\rho)x(t - h(\rho(t))) + D_{11}(\rho)w(t). \end{aligned} \quad (4.7)$$

The following theorem provides a sufficient condition guaranteeing asymptotic stability along with a prescribed level of disturbance attenuation in an \mathcal{H}_∞ setting.

Theorem 4.1 *The system $(\Sigma_{\rho w})$ is asymptotically stable for all $h \in \mathcal{H}$ and satisfies the condition $\|z\|_2 \leq \gamma \|w\|_2$, if there exist a continuously differentiable matrix function $P : \mathbb{R}^s \rightarrow \mathbb{S}_{++}^n$, constant matrices $Q, R \in \mathbb{S}_{++}^n$, and a scalar $\gamma > 0$ such that the LMI condition in (4.8) holds for all $\rho \in \mathcal{F}_\rho^v$, with $M(\rho, \nu) = A^T(\rho)P(\rho) + P(\rho)A(\rho) + \left[\sum_{i=1}^s \pm \left(\nu_i \frac{\partial P(\rho)}{\partial \rho_i} \right) \right] + Q - R$ and $N(\rho, \nu) = - \left[1 - \sum_{i=1}^s \pm \left(\nu_i \frac{\partial h}{\partial \rho_i} \right) \right] Q - R$.*

$$\begin{bmatrix} M(\rho, \nu) & P(\rho)A_h + R & P(\rho)B_1(\rho) & C_1^T(\rho) & h_{max}A^T(\rho)R \\ * & N(\rho, \nu) & 0 & C_{1h}^T(\rho) & h_{max}A_h^T(\rho)R \\ * & * & -\gamma I & D_{11}^T(\rho) & h_{max}B_1^T(\rho)R \\ * & * & * & -\gamma I & 0 \\ * & * & * & * & -R \end{bmatrix} < 0. \quad (4.8)$$

Proof. Consider the Lyapunov-Krasovskii functional,

$$V(x_t, \rho) = V_1(x, \rho) + V_2(x_t, \rho) + V_3(x_t, \rho), \quad (4.9)$$

$$V_1(x, \rho) = x^T(t)P(\rho)x(t), \quad (4.10)$$

$$V_2(x_t, \rho) = \int_{t-h(\rho(t))}^t x^T(\xi)Qx(\xi)d\xi, \quad (4.11)$$

$$V_3(x_t, \rho) = \int_{-h_{max}}^0 \int_{t+\theta}^t \dot{x}^T(\eta)h_{max}R\dot{x}(\eta)d\eta d\theta. \quad (4.12)$$

It is easy to show that $V(x_t, \rho)$ is positive definite. To ascertain the asymptotic stability of the system, the time derivative of $V(x_t, \rho)$ is computed along the trajectories of the system as

$$\dot{V}_1(x, \rho) = \dot{x}^T(t)P(\rho)x(t) + x^T(t)P(\rho)\dot{x}(t) + x^T(t)\frac{\partial P(\rho)}{\partial \rho}\dot{\rho}x(t), \quad (4.13)$$

$$\begin{aligned} \dot{V}_2(x_t, \rho) &= x^T(t)Qx(t) \\ &\quad - \left(1 - \frac{\partial h}{\partial \rho}\dot{\rho}\right) x^T(t-h(\rho(t)))Qx(t-h(\rho(t))), \end{aligned} \quad (4.14)$$

$$\dot{V}_3(x_t, \rho) = h_{max}^2 \dot{x}^T(t)R\dot{x}(t) - \int_{t-h_{max}}^t \dot{x}^T(\theta)h_{max}R\dot{x}(\theta)d\theta. \quad (4.15)$$

Since $h(t) \leq h_{max}$, then

$$- \int_{t-h_{max}}^t \dot{x}^T(\theta)h_{max}R\dot{x}(\theta)d\theta \leq - \int_{t-h(t)}^t \dot{x}^T(\theta)h_{max}R\dot{x}(\theta)d\theta. \quad (4.16)$$

Using Jensen's inequality in Lemma 4.2, it is possible to bound the integral term in $\dot{V}_3(x_t, \rho)$ as

$$\begin{aligned}
\dot{V}_3(x_t, \rho) &\leq h_{max}^2 \dot{x}^T(t) R \dot{x}(t) - \int_{t-h(t)}^t \dot{x}^T(\theta) h_{max} R \dot{x}(\theta) d\theta \\
&\leq h_{max}^2 \dot{x}^T(t) R \dot{x}(t) - \frac{h_{max}}{h(t)} \left(\int_{t-h(t)}^t \dot{x}(\theta) d\theta \right)^T R \left(\int_{t-h(t)}^t \dot{x}(\theta) d\theta \right) \\
&= h_{max}^2 \dot{x}^T(t) R \dot{x}(t) \\
&\quad - \frac{h_{max}}{h(t)} [x(t) - x(t - h(\rho(t)))]^T R [x(t) - x(t - h(\rho(t)))] . \quad (4.17)
\end{aligned}$$

Finally, bounding $-\frac{h_{max}}{h(t)}$ by -1 , we get

$$\dot{V}_3(x_t, \rho) \leq h_{max}^2 \dot{x}^T(t) R \dot{x}(t) - [x(t) - x(t - h(\rho(t)))]^T R [x(t) - x(t - h(\rho(t)))] . \quad (4.18)$$

Gathering all the derivative terms and letting $\dot{V}(x_t, \rho) < 0$, we determine the inequality condition

$$\dot{V}(x_t, \rho) \leq \zeta^T(t) \Xi(\rho, \dot{\rho}) \zeta(t) < 0, \quad (4.19)$$

with

$$\Xi(\rho, \dot{\rho}) = \begin{bmatrix} \Xi_{11} & P(\rho)A_h(\rho) + R & P(\rho)B_1(\rho) \\ \star & \Xi_{22} & 0 \\ \star & \star & 0 \end{bmatrix} + h_{max}^2 \mathbf{T}^T(\rho) R \mathbf{T}(\rho), \quad (4.20)$$

and

$$\zeta(t) = \text{col}[x(t), x(t - h(\rho(t))), w(t)], \quad (4.21)$$

$$\mathbf{T} = [A(\rho) \ A_h(\rho) \ B_1(\rho)], \quad (4.22)$$

$$\Xi_{11} = A^T(\rho)P(\rho) + P(\rho)A(\rho) + \frac{\partial P(\rho)}{\partial \rho} \dot{\rho} + Q - R, \quad (4.23)$$

$$\Xi_{22} = - \left(1 - \frac{\partial h}{\partial \rho} \dot{\rho} \right) Q - R. \quad (4.24)$$

To establish the prescribed \mathcal{H}_∞ performance level γ we further require [81]

$$\dot{V}(x_t, \rho) - \gamma^2 w^T(t)w(t) + z^T(t)z(t) \leq 0. \quad (4.25)$$

Substituting $z(t)$ from (4.7) into the inequality (4.25) above finally leads to the following inequality $\zeta^T(t)\Omega(\rho, \dot{\rho})\zeta(t) < 0$ with

$$\Omega = \begin{bmatrix} \Omega_{11} & PA_h + R + h_{max}^2 A^T RA_h + C_1^T C_{1h} & PB_1 + h_{max}^2 A^T RB_1 + C_1^T D_{11} \\ \star & \Xi_{22} + h_{max}^2 A_h^T RA_h + C_{1h}^T C_{1h} & h_{max}^2 A_h^T RB_1 + C_{1h}^T D_{11} \\ \star & \star & h_{max}^2 B_1^T RB_1 + D_{11}^T D_{11} - \gamma^2 I \end{bmatrix}, \quad (4.26)$$

and $\Omega_{11} = A^T P + PA + \frac{\partial P}{\partial \rho} \dot{\rho} + Q - R + h_{max}^2 A^T RA + C_1^T C_1$, and where the explicit dependence on the scheduling parameter vector ρ has been dropped for convenience. Applying Schur complement lemma [7] to the above inequality expression leads to LMI (4.8). Finally noting that $\dot{\rho}$ enters affinely in the LMI, it suffices to check the LMI only at the vertices of $\dot{\rho}$ and hence $\frac{\partial h}{\partial \rho} \dot{\rho}$ and $\frac{\partial P}{\partial \rho} \dot{\rho}$ are replaced by $\sum_{i=1}^s \pm \left(\nu_i \frac{\partial h}{\partial \rho_i} \right)$ and $\sum_{i=1}^s \pm \left(\nu_i \frac{\partial P(\rho)}{\partial \rho_i} \right)$, respectively.

4.3.1 LMI relaxation using slack variables

A drawback of the standard matrix inequality characterization given by Theorem 4.1 is that it involves multiple product terms including PA and RA and was found not to be suitable to derive the synthesis conditions. In this section, a reciprocal variant of Lemma 4.1 is used to derive a relaxed condition. This technique introduces the so-called *slack* variables which bring additional flexibility in the synthesis problem. Moreover, this flexibility is expected to result in far less conservative conditions than with customary approaches. The following lemma will be useful in this respect.

Lemma 4.3 *The system $(\Sigma_{\rho w})$ is asymptotically stable for all $h \in \mathcal{H}$ and satisfies the condition $\|z\|_2 \leq \gamma \|w\|_2$, if there exist a continuously differentiable matrix function*

$$\mathcal{C}(\rho) = \begin{bmatrix} -I & A(\rho) & A_h(\rho) & B_1(\rho) & 0 & I \end{bmatrix}, \quad (4.30)$$

$$\mathcal{D} = \begin{bmatrix} I & 0 & 0 & 0 & 0 & 0 \\ 0 & I & 0 & 0 & 0 & 0 \\ 0 & 0 & I & 0 & 0 & 0 \end{bmatrix}, \quad (4.31)$$

$$\Theta^T = \begin{bmatrix} V_1^T & V_2^T & V_3^T \end{bmatrix}. \quad (4.32)$$

The explicit bases of the null-space of \mathcal{C} and \mathcal{D} are given by

$$\text{Ker}(\mathcal{C}(\rho)) = \begin{bmatrix} A(\rho) & A_h(\rho) & B_1(\rho) & 0 & I \\ I & 0 & 0 & 0 & 0 \\ 0 & I & 0 & 0 & 0 \\ 0 & 0 & I & 0 & 0 \\ 0 & 0 & 0 & I & 0 \\ 0 & 0 & 0 & 0 & I \end{bmatrix}, \quad \text{Ker}(\mathcal{D}) = \begin{bmatrix} 0 & 0 & 0 \\ 0 & 0 & 0 \\ 0 & 0 & 0 \\ I & 0 & 0 \\ 0 & I & 0 \\ 0 & 0 & I \end{bmatrix}. \quad (4.33)$$

Applying Lemma 4.1 with respect to the variable Θ in (4.28) yields two inequalities, one of which is exactly the characterization given by (4.8) and the other is the LMI given by (4.34) as

$$\begin{bmatrix} -\gamma I & D_{11}^T(\rho) & 0 \\ \star & -\gamma I & 0 \\ \star & \star & (-1 - 2h_{max})R \end{bmatrix} < 0. \quad (4.34)$$

The above inequality is a relaxed form of the right bottom 3×3 block of the inequality (4.8) and is always satisfied. Hence, the feasibility of (4.27) implies the feasibility of (4.8), which along with the result of Theorem 4.1 concludes the proof. Having developed a relaxation for the bounded real lemma analysis condition we now discuss the control synthesis conditions in the subsequent sections.

4.4 \mathcal{H}_∞ State Feedback Control of Time-Delay LPV systems

In this section, the analysis results developed in the previous section are used for the synthesis of a state feedback parameter-varying \mathcal{H}_∞ controller for LPV systems with time delays. For the system (4.1), we seek to design a parameter-dependent state feedback controller of the form

$$u(t) = K(\rho(t))x(t), \quad (4.35)$$

such that the closed loop system is asymptotically stable and has induced \mathcal{L}_2 norm less than γ . Using the state feedback control law (4.35) results in a closed-loop system given by

$$\begin{aligned} \dot{x}(t) &= A_{cl}x(t) + A_hx(t-h) + B_1w(t), \\ z(t) &= C_{1,cl}x(t) + C_{1h}x(t-h) + D_{11}w(t), \end{aligned} \quad (4.36)$$

where $A_{cl} = A + B_2K$ and $C_{1,cl} = C_1 + D_{12}K$. The following theorem provides a sufficiency condition for the existence of such a control law.

Theorem 4.2 *Given the LPV system (4.1), there exists a state feedback controller of the form (4.35) such that the closed-loop system is asymptotically stable and satisfies the condition $\|z\|_2 \leq \gamma\|w\|_2$ for all $h \in \mathcal{H}$, if there exist a continuously differentiable matrix function $\tilde{P} : \mathbb{R}^s \rightarrow \mathbb{S}_{++}^n$, constant matrices \tilde{Q}, \tilde{R} and $U \in \mathbb{S}_{++}^n$, two given scalars λ_2 and $\lambda_3 \in \mathbb{R}$, a matrix function $Y : \mathbb{R}^s \rightarrow \mathbb{R}^{n_u \times n}$ and a scalar $\gamma > 0$ such that the LMI condition given by (4.38) holds, with $(2, 3) = \tilde{R} + \lambda_2 A_h U + \lambda_3 (U A^T + Y^T B_2^T)$, $E = \lambda_2 (A U + U A^T + B_2 Y + Y^T B_2^T)$, and $\tilde{\Psi}_{22}, \tilde{\Xi}_{22}$ as defined below holds true for all $\rho \in \mathcal{F}_\rho^v$. Moreover, the state feedback control law providing a guaranteed \mathcal{H}_∞ norm performance level γ is given by*

$$u(t) = Y(\rho)U^{-1}x(t). \quad (4.37)$$

$$\begin{bmatrix}
-2U & \tilde{P} - \lambda_2 U + AU + B_2 Y & -\lambda_3 U + A_h U \\
\star & \tilde{\Psi}_{22} + E & (2, 3) \\
\star & \star & \tilde{\Xi}_{22} + \lambda_3 (A_h U + U A_h^T) \\
\star & \star & \star \\
\star & \star & \star \\
\star & \star & \star \\
B_1 & 0 & U + h_{max} \tilde{R} \\
\lambda_2 B_1 & UC_1^T + Y^T D_{12}^T & \lambda_2 U - \tilde{P} \\
\lambda_3 B_1 & UC_{1h}^T & \lambda_3 U \\
-\gamma I & D_{11}^T & 0 \\
\star & -\gamma I & 0 \\
\star & \star & (-1 - 2h_{max}) \tilde{R}
\end{bmatrix} < 0. \quad (4.38)$$

Proof. The proof is an application of Lemma 4.3 to the closed-loop system (4.36). To derive the synthesis conditions we choose the three distinct slack variable matrices of the analysis condition in (4.27) as $V_1 = V \in \mathbb{S}_{++}^n$, $V_2 = \lambda_2 V$ and $V_3 = \lambda_3 V$ where λ_2 and λ_3 are any given real scalars. Defining new variables $U = V^{-1}$ and $Y = KU$, and applying the congruence transformation using matrix $diag(U, U, U, I, I, U)$ to LMI (4.27) we obtain the result of Theorem 4.2 with $\tilde{P} = U^T P U$, $\tilde{Q} = U^T Q U$, $\tilde{R} = U^T R U$, $\tilde{\Psi}_{22} = U^T \Psi_{22} U$ and $\tilde{\Xi}_{22} = U^T \Xi_{22} U$.

4.5 \mathcal{H}_∞ Output Feedback Control Design

In this section, the state feedback controller synthesis results presented in the previous section are extended to design a dynamic output feedback controller. The time delay in the system dynamics is assumed to be an exactly known or measurable function of the scheduling parameter ρ . For the system (4.1), we seek to design a

controller of the form

$$\begin{aligned}\dot{x}_k(t) &= A_k(\rho)x_k(t) + A_{hk}(\rho)x_k(t - h(\rho(t))) + B_k(\rho)y(t), \\ u(t) &= C_k(\rho)x_k(t) + C_{hk}(\rho)x_k(t - h(\rho(t))) + D_k(\rho)y(t),\end{aligned}\tag{4.39}$$

where $x_k(t) \in \mathbb{R}^n$ is the controller state vector and $x_k(t - h(\rho(t))) \in \mathbb{R}^n$ denotes the delayed state of the controller. The closed loop system formed by the interconnection of (4.1) and (4.39) is

$$\begin{aligned}\dot{x}_{cl}(t) &= \underbrace{\begin{bmatrix} A + B_2 D_k C_2 & B_2 C_k \\ B_k C_2 & A_k \end{bmatrix}}_{A_{cl}} x_{cl}(t) + \underbrace{\begin{bmatrix} B_1 + B_2 D_k D_{21} \\ B_k D_{21} \end{bmatrix}}_{B_{cl}} w(t) \\ &+ \underbrace{\begin{bmatrix} A_h + B_2 D_k C_{2h} & B_2 C_{hk} \\ B_k C_{2h} & A_{hk} \end{bmatrix}}_{A_{hcl}} x_{cl_h}, \\ z(t) &= \underbrace{\begin{bmatrix} C_1 + D_{12} D_k C_2 & D_{12} C_k \end{bmatrix}}_{C_{cl}} x_{cl}(t) + \underbrace{\begin{bmatrix} D_{11} + D_{12} D_k D_{21} \end{bmatrix}}_{D_{cl}} w(t) \\ &+ \underbrace{\begin{bmatrix} C_{1h} + D_{12} D_k C_{2h} & D_{12} C_{hk} \end{bmatrix}}_{C_{hcl}} x_{cl_h},\end{aligned}\tag{4.40}$$

with $x_{cl}(t) = \text{col}[x(t), x_k(t)]$ and $x_{cl_h} = x_{cl}(t - h(\rho(t)))$, where again the dependence on the scheduling parameter has been dropped in order to improve clarity. The following result gives sufficiency conditions for the synthesis of a delayed output feedback controller, such that the closed loop system (4.40) is asymptotically stable and has an induced \mathcal{L}_2 norm less than γ .

Theorem 4.3 *If there exists a continuously differentiable matrix function $\tilde{P} : \mathbb{R}^s \rightarrow \mathbb{S}_{++}^{2n}$, parameter dependent matrix functions $X, Y : \mathbb{R}^s \rightarrow \mathbb{S}_{++}^n$, constant matrices $\tilde{Q}, \tilde{R} \in \mathbb{S}_{++}^{2n}$, parameter dependent matrices $\hat{A}, \hat{A}_h, \hat{B}, \hat{C}, \hat{C}_h$ and D_k , two given scalars*

$$\tilde{\Psi}_{22} = \tilde{Q} - \tilde{R} + \left[\sum_{i=1}^s \pm \left(\nu_i \frac{\partial \tilde{P}(\rho)}{\partial \rho_i} \right) \right], \quad (4.49)$$

$$\tilde{\Xi}_{22} = - \left[1 - \sum_{i=1}^s \pm \left(\nu_i \frac{\partial h}{\partial \rho_i} \right) \right] \tilde{Q} - \tilde{R}, \quad (4.50)$$

then there exists a controller of the form (4.39) such that:

1. The closed-loop system (4.40) with $h \in \mathcal{H}$ is asymptotically stable for any $\rho \in \mathcal{F}_p^\nu$.
2. The \mathcal{H}_∞ norm (induced \mathcal{L}_2 norm) of the closed loop system is bounded by the positive scalar γ .

Moreover, once the parameter dependent matrices satisfying the LMI condition (4.41) are determined the delayed output feedback control matrices can be computed using the following steps:

1. Obtain M and N from the factorization problem

$$I - XY = NM^T. \quad (4.51)$$

2. Once the decision matrices are determined from the LMI optimization problem, compute the controller matrices as follows:

$$\begin{aligned} C_{hk} &= (\hat{C}_h - D_k C_{2h} Y) M^{-T}, \\ C_k &= (\hat{C} - D_k C_2 Y) M^{-T}, \\ B_k &= N^{-1}(\hat{B} - X B_2 D_k), \\ A_{hk} &= -N^{-1}(X A_h Y + X B_2 D_k C_{2h} Y + N B_k C_{2h} Y + \\ &\quad X B_2 C_{hk} M^T - \hat{A}_h) M^{-T}, \\ A_k &= -N^{-1}(X A Y + X B_2 D_k C_2 Y + N B_k C_2 Y + X B_2 C_k M^T - \hat{A}) M^{-T}. \end{aligned} \quad (4.52)$$

It is to be noted that the matrices M and N are always square and invertible in the case of full-order controllers.

where we have $\tilde{P} = Z^T P Z$, $\tilde{R} = Z^T R Z$, $\tilde{\Psi}_{22} = Z^T \Psi_{22} Z$ and $\tilde{\Xi}_{22} = Z^T \Xi Z$. Note that

$$Z^T V Z = \begin{bmatrix} Y & I \\ I & X \end{bmatrix} \quad \text{and} \quad Z^T V = \begin{bmatrix} I & 0 \\ X & N \end{bmatrix}. \quad (4.57)$$

With this, the following identities can be obtained:

$$\begin{aligned} Z^T V A_{cl} Z &= \mathcal{A}, & Z^T V B_{cl} &= \mathcal{B}, \\ Z^T V A_{hcl} Z &= \mathcal{A}_h, & Z^T C_{cl}^T &= \mathcal{C}^T, \\ Z^T C_{hcl}^T &= \mathcal{C}_h^T, & D_{cl} &= \mathcal{D}. \end{aligned} \quad (4.58)$$

The nonlinear transformations employed to linearize the inequality are

$$\begin{aligned} \hat{A} &= X A Y + X B_2 D_k C_2 Y + N B_k C_2 Y + X B_2 C_k M^T + N A_k M^T, \\ \hat{A}_h &= X A_h Y + X B_2 D_k C_{2h} Y + N B_k C_{2h} Y + X B_2 C_{hk} M^T + N A_{hk} M^T, \\ \hat{B} &= X B_2 D_k + N B_k, \\ \hat{C} &= D_k C_2 Y + C_k M^T, \\ \hat{C}_h &= D_k C_{2h} Y + C_{hk} M^T. \end{aligned} \quad (4.59)$$

Thus the inequality has been linearized with respect to the new variables (\hat{A} , \hat{A}_h , \hat{B} , \hat{C} , \hat{C}_h and D_k) and it represents the LMI condition presented in Theorem 4.3. It is to be noted that the output feedback controller designed using the result of Theorem 4.3 includes a delay in its dynamics.

Remark 4.1 *It should be observed that the inequality (4.41) is not an LMI unless the scalars λ_2 and λ_3 are fixed. It is observed through simulations that the results obtained are very sensitive to the chosen scalar values. To achieve improved results one should perform a 2-dimensional search over the scalars and use those in the LMI optimization for γ .*

Remark 4.2 *Previous work in literature on \mathcal{H}_∞ control design for LPV time-delay systems in case of a time-varying delay required the rate of variation of the time*

delay to be less than one, i.e., $|\dot{h}| < 1$. With the results presented in this chapter, this restriction does not exist and the proposed LMI formulation can even handle unbounded delay rates.

4.6 Numerical Examples

It was mentioned in section 4.3.1 that the introduction of slack variables is expected to result in reduced conservativeness in the design methodology. In this section we present two numerical examples to assess the performance of the new controller synthesis conditions presented in this chapter.

Example 1. Consider the following linear time-varying state-delayed system adopted from [88]

$$\begin{aligned} \dot{x}(t) = & \begin{bmatrix} 0 & 1 + 0.2\sin(t) \\ -2 & -3 + 0.1\sin(t) \end{bmatrix} x(t) + \begin{bmatrix} 0.2\sin(t) & 0.1 \\ -0.2 + 0.1\sin(t) & -0.3 \end{bmatrix} x(t - h(t)) \\ & + \begin{bmatrix} 0.2 \\ 0.2 \end{bmatrix} w(t) + \begin{bmatrix} 0.2\sin(t) \\ 0 & 1 + 0.1\sin(t) \end{bmatrix} u(t), \end{aligned} \quad (4.60)$$

$$z(t) = \begin{bmatrix} 0 & 10 \\ 0 & 0 \end{bmatrix} x(t) + \begin{bmatrix} 0 \\ 0.1 \end{bmatrix} u(t). \quad (4.61)$$

Defining $\rho(t) = \sin(t)$ leads to an LPV system with the parameter space $\rho(t) \in [-1 \ 1]$. The control objective is to minimize the effect of disturbance $w(t)$ on the state $x_2(t)$ and maintain a reasonable control effort. The matrix D_{12} is used to penalize the control effort. To apply the synthesis results presented in Theorem 4.2 the parameter space is gridded uniformly using 20 points. To allow a fair comparison we choose the same parameter dependence for the controller as chosen in the control design methods in [88, 89] as

$$Y(\rho) = Y_0 + \rho Y_1 + \frac{\rho^2}{2} Y_2. \quad (4.62)$$

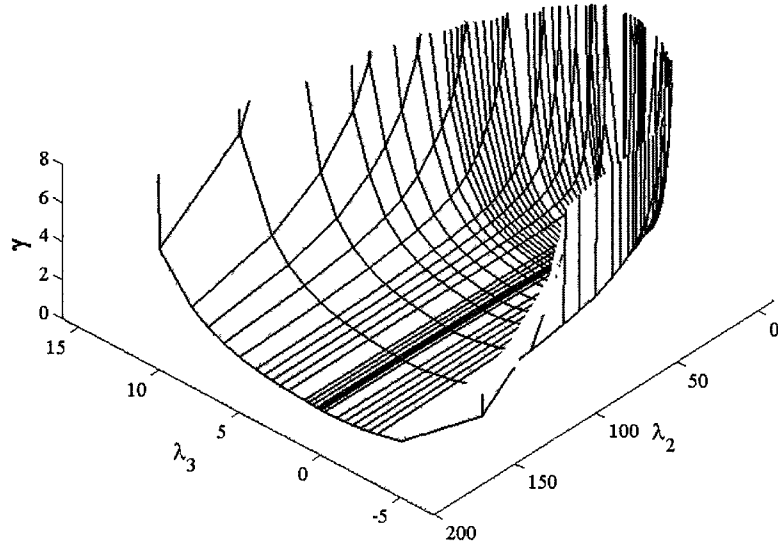


Figure 4.1: γ varying with λ_2 and λ_3

The induced \mathcal{L}_2 performance levels with respect to different maximum time delays h_{max} and different delay variation rates μ are computed using the results of Theorem 4.2. As mentioned in Remark 4.1, we perform a search over the two scalar variables λ_2 and λ_3 . Fig. 4.1 shows a zoomed-in plot of the obtained γ variation with changing λ_2 and λ_3 . The two scalars λ_2 and λ_3 are chosen to be 1 and 7, respectively, leading to the minimum value of γ . Tables 4.1 and 4.2 present a comparison of the \mathcal{H}_∞ norms obtained, whereas Table 4.3 compares the allowable maximum time-delay values using the results of this chapter with those in [89] and [98]. It can be observed from the tables 4.1 and 4.2 that \mathcal{H}_∞ performance index deteriorates with increasing time delay h_{max} and increasing delay variation rate μ as expected. It is also evident that the controller design method proposed in this chapter outperforms the previous results in terms of the achievable \mathcal{H}_∞ costs for same values of h_{max} and μ . In addition, it is observed that the proposed controller design methodology works for delay variation rates $\mu \geq 1$, whereas the past results fail. Furthermore, when $h_{max} = 1.7$ and $\mu = 0.5$, the state feedback controller synthesis problem is solvable using the method of this chapter, while the synthesis condition in [88] becomes infeasible. Table 4.3 shows that

Table 4.1: The resulting \mathcal{H}_∞ norms for $h_{max} = 1$ (Numbers as reported in the corresponding papers)

Method	$\mu = 0$	$\mu = 0.5$	$\mu = 0.7$	$\mu = 1$
[88]	6.489	6.499	6.515	Infeasible
[89]	2.129	2.239	2.531	Infeasible
Theorem 4.2, of this chapter	1.803	1.82	1.827	1.834

the maximum time-delay allowing the controller synthesis as obtained in this chapter is much larger than the results in both [89] and [98]. This indicates that the method in this chapter would be less conservative and allow for a larger delay range.

Table 4.2: The resulting \mathcal{H}_∞ norms for $h_{max} = 1.5$ (Numbers as reported in the corresponding papers)

Method	$\mu = 0$	$\mu = 0.5$	$\mu = 0.7$	$\mu = 1$
[88]	27.531	28.079	28.83	Infeasible
[89]	2.172	2.573	3.367	Infeasible
Theorem 4.2, of this chapter	1.864	1.889	1.91	1.958

Table 4.3: The maximum allowable time-delay

Method	$\mu = 0$	$\mu = 0.5$	$\mu = 0.7$
[89]	9.1	3.1	2.0
[98]	3.2	1.8	1.1
Theorem 4.2, of this chapter	48.4	45.2	42.3

Example 2. This example is motivated by the control of chattering during the milling process [82]. In a typical milling process, the work-piece is clamped and fed to a rotating multi-tooth cutter. The geometry of the cutting process of a milling machine is as shown in Fig. 4.2. The cutter has two blades that are used to remove material from the workpiece. The force acting on the tool is a function of not only the current displacement of the tool, but also the surface characteristics, and hence the displacement at the previous tool pass. This induces a delay into the system.

The force depends also on the angular position of the blade, which plays the role of a time-varying parameter. The equations of motion for the system are derived as given below, where we have

$$m_1\ddot{x}_1 + k_1(x_1 - x_2) = k \sin(\phi + \beta)l(t) - w, \quad (4.63)$$

$$m_2\ddot{x}_2 + c\dot{x}_2 + k_1(x_2 - x_1) + k_2x_2 = u, \quad (4.64)$$

and $l(t) = \sin(\phi)[x_1(t - h(t)) - x_1(t)]$, k_1 and k_2 are the stiffness of the two springs, c is the damping coefficient, m_1 and m_2 are the masses of the blade and the tool, and x_1 and x_2 are the displacements of the blade and the tool, respectively. The angle β depends on the particular material and the tool used. The angle ϕ denotes the angular position of the blade, k denotes the cutting force coefficient and w denotes the disturbance. The time delay which is the time interval between two successive cuts is denoted by $h(t)$ and is approximated to be $\frac{\pi}{\omega}$ where ω is the rotation speed of the blade. The plant we are considering can be rewritten as

$$\ddot{x}_1 = \frac{1}{m_1}[-k_1x_1 + k_1x_2 - k \sin(\phi + \beta) \sin(\phi)x_1 \quad (4.65)$$

$$+ k \sin(\phi + \beta) \sin(\phi)x_1(t - h(t)) - w], \quad (4.66)$$

$$\ddot{x}_2 = \frac{1}{m_2} [k_1x_1 - k_1x_2 - k_2x_2 - c\dot{x}_2 + u]. \quad (4.67)$$

We consider the following problem data: $m_1 = 1$, $m_2 = 2$, $k_1 = 10$, $k_2 = 20$, $k = 2$, $c = 0.5$, $\beta = 70^\circ$. It is noted that

$$\begin{aligned} \sin(\phi + \beta) \sin(\phi) &= 0.5 [\cos(\beta) - \cos(2\phi + \beta)] \\ &= 0.1710 - 0.5 \cos(2\phi + \beta). \end{aligned} \quad (4.68)$$

The system equations can be put in an LPV form with the scheduling parameter vector $\rho(t) = [\rho_1(t) \ \rho_2(t)]^T$, where $\rho_1(t) = \cos(2\phi + \beta)$ and $\rho_2(t) = \omega$ are measurable in real-time and can be used to develop a gain-scheduled controller. The rotation speed of the blade is assumed to be between 200 rpm and 2000 rpm, and the maximum variation rate is 1000 rpm/sec. Hence, we have $\rho_1(t) \in [-1 \ 1]$ and $|\frac{d\rho_1}{dt}| = |-2\sin(2\phi +$

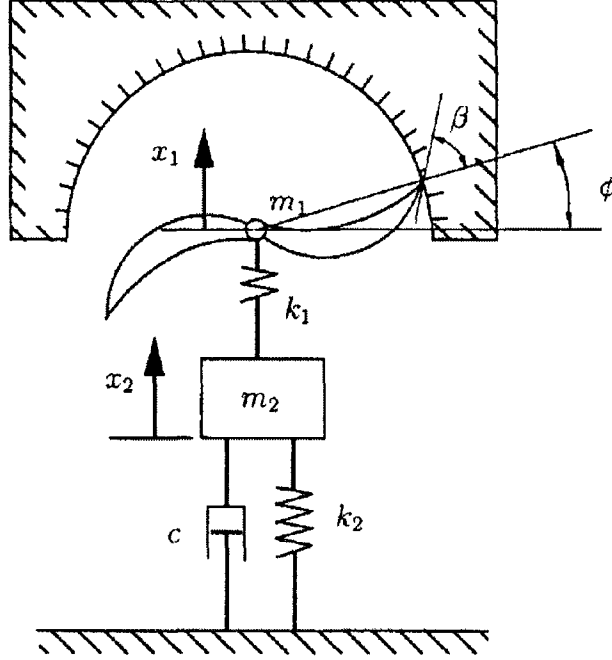


Figure 4.2: Milling process

$\beta)\omega| \leq 2 \times 2000 \times 2\pi/60 = 418.9(\text{rad}/\text{sec})$, $\rho_2(t) \in [200 \times 2\pi/60 \ 2000 \times 2\pi/60] = [20.94 \ 209.4](\text{rad}/\text{sec})$ and $|\frac{d\rho_2}{dt}| = 1000 \times 2\pi/60 = 52.35(\text{rad}/\text{sec}^2)$. The delay rate $|\frac{dh(t)}{dt}| = |\frac{-\pi}{\omega^2} \times \frac{d\omega}{dt}| \leq \frac{\pi}{(200 \times 2\pi/60)^2} \times 1000 \times 2\pi/60 = 0.75 < 1$. We seek to design an LPV controller to attenuate the effect of the disturbance force w . The controlled variable vector z is composed of the displacements of the two masses and the control force. Considering the state vector as $x = [x_1 \ x_2 \ \dot{x}_1 \ \dot{x}_2]^T$, the state-space matrices corresponding to the time-delay LPV plant to be controlled are as given by (4.69). Note that the penalty on control effort is 0.1. We use the synthesis results presented in this chapter and compare with the results obtained using the method in [88]. For simplicity both the Lyapunov matrix \tilde{P} and the slack variable matrix U are assumed to be constant matrices. We grid the parameter space using 5 grid points. It is worth noting that the synthesis conditions do not depend of the parameter ρ_2 explicitly as it appears only in the delay and nowhere in the state-space matrices. Solving the LMI problem in Theorem 4.3 we obtain an \mathcal{H}_∞ performance bound $\gamma = 1.031$ and

using the result in [88] we have $\gamma = 1.057$. The data matrices used are

$$\begin{aligned}
 A &= \begin{bmatrix} 0 & 0 & 1 & 0 \\ 0 & 0 & 0 & 1 \\ -10.34 + \rho_1 & 10 & 0 & 0 \\ 5 & -15 & 0 & -0.25 \end{bmatrix}, \quad B_1 = \begin{bmatrix} 0 \\ 0 \\ -1 \\ 0 \end{bmatrix}, \\
 A_h &= \begin{bmatrix} 0 & 0 & 0 & 0 \\ 0 & 0 & 0 & 0 \\ 0.34 - \rho_1 & 0 & 0 & 0 \\ 0 & 0 & 0 & 0 \end{bmatrix}, \quad B_2 = \begin{bmatrix} 0 \\ 0 \\ 0 \\ 0.5 \end{bmatrix}, \\
 C_1 &= \begin{bmatrix} 1 & 0 & 0 & 0 \\ 0 & 1 & 0 & 0 \\ 0 & 0 & 0 & 0 \end{bmatrix}, \quad D_{11} = \begin{bmatrix} 0 \\ 0 \\ 0.1 \end{bmatrix}.
 \end{aligned} \tag{4.69}$$

Simulations performed validate the disturbance attenuation performance of the designed controller. The disturbance $w(t)$ used in the simulation is a rectangular signal of unity magnitude for $0 \leq t \leq 4$ and zero elsewhere. The blade rotating speed ω is as shown in Fig. 4.3. Under the proposed control scheme, the control signal is shown in Fig. 4.6 and the displacements of the two masses are shown in Figs. 4.4 and 4.5. As is evident from the figures the disturbance attenuation performance using the two compared methods is similar. However, the control effort required using the method of [88] exhibits significant chatter, whereas the results of the present chapter yield a much smoother control effort.

4.7 Application to Fueling Control of SI Engines

To demonstrate the application of the output feedback controller synthesis conditions presented in this chapter, we consider the problem of controlling the air-fuel

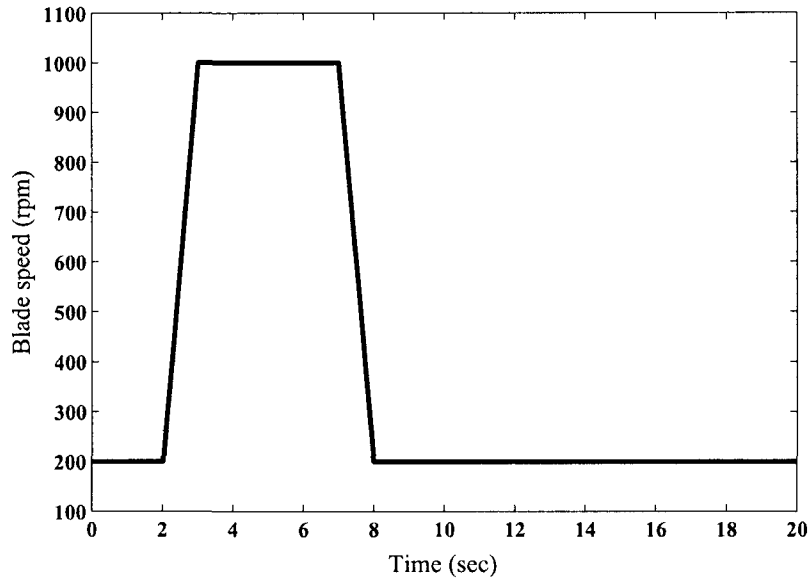


Figure 4.3: Blade rotation speed (rpm)

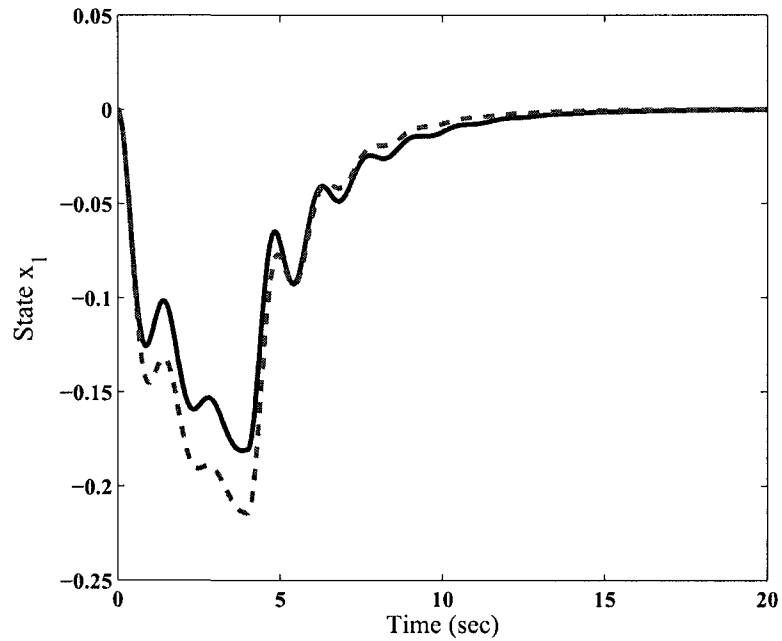


Figure 4.4: Displacement of mass 1 using results in Zhang et al. 2005 (solid line), and our results (dashed line)

ratio (AFR) in an SI engine. Precise control of AFR in SI engines is necessary to minimize emissions. Stringent norms on the emission levels of exhaust gases from

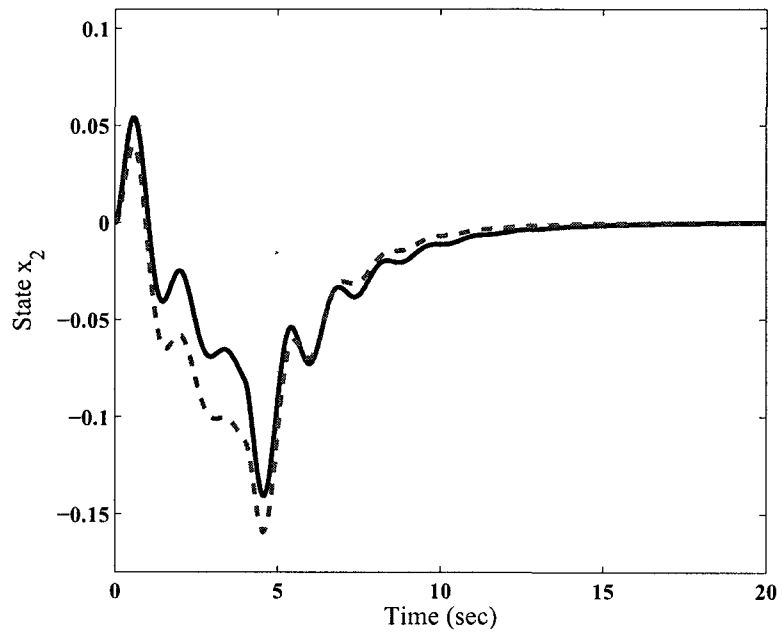


Figure 4.5: Displacement of mass 2 using results in Zhang et al. 2005 (solid line), and our results (dashed line)

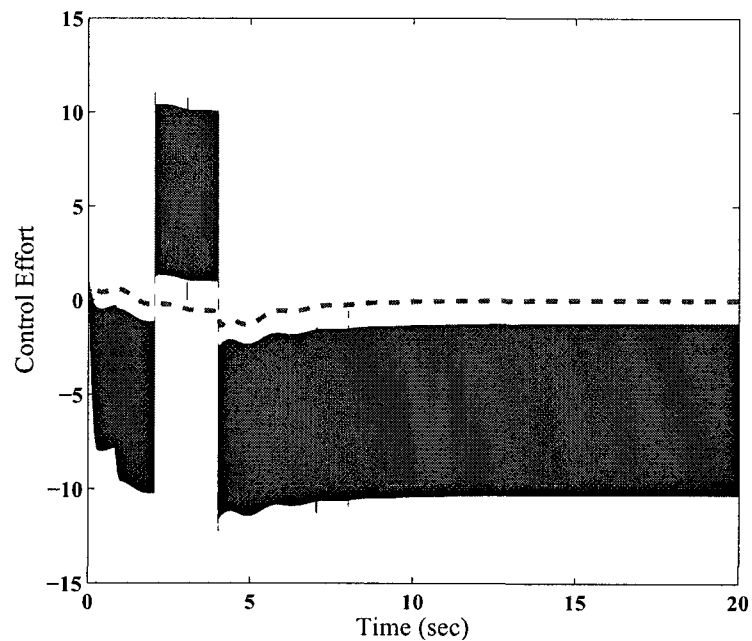


Figure 4.6: Control effort for the milling process example using results in Zhang et al. 2005 (solid line), and our results (dashed line)

automotive engines demand development of robust fueling strategies which take into account the engine, as well as, the catalyst dynamics. The three way catalyst (TWC) converter is a standard component of today's automobiles. The TWC reduces exhaust emissions by oxidizing the unburnt hydrocarbons (HC) and carbon monoxide (CO) and by reducing nitrogen oxides (NOx). The TWC performance is only as good as the quality of the exhaust gas mixture supplied to it, leading to best results only in a narrow region around stoichiometry. Short excursions about the stoichiometric point are allowed due to the oxygen storage behavior of the catalysts. When the engine is operating lean, the excess oxygen in the pre-catalyst exhaust gas is stored onto the catalyst surface through chemisorption, preventing lean (NOx) tailpipe emissions. When operating rich, the previously stored oxygen is released from the catalyst, resulting in oxidation of the reducing species HC and CO, and hence lowering their content at the tailpipe. Cycling the pre-catalyst air-fuel ratio across stoichiometry at a frequency determined during engine calibration or based on a feedback sensor signal downstream of the TWC, has been a common practice. Key to the correct operation of a TWC is the oxygen storage and release mechanism and the ability of the control strategy to maintain the oxygen level at the midpoint of the catalyst's current storage capacity. Sophisticated control strategies try to maintain the catalyst oxygen level. This has been the driving motivation behind the development of tight AFR control.

The plant to be controlled is the fuel path of an SI engine from the point 'a' to the point 'b' as shown in Fig. 4.7. The input of interest is the fuel injector pulse-width. The normalized AFR λ_{up} , as measured by UEGO sensor upstream of the TWC and the mass of oxygen stored in the TWC, i.e. m_{O_2} , form the vector of controlled variables. The overall dynamics from the fuel injector to the UEGO sensor can be modeled as a series combination of a first order lag and a delay element as given by [99]

$$G(s) = \frac{\Delta\lambda_{up}}{\Delta F_\lambda} = \frac{1}{s\tau + 1} e^{-sT}, \quad (4.70)$$

where $\Delta\lambda_{up} = \lambda_{up} - 1$, F_λ is the fuel injector pulse-width multiplier, $\Delta F_\lambda = F_\lambda - 1$ is

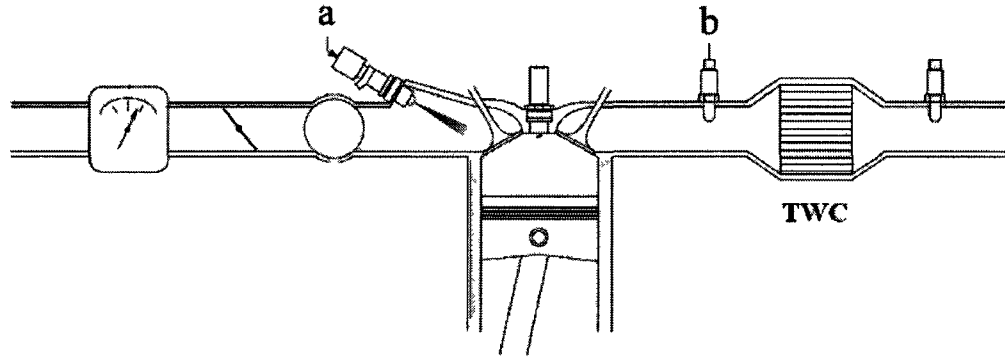


Figure 4.7: Fuel path of an SI engine

the incremental fuel injector pulse-width and the subscript “*up*” refers to upstream of the TWC. The time constant τ and the time delay T depend on the operating speed of the engine ω and this defines an LPV system with a parameter varying time-delay. The dependence of these parameters on the engine speed ω and the mass air flow is as given below.

T_{exh} : depends on the mass air flow and the engine speed ω , and typically varies between 20 and 500ms.

T_{burn} : depends on the engine speed and approximates to $\frac{90}{\omega}$.

τ depends on the engine speed ω and approximates to $\frac{2(CYL-1)}{\omega CYL}$ [99], where CYL denotes the number of cylinders in the engine. The total time delay can be summed up as $T = T_{burn} + T_{exh}$. Assuming a six cylinder engine and the relations above with the assumption of $T_{exh} \approx T_{burn}$, the parameters can be approximated as

$$\tau = 100/\omega, \quad T = 180/\omega. \quad (4.71)$$

Using (4.71) in (4.70) we get the following LPV state space representation of the plant

$$\begin{aligned} \dot{x}(t) &= -\frac{\omega}{100}x(t) + \frac{\omega}{100}u\left(t - \frac{180}{\omega}\right), \\ y_p(t) &= x(t) + d_o(t), \end{aligned} \quad (4.72)$$

where u is the input corresponding to the fuel pulse-width multiplier, y is the output air-fuel ratio upstream of the TWC and d_o is a disturbance acting on the output.

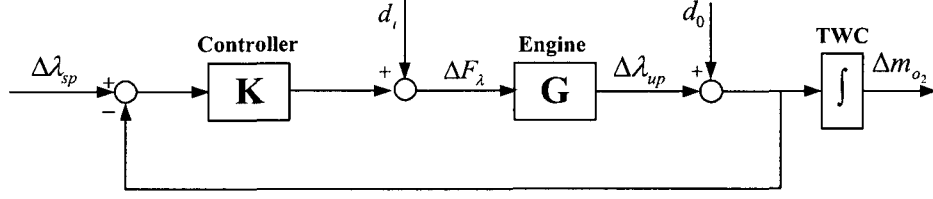


Figure 4.8: Interconnection of the engine model and the controller

The control objective is to minimize the impact of disturbance inputs on the oxygen storage level in the TWC by measuring the upstream lambda signal, and track any commanded changes in the lambda setpoint. The oxygen storage behavior of the TWC is modeled as [19]

$$\Delta m_{O_2} = \frac{1}{s}(m_{O_2,up})\Delta\lambda_{up}, \quad (4.73)$$

where $m_{O_2,up}$ represents the mass of oxygen flow upstream of the TWC, which is assumed to be unity for design purposes.

4.7.1 LPV time-delayed Controller Design

Fig. 4.8 shows the interconnection of the engine model and the controller. The simplified engine model developed in the previous section needs to be refined to suit the LPV time-delay systems controller design framework. For this purpose, the delay appearing in the input needs to be converted to a delay in state allowing us to use the results of the theorems stated in this chapter. To address this problem we introduce an artificial dynamic feedback control law $u_a(t) \in \mathbb{R}^{n_u}$ as $u(s) = (sI + \Lambda)^{-1}\Omega u_a(s)$ where Ω is a non-singular gain matrix and $\Lambda > 0$ is a parameter matrix that can be selected based on the bandwidth of the actuators. We choose $\Lambda = \Omega = 50$ for our work. By defining the new state vector $x_a^T = [x^T u^T]$, we obtain the following

state-delayed LPV system

$$\begin{aligned} \dot{x}_a(t) &= \begin{bmatrix} -\frac{\omega}{100} & 0 \\ 0 & -\Lambda \end{bmatrix} x_a(t) + \begin{bmatrix} 0 & \frac{\omega}{100} \\ 0 & 0 \end{bmatrix} x_a\left(t - \frac{180}{\omega}\right) + \begin{bmatrix} 0 \\ \Omega \end{bmatrix} u_a(t), \\ y_a(t) &= \begin{bmatrix} 1 & 0 \end{bmatrix} x_a(t) + d_o(t). \end{aligned} \quad (4.74)$$

The problem of AFR control is to achieve the reference tracking and attenuate the effect of disturbances. To achieve this, we augment the state-space representation of the plant in (4.74) with two additional states x_3 and x_4 , where $\dot{x}_3 = r - y_a$, with r being the reference signal to be tracked and $\dot{x}_4 = x_3$. The state x_4 is necessary as we are interested in minimizing the effect of disturbances on the storage level of oxygen in the TWC. This leads to the final LPV time-delay system representation of the form (4.1) where the scheduling parameter $\rho(t)$ is the engine speed $\omega(t)$ and the parameter varying time-delay is given by $h(\rho(t)) = 180/\omega(t)$. The state space matrices are

$$\begin{aligned} A(\rho) &= \begin{bmatrix} -\frac{\rho}{100} & 0 & 0 & 0 \\ 0 & -\Lambda & 0 & 0 \\ -1 & 0 & -\varepsilon_1 & 0 \\ 0 & 0 & 1 & -\varepsilon_2 \end{bmatrix}, \quad A_h(\rho) = \begin{bmatrix} 0 & \frac{\rho}{100} & 0 & 0 \\ 0 & 0 & 0 & 0 \\ 0 & 0 & 0 & 0 \\ 0 & 0 & 0 & 0 \end{bmatrix}, \quad B_2(\rho) = \begin{bmatrix} 0 \\ \Omega \\ 0 \\ 0 \end{bmatrix}, \\ B_1(\rho) &= \begin{bmatrix} 0 & 0 \\ 0 & 0 \\ 1 & -1 \\ 0 & 0 \end{bmatrix}, \quad C_1(\rho) = \begin{bmatrix} 0 & 0 & \phi & 0 \\ 0 & 0 & 0 & \psi \\ 0 & 0 & 0 & 0 \end{bmatrix}, \quad D_{12}(\rho) = \begin{bmatrix} 0 \\ 0 \\ \xi \end{bmatrix}, \\ C_2(\rho) &= \begin{bmatrix} -1 & 0 & 0 & 0 \end{bmatrix}, \quad D_{21}(\rho) = \begin{bmatrix} 1 & -1 \end{bmatrix}. \end{aligned} \quad (4.75)$$

$D_{11}(\rho)$ is a zero matrix and the scalars ε_1 and ε_2 exist for numerical solvability reasons. As observed from the matrices above, the vector of controlled outputs is $z = [\phi x_3 \ \psi x_4 \ \xi u]^T$. This penalizes the tracking error (as given by the state x_3), the integral of the tracking error (given by state x_4), as well as the control effort. It is necessary to have this choice of variables as our controlled outputs. The penalty

on the state x_4 is necessary as one of our design objectives is to minimize the effect of disturbances on the storage level of oxygen in the TWC. If we do not penalize the state x_4 , tracking would still be achieved; however, it would take a long time to bring the level of oxygen stored in the TWC back to its desired midpoint value. The scalars ϕ, ψ , and ξ decide the relative weighting in the optimization scheme. The vector of exogenous disturbance is $w = [r \ d_o]^T$. The design objective is to guarantee the closed loop stability and \mathcal{H}_∞ performance over the entire operating range of the engine. The engine speed variation is assumed to be from idle ≈ 800 rpm to high speeds ≈ 4000 rpm. The controller design follows in a straightforward way using the result of Theorem 4.3. As pointed out in Remark 1.3, Theorem 4.3 leads to an infinite dimensional convex optimization problem with an infinite number of LMIs and infinite number of decision variables. To convert this problem to a finite dimensional convex optimization problem, we follow the approach proposed in [13] and choose the functional dependence as

$$M(\omega) = M_0 + \omega M_1, \quad (4.76)$$

where M represents any of the parameter dependent matrices appearing in (4.41). This choice of the basis functions mimics the dependence of the plant state-space matrices on the gain scheduling parameter $\rho(t)$. As mentioned above we assume $\omega(t) \in [800 \ 4000]$, which defines the value of maximum time-delay $h(\rho(t))$ to be used in the synthesis of the controller. The maximum rate of variation of the parameter is assumed to be 100 rpm/sec. As described in Remark 4.1, a search is performed over the scalars λ_2 and λ_3 and we choose $\lambda_2 = 10$ and $\lambda_3 = -0.05$. Finally, gridding the parameter space (range of engine speed variation) over the intervals of 500 rpm leads to a finite set of LMIs to be solved for the unknown matrices and γ . The LMI solver in MATLAB gives a performance level of $\gamma = 2.001$.

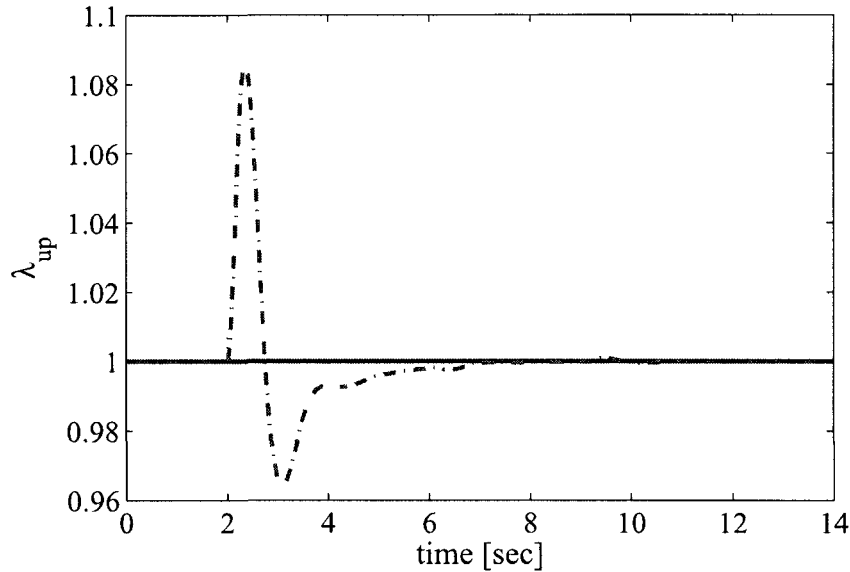


Figure 4.9: λ_{up} variation in response to disturbance with engine operating speed 1000 rpm

4.7.2 Simulation Results

Simulations were performed to validate the closed-loop performance in terms of reference tracking and disturbance rejection. A 10% step disturbance, corresponding to an absolute value of $\lambda_{up} = 0.1$ was applied at the system output at time $t = 2$ sec. To validate the controller performance over the entire operating range of engine we analyze the disturbance rejection at a low speed corresponding to larger time-delay and at a high speed, where the time-delay is comparatively smaller. Figs. 4.9 - 4.12 show the disturbance rejection performance of the designed gain scheduled LPV time-delayed controller for different engine speeds of 1000 rpm and 3500 rpm. As is evident from the figures the disturbance has been rejected and the deviation in the level of oxygen stored in the TWC is brought back to zero within approximately 12 seconds for both the cases of differing engine speeds.

Fig. 4.15 illustrates the closed-loop tracking performance of the system. The engine speed was varied as shown in Fig. 4.13. In this particular speed profile we capture the effects of running at low speed, acceleration followed by cruise and a

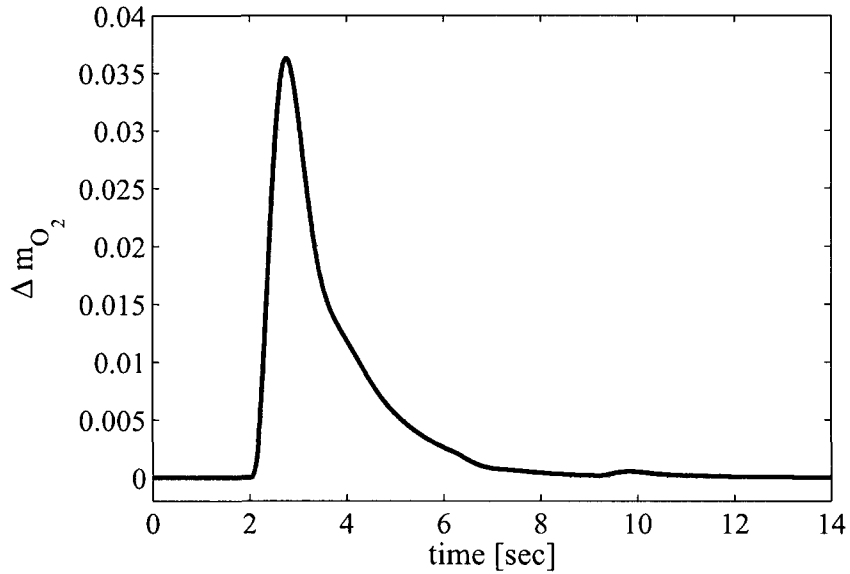


Figure 4.10: Δm_{O_2} variation in response to disturbance with engine operating speed 1000 rpm

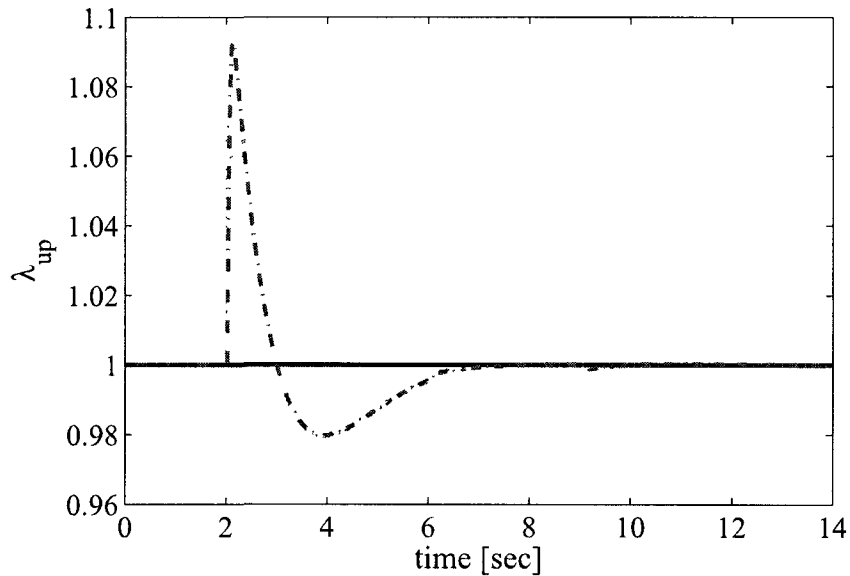


Figure 4.11: λ_{up} variation in response to disturbance with engine operating speed 3500 rpm

braking. The λ setpoint alternates between values $\lambda_{sp} = 1.1$ and 0.9. Pulsating input disturbance as shown in Fig. 4.14 is applied to the system to evaluate the overall tracking behavior in the presence of external disturbances. Fig. 4.16 shows tracking

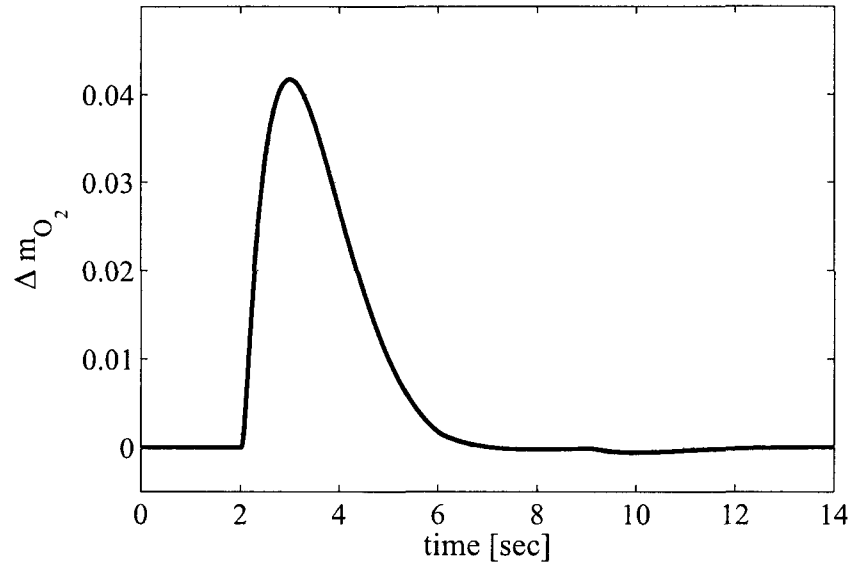


Figure 4.12: Δm_{O_2} variation in response to disturbance with engine operating speed 3500 rpm

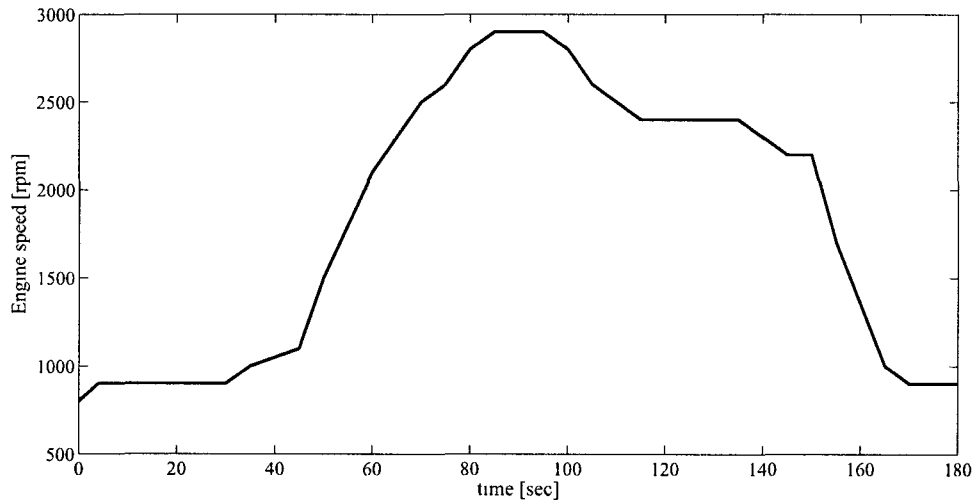


Figure 4.13: Engine speed variation

performance when zoomed-in on time from 90 sec to 165 sec. As can be seen the closed loop system tracks both a positive as well as negative step in reference input in < 10 sec. Thus the simulation validates the novel results proposed in this chapter.

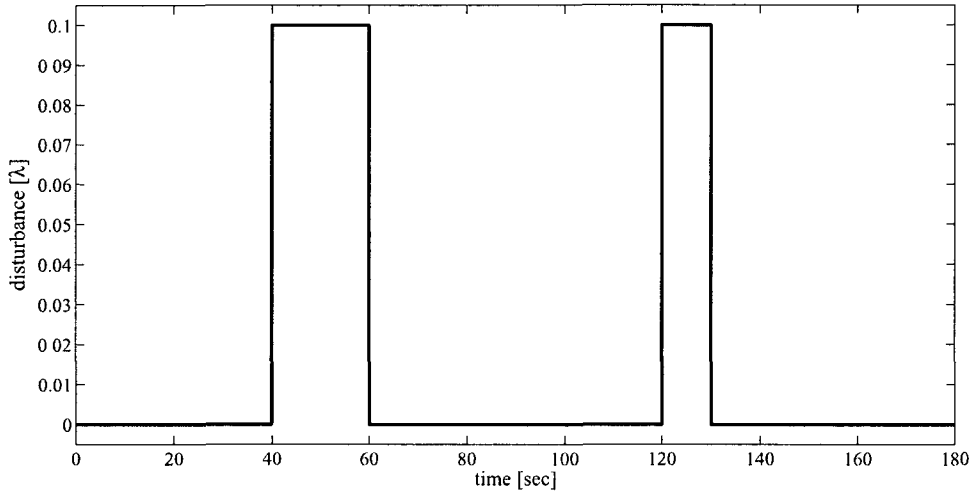


Figure 4.14: Disturbance profile

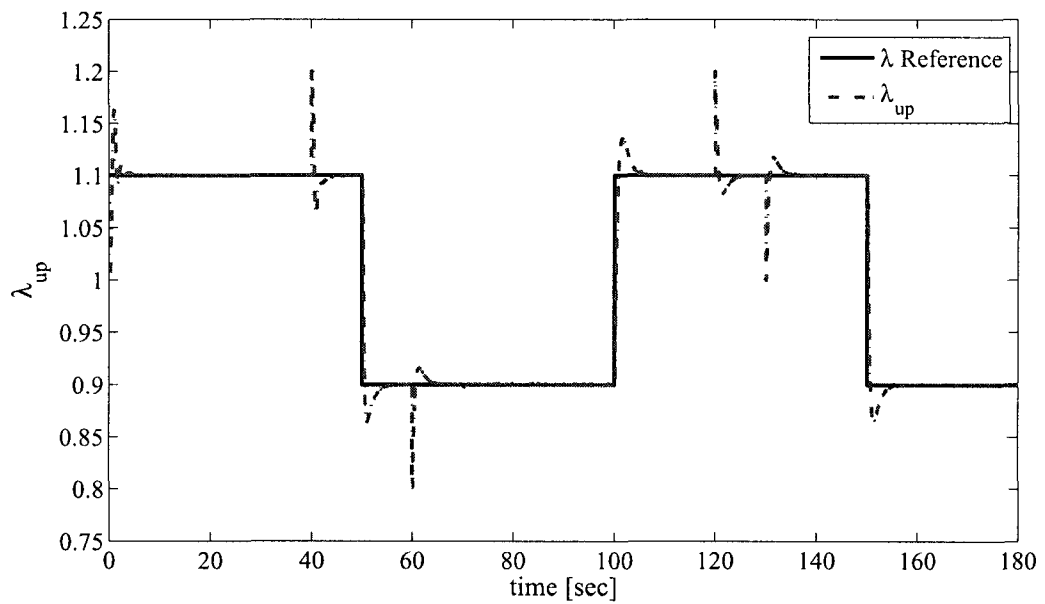


Figure 4.15: Closed loop λ tracking performance

4.8 Chapter Conclusions

In this chapter, we presented a procedure to design an output feedback controller for LPV systems with parameter-varying time delays. The presented results of this

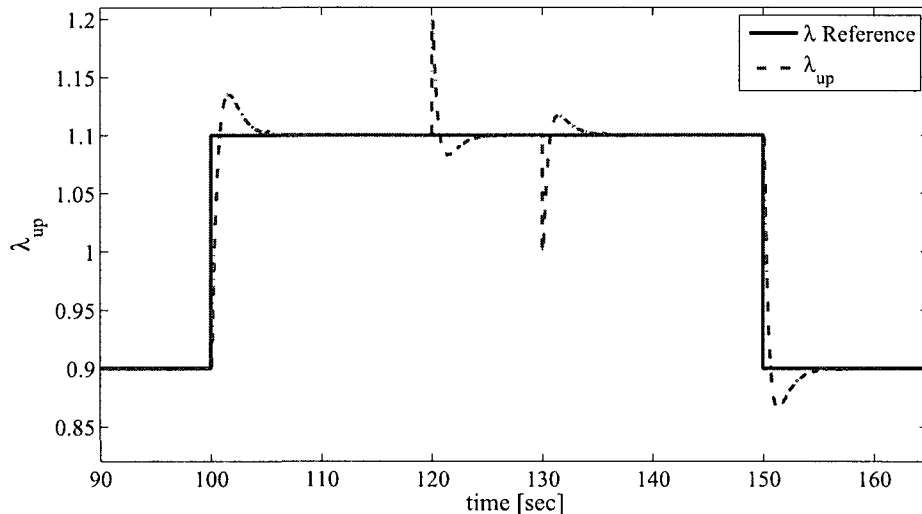


Figure 4.16: Tracking performance: 90 -165 sec

chapter are the first in the literature to provide a solution to the output feedback synthesis problem based on delay-dependent analysis conditions. The developed delay-dependent induced \mathcal{L}_2 gain performance analysis conditions are expressed in terms of LMIs that can be solved efficiently using the commercial solvers. The obtained matrix inequality-based optimization problem is then relaxed by the introduction of additional slack variables that allow the synthesis conditions to be formulated as a convex optimization problem in an LMI form. The proposed systematic procedure for the gain-scheduled output feedback control design leads to less conservative results due to the use of parameter-dependent Lyapunov-Krasovskii functional, inclusion of the delay term in the feedback control dynamics and final delay-dependent synthesis conditions. The developed delay-dependent conditions for existence of a state feedback controller guaranteeing a prescribed level of \mathcal{H}_∞ performance are compared with results existing in literature using two numerical examples. The output feedback design methodology is validated using simulations to control the air-fuel mixture ratio in an SI engine.

Chapter 5 Conclusions, Contributions and Future Work

5.1 Summary and Assessment of the Dissertation

The main objective of this dissertation was to develop and implement novel model estimation and control strategies for use in SI engines. We can broadly categorize the work in two parts. Chapter 2 constitutes the first part of this dissertation. In this part we address the problem of ethanol-blend estimation in flex fuel vehicles. The second part of the dissertation includes chapter 3 and chapter 4 where we investigate the use of linear parameter varying systems theory and apply it to identify engine dynamics and propose control methods. This work has provided a motivation for use of LPV techniques for

In chapter 2 we investigated the problem of estimating the percentage of ethanol by volume for a given ethanol-gasoline blend in a flex fuel vehicle. The use of ethanol as an alternative fuel to gasoline has spurred a lot of research concerning the use and effects of ethanol fuel on SI engines. A blend of 10% ethanol and 90% gasoline by volume is commonly available at all the gas stations in the United States. Ethanol and gasoline have differing physical and chemical properties and ethanol provides some benefits over gasoline. For example the higher octane rating of ethanol can provide for improvements in engine performance if the engine spark timing is optimized. These benefits can be reaped only if we accurately know the ethanol content in the fuel blend. Furthermore, not knowing the ethanol content correctly may result in increased emissions due to incorrect fueling and also lead to starting problems in cold conditions. In chapter 2 we proposed a model-based method for ethanol blend estimation. From first-principles, we developed a steady-state model with engine speed, throttle position

and UEGO sensor measured air-fuel ratio as inputs and the fuel injector's pulse-width as an output. This model was validated with experiments performed at the UH-ECRL. Next, we presented a method to use the change in model parameters with changing ethanol-content to predict the ethanol-blend percentage. We have shown that the 2-norm of the vector formed by the three model coefficients is a good metric to infer the ethanol content. The proposed ethanol estimation methodology is tested using seven different ethanol-gasoline blends. Finally, we provided a validation of the proposed approach based on the physics of the process and combustion chemistry.

In chapter 3 we examined the problem of identifying parameters of an LPV system. We presented a procedure to convert the problem of LPV system identification to a simpler problem of linear regression. We started with a discrete time input-output representation of an LPV system. We have introduced a new regressor vector to augment the basis functions and the system data using the Kronecker product. The proposed methodology can be used to identify single-input single-output as well as multiple-input multiple-output systems. The results presented were applied to identify the intake manifold dynamics of an SI engine. A quasi-LPV model was initially extracted from the non-linear system dynamics. For the input-output representation we chose the mass air flow as an output and the engine speed, manifold pressure and throttle angle as the inputs. We presented simulation study using GT-Power and also validated the methodology using data from experiments performed on a Ford engine.

Chapter 4 started with a discussion of LPV time-delay systems. We presented a brief survey of existing methods dealing with the analysis and control of time-delays systems and LPV time-delay systems in particular. Stability of time-delay systems using Lyapunov based methods is analyzed either using the delay-independent conditions or the delay-dependent conditions. Most of the existing results for synthesis of \mathcal{H}_∞ output feedback controllers for LPV time-delay systems use the delay-independent criteria. In-depth study revealed the conservativeness of these existing

controller synthesis conditions. Hence, we proposed the use of delay-dependent criteria based Lyapunov-Krasovskii functionals to analyze the stability and \mathcal{H}_∞ norm-based performance of LPV time-delay systems. The proposed approach can tackle parameter-varying delays as well as fast varying delays where the rate of change of delay variation is not restricted to unity. Substitution of the closed-loop matrices in the analysis conditions in order to derive the synthesis conditions resulted in a bi-linear matrix inequality. To alleviate this problem the analysis conditions were relaxed by introducing the so called slack variables. We proposed a clever use of the slack variables which leads to reduced conservativeness and a form better suited to developing controller synthesis conditions. Finally we derived conditions for the existence of a state-feedback controller and an time-delayed output-feedback controller in terms of linear matrix inequalities. It is shown in simulation using numerical examples from literature that our proposed method may lead to performance improvements for the state-feedback controller designed. The results presented for the design of output-feedback based controllers utilizing the delay-dependent conditions are the first in literature. To demonstrate the viability of the presented output-feedback results we used the fueling control in SI engines as an application. We derived the LPV system representation for the air and fuel path dynamics in an SI engine. It was shown that these dynamics constitute an LPV system with a parameter-varying time-delay with engine speed as the scheduling parameter. The novel results presented were thus successfully validated.

5.2 Future Research Directions

In this section we give directions for future research work based on the findings and learning from this thesis.

- The novel model-based low cost solution to the problem of ethanol blend estimation proposed in this work makes use of the steady state operating conditions for the engine. The implementation aspect of the proposed method requires an additional effort in terms of extracting steady state or quasi-steady state data from a normal street drive data. The steady-state model developed in this thesis can be further extended to non-steady state conditions and making possible the prediction of percentage of ethanol in the blend based on a normal street drive data. One suggested way of accomplishing this is the use of manifold pressure sensor.
- The methodology presented in chapter 2 proposed the use of the length of the vector to predict ethanol percentage. This vector based approach can be used to address any sensor measurement inaccuracies/uncertainties by looking at the direction of the vector along with the length. This can provide an additional diagnostic capability which could be integrated as a part of current on-board diagnostics algorithms.
- Manifold pressure sensor based algorithm for ethanol estimation relies on accurate modeling of the volumetric efficiency of an SI engine. The volumetric efficiency depends on ethanol content in the fuel and ambient humidity among other more obvious factors. Studying the effects of changing ambient humidity as well as changing ethanol content on the volumetric efficiency and hence ethanol estimation provides a new direction for future research work.
- Ethanol blend estimation is important among other factors, to achieve stoichiometric air-fuel ratio control. Future work utilizing the knowledge of the estimated ethanol content in the fuel blend would include developing a gain-scheduled fueling controller. In one of the current works at the UH-ECRL we plan to investigate a universal fueling control strategy for use in flex-fuel vehicles independent of the fuel type.

- In chapter 4 we derived conditions for existence of an output-feedback controller using the delay-dependent Lyapunov-Krasovskii functional. The choice of Lyapunov-Krasovskii functional was rather standard. This work can be extended further by investigating the use of other forms of Lyapunov-Krasovskii functionals. More specifically one can look at Lyapunov-Krasovskii functionals with input dynamics so that the delay at the input would not have to be transformed to a delay in the state.
- The output feedback controller proposed for LPV time-delay systems included delayed dynamics. Developing LMI based synthesis conditions leading to an output-feedback controller with no delay in its states could be a topic of future research.

References

- [1] J. Heywood. Internal Combustion Engine Fundamentals, McGraw Hill, 1988.
- [2] J. Goettemoeller and A. Goettemoeller. Sustainable Ethanol: Biofuels, Biorefineries, Cellulosic Biomass, Flex-fuel Vehicles and Sustainable Farming for Energy Independence, Prairie Oak Publishing, 2007.
- [3] G. Davis, E. Heil, and R. Rust, “Ethanol Vehicle Cold Start Improvement when using a Hydrogen supplemented E85 Fuel,” *Proceedings of the 35th Intersociety Energy Conversion Engineering Conference and Exhibit, 2000*, vol. 1, pp. 303–308, 2000.
- [4] J. S. Shamma and M. Athans, “Guaranteed Properties of Gain Scheduled Control of Linear Parameter-Varying Plants,” *Automatica*, vol. 27, no. 1, pp. 898–907, 1991.
- [5] W. J. Rugh and J. S. Shamma, “Research on Gain Scheduling,” *Automatica*, vol. 36, pp. 1401–1425, 2000.
- [6] F. D. Bianchi, H. De Battista, and R. J. Mantz, Wind Turbine Control Systems, Springer-Verlag, London, 2007.
- [7] S. Boyd, L. El Ghaoui, E. Feron, and V. Balakrishnan, Linear Matrix Inequalities in System and Control Theory, Society for Industrial and Applied Mathematics, 1994.
- [8] L. El Ghaoui and S.-I. Niculescu, Advances in Linear Matrix Inequality Methods in Control, Society for Industrial and Applied Mathematics, 2000.
- [9] C. Scherer and S. Weiland, Linear Matrix Inequalities in Control, Lecture Notes at Delft Centre for Systems and Control, Delft University of Technology, 2000.

- [10] S. P. Boyd and L. Vanderberghe, Convex Optimization, Cambridge University Press, 2004.
- [11] F. Wu, “Control of Linear Parameter Varying Systems,” Ph.D. dissertation, University of California at Berkeley, 1995.
- [12] F. Wu, X. Yang, A. Packard, and G. Becker, “Induced \mathcal{L}_2 -Norm Control for LPV Systems with Bounded Parameter Variation Rates,” *International Journal of Robust and Nonlinear Control*, vol. 6, no. 9-10, pp. 983–998, 1996.
- [13] P. Apkarian and R. Adams, “Advanced gain-scheduling techniques for uncertain systems,” *IEEE Transactions on Control Systems Technology*, vol. 6, no. 1, pp. 21–32, 1998.
- [14] J. A. Cook, J. W. Grizzle, and J. Sun, The Control Handbook, IEEE Press, New York, 1996.
- [15] R. A. Zope, M. A. Franchek, K. Grigoriadis, G. Surnilla, and S. Smith, “Model-based estimation of ethanol content in Flexible Fuel Vehicles,” *Proceedings of the American Control Conference, San Fransisco, CA*, 2011.
- [16] R. A. Zope, M. A. Franchek, K. Grigoriadis, G. Surnilla, and S. Smith, “Model-based ethanol blend estimation in flexible-fuel vehicles,” *International Journal of Engine Research*, In Press.
- [17] R. A. Zope, J. Mohammadpour, M. A. Franchek, K. Grigoriadis, R. Tafreshi, and H. Masoudi, “Identification of Air-Fuel Ratio Dynamics in SI Engines using Linear Parameter Varying Techniques,” *Proceedings of the IASTED Conference on Control and Applications, Vancouver, Canada*, 2011.

- [18] R. A. Zope, J. Mohammadpour, M. A. Franchek, K. Grigoriadis, and Y.-Y. Wang, "Parameter dependent identification of the intake manifold system dynamics in spark ignition engines using LPV methods," *Proceedings of the ASME Dynamic Systems and Control Conference, Arlington, VA*, 2011.
- [19] R. A. Zope, J. Mohammadpour, K. Grigoriadis, and M. A. Franchek, "Air-Fuel Ratio Control of Spark Ignition Engines with TWC using LPV Techniques," *Proceedings of the 2nd Annual ASME Dynamic Systems and Control Conference, 2009*, vol. 1, pp. 897–903, 2009.
- [20] R. A. Zope, J. Mohammadpour, K. Grigoriadis, and M. A. Franchek, "Robust Fueling Strategy for an SI Engine modeled as Linear Parameter-Varying Time-Delayed System," *Proceedings of the American Control Conference, Baltimore, MD*, 2010.
- [21] R. A. Zope, J. Mohammadpour, K. Grigoriadis, and M. A. Franchek, "Delay-dependent \mathcal{H}_∞ control for LPV Systems with fast-varying time-delays," *To appear in Proceedings of the American Control Conference, Montreal, Canada*, 2012.
- [22] R. A. Zope, J. Mohammadpour, K. Grigoriadis, and M. A. Franchek, "Delay-dependent Output Feedback Control of LPV time-delay Systems," *Automatica*, Submitted.
- [23] Department of Energy, "Alternatives to Traditional Transportation Fuels," *EIA*, Table C1, 2005.
- [24] Department of Energy, "The Energy Independence and Security Act," <http://www1.eere.energy.gov/femp/regulations/eisa.html>, 2007.
- [25] K. Nakata, S. Utsumi, A. Ota, K. Kawatake, and T. Tsunooka, "The Effect of Ethanol Fuel on Spark Ignition Engine," *SAE International*, vol. 2006-01-3380, 2006.

- [26] M. B. Celik, "Experimental Determination of Suitable Ethanol Gasoline Blend Rate at High Compression Ratio for Gasoline Engine," *Applied Thermal Engineering*, vol. 28, p. 396404, 2008.
- [27] F. Salih and G. Andrews, "The Influence of Gasoline/Ethanol Blends on Emissions and Fuel Economy," *SAE International*, vol. 922378, 1992.
- [28] M. Koc, Y. Sekmen, T. Topgul, and H. Yucesu, "The Effects of Ethanol-Unleaded Gasoline Blends on Engine Performance and Exhaust Emissions in a Spark-Ignition Engine," *Renewable Energy*, vol. 34, pp. 2101–2106, 2009.
- [29] J. S. Cowart, W. E. Boruta, J. D. Dalton, R. F. Dona, F. L. Rivard II, R. S. Furby, J. A. Piontkowski, R. E. Seiter, and R. M. Takai, "Powertrain Development of the 1996 Ford Flexible Fuel Taurus," *SAE International*, vol. 952751, 1995.
- [30] S. S. Wang, Y. Lin, N. H. Resendiz, L. E. Granados, and H. H. Rodriguez, "Ethanol Concentration Sensor," *SAE International*, vol. 2008-01-2452, 2008.
- [31] K. Ahn, M. Jankovic, and A. Stefanopoulou, "Estimation of Ethanol Content in Flex-Fuel Vehicles using an Exhaust Gas Oxygen Sensor: Model, Tuning and Sensitivity," *Proceedings of the 1st ASME-Dynamic Systems and Control Conference, Ann Arbor, MI*, pp. 1309–1316, 2008.
- [32] F. Theunissen, "Percent Ethanol Estimation on Sensorless Multi-Fuel Systems; Advantages and Limitations," *SAE International*, vol. 2003-01-3562, 2003.
- [33] N. H. Oliverio, L. Jiang, H. Yilmaz, and A. Stefanopoulou, "Modeling the Effect of Fuel Ethanol Concentration on Cylinder Pressure Evolution in Direct-Injection Flex-Fuel Engine," *Proceedings of the American Control Conference, St. Louis, MO*, pp. 2037–2044, 2009.

- [34] D. B. Snyder, G. H. Adi, M. P. Bunce, C. A. Satkoski, and G. M. Shaver, "Fuel Blend Fraction Estimation for Fuel-Flexible Combustion Control: Uncertainty Analysis," *Control Engineering Practice*, vol. 18, pp. 418–432, 2010.
- [35] K. Ahn, M. Jankovic, and A. Stefanopoulou, "Tolerant Ethanol Estimation in Flex-Fuel Vehicles during MAF Sensor Drifts," *Proceedings of the 2nd ASME-Dynamic Systems and Control Conference, Los Angeles, CA*, pp. 581–588, 2009.
- [36] E. Hendricks, M. J. Chevalier, S. C. Sorensen, D. Trumpy, and J. Asik, "Modeling of the Intake Manifold Filling Dynamics," *SAE International*, vol. 960037, 1996.
- [37] B. K. Powell, "A Dynamic Model for Automotive Engine Control Analysis," *Proceedings of the 18th IEEE Conference on Decision and Control including the Symposium on Adaptive Processes*, vol. 18, pp. 120–126, 1979.
- [38] L. Guzzella and C. Onder, Introduction to Modeling and Control of Internal Combustion Engine Systems, Springer-Verlag Berlin Heidelberg, 2004.
- [39] M. A. Franchek, J. Mohrfield, and A. Osburn, "Transient Fueling Controller Identification for Spark Ignition Engines," *Journal of Dynamic Systems and Control, Transactions of the ASME*, vol. 128, no. 3, pp. 499–509, 2006.
- [40] C. F. Aquino, "Transient A/F Control Characteristics of the 5 Liter Central Fuel Injection Engine," *SAE International*, vol. 810494, 1981.
- [41] L. Ljung, System Identification: Theory for the User, 2nd Edition, Prentice Hall, 1999.
- [42] T. Soderstrom and P. Stoica, System Identification, Prentice Hall International (UK) Ltd, 1989.
- [43] C. R. Rao, Linear Statistical Inference and its Applications, 2nd Edition, Wiley, New York, 1973.

- [44] M. Nemani, R. Ravikanth, and B. Bamieh, “Identification of Linear Parametrically Varying Systems,” *Proceedings of the 34th Conference on Decision and Control*, 1995.
- [45] V. Verdult, “Nonlinear System Identification: A State-Space Approach,” Ph.D. dissertation, University of Twente, Netherlands, 2001.
- [46] V. Verdult and M. Verhaegen, “Kernel Methods for Subspace Identification of Multivariable LPV and Bilinear Systems,” *Automatica*, vol. 41, no. 9, pp. 1557–1565, September 2005.
- [47] B. Bamieh and L. Giarré, “Identification of Linear Parameter Varying Models,” *International Journal of Robust and Nonlinear Control*, vol. 12, no. 9, pp. 841–853, 2002.
- [48] X. Wei and L. Del Re, “Gain Scheduled \mathcal{H}_∞ Control for Air Path System of Diesel Engines using LPV Techniques,” *IEEE Transactions on Control System Technology*, vol. 15, no. 3, 2007.
- [49] L. Giarré, D. Bauso, P. Falguni, and B. Bamieh, “LPV Model Identification for Gain Scheduling Control: An Application to Rotating Stall and Surge Control Problem,” *Control Engineering Practice*, vol. 14, no. 4, pp. 351–361, 2006.
- [50] R. Toth, “Modeling and Identification of Linear Parameter-Varying systems: An Orthonormal Basis Function Approach,” Ph.D. dissertation, Delft University of Technology, 2008.
- [51] A. Kwiatkowski, J. Blath, H. Werner, and M. Schultalbers, “Application of LPV Gain Scheduling to Charge Control of a SI Engine,” *Proceedings of the IEEE International Symposium on Intelligent Control*, pp. 2327–2331, 2006.

- [52] A. Kwiatkowski, H. Werner, J. Blath, and M. Schultalbers, "LPV Controller Synthesis for Charge Control of a Car Engine - A Hybrid Evolutionary Algebraic Approach," *Proceedings of the European Control Conference, Greece, 2007*.
- [53] J. Hale and S. Lunel, Introduction to Functional Differential Equations (Applied Mathematical Sciences), Springer, 1993.
- [54] M. Malek-Zavarei and M. Jamshidi, Time-Delay Systems: Analysis, Optimization and Applications, Elsevier Science Inc., 1987.
- [55] K. Watanabe, E. Nobuyama, and A. Kojima, "Recent Advances in Control of Time Delay Systems - a Tutorial Review," *Proceedings of the 35th IEEE Decision and Control, 1996*, vol. 2, pp. 2083–2089, 1996.
- [56] S. Niculescu, E. Verriest, L. Dugard, and J.-M. Dion, Stability and Robust Stability of Time-Delay System: A Guided Tour, Springer, 1998.
- [57] M. Mahmoud, Robust Control and Filtering for Time-Delay Systems, CRC, 2000.
- [58] S. Niculescu, Delay Effects on Stability: A Robust Control Approach, Springer Verlag, 2001.
- [59] K. Gu, V. Kharitonov, and J. Chen, Stability of Time-Delay Systems (Control Engineering), Birkhauser, 2003.
- [60] Q. Zhong. Robust Control of Time-Delay Systems. Springer Verlag, 2006.
- [61] J. Richard, "Time-Delay Systems: An Overview of Some Recent Advances and Open Problems," *Automatica*, vol. 39, no. 10, pp. 1667–1694, 2003.
- [62] R. Lewis and B. Anderson, "Necessary and Sufficient Conditions for Delay-Independent Stability of Linear Autonomous Systems," *IEEE Transactions on Automatic Control*, vol. 25, no. 4, pp. 735–739, 1980.

- [63] S. Brierley, J. Chiasson, E. Lee, and S. Zak, "On Stability Independent of Delay for Linear Systems," *IEEE Transactions on Automatic Control*, vol. 27, no. 1, pp. 252–254, 1982.
- [64] T. Mori, "Criteria for Asymptotic Stability of Linear Time-Delay Systems," *IEEE Transactions on Automatic Control*, vol. 30, no. 2, pp. 158–161, 1985.
- [65] S. Phoojaruenchanachai and K. Furuta, "Memoryless stabilization of uncertain linear systems including time-varying state delays," *IEEE Transactions on Automatic Control*, vol. 37, no. 7, pp. 1022–1026, 1992.
- [66] M. Mahmoud and N. Al-Muthairi, "Design of Robust Controllers for Time-Delay Systems," *IEEE Transactions on Automatic Control*, vol. 39, no. 5, pp. 995–999, 1994.
- [67] J. Chen and H. Latchman, "Asymptotic Stability Independent of Delays: Simple Necessary and Sufficient Conditions," *Proceedings of the American Control Conference*, pp. 1027–1031, 1994.
- [68] V. Kolmanovskii and J. Richard, "Stability of Some Linear Systems with Delays," *IEEE Transactions on Automatic Control*, vol. 44, no. 5, pp. 984–989, 1999.
- [69] T. Mori and H. Kokame, "Stability of $x(t) = Ax(t) + Bx(t - \tau)$," *IEEE Transactions on Automatic Control*, vol. 34, no. 4, pp. 460–462, 1989.
- [70] E. Verriest, "Robust Stability of Time Varying Systems with Unknown Bounded Delays," *Proceedings of the 33rd IEEE Conference on Decision and Control, 1994.*, vol. 1, pp. 417–422, 1994.
- [71] T. Su and C. Huang, "Robust Stability of Delay Dependence for Linear Uncertain Systems," *IEEE Transactions on Automatic Control*, vol. 37, no. 10, pp. 1656–1659, 1992.

- [72] S. Niculescu, T. Nito, J. Dion, and L. Dugard, “Delay-Dependent Stability of Linear Systems with Delayed State: An LMI Approach,” *Proceedings of the 34th IEEE Conference on Decision and Control*, vol. 2, pp. 1495–1496, 1995.
- [73] X. Li and C. De Souza, “Delay-Dependent Robust Stability and Stabilization of Uncertain Linear Delay Systems: a Linear Matrix Inequality Approach,” *IEEE Transactions on Automatic Control*, vol. 42, no. 8, pp. 1144–1148, 1997.
- [74] Y. Moon, P. Park, W. Kwon, and Y. Lee, “Delay-Dependent Robust Stabilization of Uncertain State-Delayed Systems,” *International Journal of Control*, vol. 74, no. 14, pp. 1447–1455, 2001.
- [75] E. Fridman and U. Shaked, “Delay-Dependent Stability and \mathcal{H}_∞ Control: Constant and Time-Varying Delays,” *International Journal of Control*, vol. 76, no. 1, pp. 48–60, 2003.
- [76] M. Wu, Y. He, J. She, and G. Liu, “Delay-Dependent Criteria for Robust Stability of Time-Varying Delay Systems,” *Automatica*, vol. 40, no. 8, pp. 1435–1439, 2004.
- [77] S. Xu, J. Lam, and Y. Zou, “New Results on Delay-Dependent Robust \mathcal{H}_∞ Control for Systems with Time-Varying Delays,” *Automatica*, vol. 42, no. 2, pp. 343–348, 2006.
- [78] A. Packard, “Gain Scheduling via Linear Fractional Transformations,” *Systems & Control Letters*, vol. 22, no. 2, pp. 79–92, 1994.
- [79] G. Becker and A. Packard, “Robust Performance of Linear Parametrically Varying Systems using Parametrically-Dependent Linear Feedback,” *Systems & Control Letters*, vol. 23, no. 3, pp. 205–215, 1994.

- [80] P. Apkarian and P. Gahinet, "A Convex Characterization of Gain-Scheduled \mathcal{H}_∞ Controllers," *IEEE Transactions on Automatic Control*, vol. 40, no. 5, pp. 853–864, 1995.
- [81] F. Wu and K. Grigoriadis, "LPV Systems with Parameter-Varying Time Delays: Analysis and Control," *Automatica*, vol. 37, no. 2, pp. 221–229, 2001.
- [82] X. Zhang, P. Tsiotras, and C. Knospe, "Stability Analysis of LPV Time-Delayed Systems," *International Journal of Control*, vol. 75, no. 7, pp. 538–558, 2002.
- [83] M. Mahmoud and N. Al-Muthairi, "Linear Parameter-Varying State-Delay (LPVSD) Systems: Stability and L_2 -Gain Controllers," *Systems Analysis Modelling Simulation*, vol. 43, no. 7, pp. 885–915, 2003.
- [84] K. Tan, K. Grigoriadis, and F. Wu, " \mathcal{H}_∞ and \mathcal{L}_2 -to- \mathcal{L}_∞ Gain Control of Linear Parameter-Varying Systems with Parameter-Varying Delays," *IEE Proceedings on Control Theory and Applications*, vol. 150, no. 5, pp. 509–517, 2003.
- [85] K. Tan and K. Grigoriadis, " $\mathcal{L}_2 - \mathcal{L}_2$ and $\mathcal{L}_2 - \mathcal{L}_\infty$ Output Feedback Control of Time-Delayed LPV Systems," *Proceedings of the 39th IEEE Conference on Decision and Control*, vol. 5, pp. 4422–4427, 2000.
- [86] J. Wang, C. Wang, and W. Yuan, "A Novel \mathcal{H}_∞ Output Feedback Controller Design for LPV Systems with a State-Delay," *Nature and Science*, vol. 2, no. 1, pp. 53–60, 2004.
- [87] F. Wu, "Delay Dependent Induced \mathcal{L}_2 -Norm Analysis and Control for LPV Systems with State Delays," *Proceedings of the 2001 International Mechanical Engineering Congress and Exposition*, 2001.
- [88] F. Zhang and K. Grigoriadis, "Delay-Dependent Stability Analysis and \mathcal{H}_∞ Control for State-Delayed LPV System," *Proceedings of the 2005 IEEE International*

Symposium on Intelligent Control, Mediterrean Conference on Control and Automation, pp. 1532–1537, 2005.

- [89] M. Sun, Y. Jia, J. Du, and S. Yuan, “Delay-Dependent \mathcal{H}_∞ Control for LPV Systems with Time Delays,” *International Journal of Systems, Control and Communications*, vol. 1, no. 2, pp. 256–265, 2008.
- [90] E. Fridman and U. Shaked, “A Descriptor System Approach to \mathcal{H}_∞ Control of Linear Time-Delay Systems,” *IEEE Transactions on Automatic Control*, vol. 47, no. 2, pp. 253–270, 2002.
- [91] P. Park, “A Delay-Dependent Stability Criterion for Systems with Uncertain Time-Invariant Delays,” *IEEE Transactions on Automatic Control*, vol. 44, no. 4, pp. 876–877, 1999.
- [92] C. Briat, O. Sename, and J. Lafay, “A LFT/ \mathcal{H}_∞ State-Feedback Design for Linear Parameter Varying Time Delay Systems,” *Proceedings of the European Control Conference*, 2007
- [93] C. Briat, O. Sename, and J. Lafay, “Parameter Dependent State-Feedback Control of LPV Time-Delay Systems with Time-Varying Delays using a Projection Approach,” *IFAC World Congress, Seoul*, vol. 17, no. 1, 2008
- [94] J. Mohammadpour and K. Grigoriadis, “Delay-Dependent \mathcal{H}_∞ Filtering for Time-Delayed LPV Systems,” *Systems & Control Letters*, vol. 57, no. 4, pp. 290–299, 2008.
- [95] C. Briat, “Robust Control and Observation of LPV Time-Delay Systems,” Ph D. dissertation, Universitadegli Studi di Siena, 2008.
- [96] P. Gahinet and P. Apkarian, “A Linear Matrix Inequality Approach to \mathcal{H}_∞ Control,” *International Journal of Robust and Nonlinear Control*, vol. 4, no. 4, pp. 421–448, 1994.

- [97] H. Tuan, P. Apkarian, and T. Nguyen, “Robust and Reduced-Order Filtering: New LMI-Based Characterizations and Methods,” *IEEE Transactions on Signal Processing*, vol. 49, no. 12, pp. 2975–2984, 2001.
- [98] M. Sun, Y. Jia, J. Du, and S. Yuan, “Delay-Dependent \mathcal{H}_∞ Control for LPV Systems with Time Delays,” *Proceedings of the IEEE Conference on Decision and Control, 2008*, pp. 2089–2093, 2008.
- [99] U. Kienke and L. Nielsen, Automotive Control Systems, Springer SAE International, Warrendale, PA, 2000.